NACA TM 1418

7968

TECH LIBRARY KAFB, NM
0144511

NATIONAL ADVISORY COMMITTEE FOR AERONAUTICS

TECHNICAL MEMORANDUM 1418

THE INTERACTION OF A REFLECTED SHOCK WAVE WITH THE BOUNDARY LAYER IN A SHOCK TUBE

By Herman Mark

Cornell University
Ithaca, New York

Washington
March 1958

AFMDC
TECHNICAL LIBRARY
AFL 2811

TECH LIBRARY KAFB, NM
0144511

TABLE OF CONTENTS

Page

SUMMARY 1

I - INTRODUCTION 3

II - THE IDEAL REFLECTED SHOCK 6

THE INITIAL SHOCK WAVE 6
THE REFLECTED SHOCK WAVE 12

III - THE REFLECTED SHOCK WAVE IN A REAL SHOCK TUBE 16

THE LAMINAR BOUNDARY LAYER IN THE FLOW BEHIND THE INITIAL SHOCK WAVE 16
ATTENUATION OF THE INITIAL SHOCK 19
THE INTERACTION OF THE REFLECTED SHOCK WITH THE BOUNDARY LAYER IN A REAL SHOCK TUBE 23

IV - EXPERIMENTAL DETERMINATIONS 35

DESCRIPTION OF THE EXPERIMENTAL SETUP AND EQUIPMENT 35
The Shock Tube 35
The Spark Schlieren System and Photographic Techniques 37
The Spark-Triggering System 39
Description of Experimental Methods 40

DISCUSSION OF EXPERIMENTAL RESULTS AND THE PROPOSED MODEL FOR INTERACTION IN REGION 2 (fig. 12) 43
Variation of Shock Mach Number 43
Reynolds Number Effects 72

DISCUSSION OF THE GROWTH OF THE INTERACTION AS FURTHER VERIFICATION OF THE PROPOSED MODEL 90

V - ATTENUATION OF THE REFLECTED SHOCK 98

MODEL FOR THE ATTENUATION PHENOMENON 98
CALCULATION OF ATTENUATION OF THE REFLECTED SHOCK SPEED AT $M_1 = 2.15$ IN AIR 101

VI - A SUMMARY AND SOME SUGGESTED FURTHER STUDIES 109

APPENDIXES
A - MACH NUMBER DISTRIBUTION ACROSS THE BOUNDARY LAYER 112

B - A WEAK SHOCK REFLECTED AT A WALL 117

Page

C - CALCULATION OF ANGLES OF THE INTERACTION PATTERN 119

D - REYNOLDS NUMBER FOR THE REFLECTED SHOCK - BOUNDARY-LAYER INTERACTION 122

E - CALCULATION OF THE SIZE OF THE SHOCK-WAVE - BOUNDARY-LAYER INTERACTION 124

REFERENCES 126

NATIONAL ADVISORY COMMITTEE FOR AERONAUTICS

TECHNICAL MEMORANDUM 1418

THE INTERACTION OF A REFLECTED SHOCK WAVE WITH THE BOUNDARY LAYER IN A SHOCK TUBE[1]

By Herman Mark[2]

4785

SUMMARY

Ideally, the reflection of a shock from the closed end of a shock tube provides, for laboratory study, a quantity of stationary gas at extremely high temperature. Because of the action of viscosity, however, the flow in the real case is not one-dimensional, and a boundary layer grows in the fluid following the initial shock wave.

In this paper simplifying assumptions are made to allow an analysis of the interaction of the shock reflected from the closed end with the boundary layer of the initial shock afterflow. The analysis predicts that interactions of several different types will exist in different ranges of initial shock Mach number. It is shown that the cooling effect of the wall on the afterflow boundary layer accounts for the change in interaction type.

An experiment is carried out which verifies the existence of the several interaction regions and shows that they are satisfactorily predicted by the theory. Along with these results, sufficient information is obtained from the experiments to make possible a model for the interaction in the most complicated case. This model is further verified by measurements made during the experiment.

The case of interaction with a turbulent boundary layer is also considered. Identifying the type of interaction with the state of turbulence of the interacting boundary layer allows for an estimate of the state of turbulence of the boundary layer based on an experimental investigation of the type of interaction.

---

[1]The information presented herein was offered as a thesis in partial fulfillment of the requirements for the degree of Doctor of Philosophy, Cornell University, Ithaca, New York, June 1957.

[2]Now at the Lewis Flight Propulsion Laboratory, Cleveland, Ohio.

A method is proposed whereby the effect of the boundary-layer interaction on the strength of the reflected shock may be calculated. The calculation indicates that the reflected shock is rapidly attenuated for a short distance after reflection, and this result compares favorably with available experimental results.

4785

I - INTRODUCTION

In recent years the shock tube has become an extremely important laboratory instrument for the study of nonstationary problems in fluid mechanics. A great deal of fundamental work has been done since Vieille first used the shock tube to study the "Discontinuités Produites par la Détente Brusque de Gas Comprimés" (Comptes Rendus de l'Academie des Sciences, 1899, pp. 129-1288). Studies have been made of nonstationary wave phenomena, for example, refractions of shocks and expansions at contact surfaces, interactions between one-dimensional wave elements, shock waves traveling over bodies, and so forth. Other studies using the shock tube include the investigations of flows in the subsonic, transonic, and supersonic regimes and the investigation of various flame propagation phenomena. (A large bibliography may be found in refs. 1 and 2.) More recently the shock tube has been used as the primary tool in studying the phenomena of magneto-hydrodynamics and chemical kinetics. In fact, the shock tube can so conveniently provide high-temperature gases that with but slight modification it can be used to produce nitric oxide from ordinary air (ref. 3). It is conceivable that such a process may become a commercial method for producing the chemical ingredients of fertilizers (nitrates)! Indeed then, the shock tube has proven to be very versatile in its applications as a research tool.

4785

CY-1 back

In its simplest form the shock tube is essentially a long straight tube of constant cross section, closed at both ends and separated into two chambers by a thin diaphragm (fig. 1(a)). One chamber is filled with a gas at high pressure, while the other chamber is evacuated, that is, contains gas at a much lower pressure. If the diaphragm is sufficiently stressed, it will burst when punctured, and a compression wave which steepens rapidly (several diameters) into a shock travels into the low-pressure gas. At the same time an expansion wave broadening with time travels into the high-pressure gas. It is assumed that a plane surface separates the gases which were originally separated by the diaphragm. This "contact surface" travels down the tube in the direction of the low-pressure chamber and acts as the piston for setting the gas in motion. The whole wave system can be most easily visualized in the xt plane (fig. 1(b)). In this figure the traveling waves can be followed along the tube and in time. It is generally assumed that the gas in each of the regions of figure 1(b) is in a uniform state (i.e., uniform across the tube in all flow and thermodynamic variables associated with that state). In figure 1(c) two pressure distributions along the tube are shown; one at time $t = 0$, and the other at time $t > 0$. When the waves generated reach the closed ends of the tube, they are reflected as shown in figure 1(b).

With the picture just described, it is possible to calculate the conditions for all the states involved, if the pressure ratio across the diaphragm is given, and the properties of the gases separated by the diaphragm are known.

Ideally then, the shock wave propagating into the low-pressure chamber generates in the gas through which it has passed a following flow with uniform temperature, pressure, and velocity. The gas velocity is somewhat lower than that of the wave and may be subsonic or supersonic depending on the strength of the shock wave. (It is supersonic in air if the shock-wave Mach number is greater than 2.068.) This uniform region lasts until the arrival of the contact surface (where the temperature and sound speed drop sharply) and may be used for testing models (i.e., as a wind tunnel) albeit for a short time. It may be used directly or, if supersonic, after expansion to higher Mach numbers. If the shock is allowed to reach the end of the tube, however, it is reflected at the closed end; and the reflected shock, traveling back up the tube (again ideally), signals the fluid following the initial shock of the presence of the closed end, and brings this flow to rest (region 5, fig. 1(b)). Thus, ideally, this reflection process provides a slug of stationary high-temperature gas very useful for study in a number of important applications. With the advent of intercontinental ballistics missiles and hypersonic flow has come a great need for information about the properties of air (and other gases) at extremely elevated temperatures. There is hardly a more convenient way of producing gases at elevated temperatures for laboratory study than the process outlined here, which (ideally) provides hot, stationary gases behind the reflected shock wave in a shock tube.

In the work discussed so far, no mention has been made of the role played by viscosity. There were so many interesting problems to be investigated, theoretically and experimentally, without considering viscosity, that it was not until very recently that any extensive work was done to examine the features of the ideal picture which would be modified because of the effects of viscosity. Certainly, in the flow following the initial shock wave, there is generated a boundary layer near the walls of the shock tube, across which the velocity of the flow decreases from that in the main stream to zero at the walls. Nonuniformities are thus introduced in the flow and thermodynamic variables that were previously considered uniform across the tube. Some of the consequences of these nonuniformities have already been investigated (refs. 4 to 11). The most noticeable effect is the attenuation of the shock wave as it travels down the tube. The boundary layer is usually very thin, and the shape of the initial shock wave is very little influenced. The boundary layer does act, however, to slow down the shock wave, and references 6 and 8 have analyzed the effect and obtained results which check quite well with experiment.

The problem which is involved when the shock reaches the closed end of the tube and reflects into the nonuniform flow following the initial shock is more complicated but poses many interesting questions. First of all, the question arises as to how the shock itself is modified

4785

(in shape and strength) by interacting, not with the ideal flow, but with the boundary-layer flow which follows the initial shock. Then, too, it is desirable to know whether the high-temperature gas behind the reflected shock is stationary or, if the flow has been modified, at least to know whether this gas is still available for chemical kinetic studies and the like. It was with some of these questions in mind that the present work was undertaken. The report herein contained is of an analytical and experimental study made at Cornell University to determine and to clarify the phenomena involved in the real shock tube when the reflected shock interacts with the boundary-layer flow which follows the initial shock. First, an analysis is made to determine the kinds of interactions that can possibly occur, and under what conditions they are to be expected. This analysis is verified experimentally. The most complicated interaction is then studied in detail, and a model for the phenomenon is proposed. The features of the phenomenon are analyzed based on this model and these, too, are checked experimentally. Finally, assuming that this complicated interaction has been correctly described, a model is then proposed for calculating the attenuation of the reflected shock. This calculation is carried through for a given case, and comparison with experimental results on the attenuation of the reflected shock is presented. The results and the shortcomings of the present work are discussed, and some suggestions for further work are outlined.

The author would like to express his sincere gratitude to Professor N. Rott of Cornell University, Graduate School of Aeronautical Engineering, for his able guidance throughout and for a number of particularly invaluable discussions. The author would also like to express his gratitude to Professor W. R. Sears, Director of the School, for helpful criticism of the work in progress, and to Professor E. L. Resler, Jr. for several important suggestions in the laboratory. The author is grateful for financial assistance to the Office of Scientific Research, and to the Office of Naval Research for financing the experiments.

4785

II - THE IDEAL REFLECTED SHOCK WAVE

THE INITIAL SHOCK WAVE

In an ideal shock tube (fig. 1(a)) it is assumed that the diaphragm separating the high-pressure chamber from the low-pressure chamber bursts instantaneously when punctured. Immediately a shock wave travels into the low-pressure gas and compresses it to some intermediate pressure. At the same time expansion waves moving in the other direction allow the high-pressure gas to expand to this same intermediate pressure. The shock wave travels along the tube at constant speed U_1, and its strength is usually denoted by referring this speed to the speed of sound in the quiescent gas ahead of the shock a_1(i.e., by the Mach number $M_1 = U_1/a_1$). It is assumed that the gas compressed by the shock is in a completely uniform state and is contained between the shock and the gas which has expanded from the high-pressure chamber. The sequence of events which follow the bursting of the diaphragm is shown in figure 1(b). A typical pressure distribution before the diaphragm burst (time $t = 0$) and shortly afterwards ($t = t_1 > 0$) is shown in figure 1(c). The gases in states 2 and 3 of figure 1(b) are at the same pressure and are moving at the same velocity but, since the gas in 2 was compressed from state 1 and the gas in 3 was expanded from state 4 (states 1 and 4 were originally in temperature equilibrium), the temperatures in the two states are not the same. Thus we have

$$T_3 \neq T_2;\ p_3 = p_2;\ u_3 = u_2 \tag{II-1}$$

where T is the temperature, p the pressure, and u the particle velocity. No fluid crosses the contact surface separating regions 2 and 3, and so it, too, moves at $u_2 = u_3$.

If, in considering the shock, we change the axis of reference to one moving with the shock, we may write the Rankine-Hugoniot relations across the shock.

Conservation of mass:

$$\rho_1 U_1 = \rho_2(U_1 - u_2) \tag{II-2}$$

Conservation of momentum:

$$p_1 + \rho_1 U_1^2 = p_2 + \rho_2(U_1 - u_2)^2 \tag{II-3}$$

4785

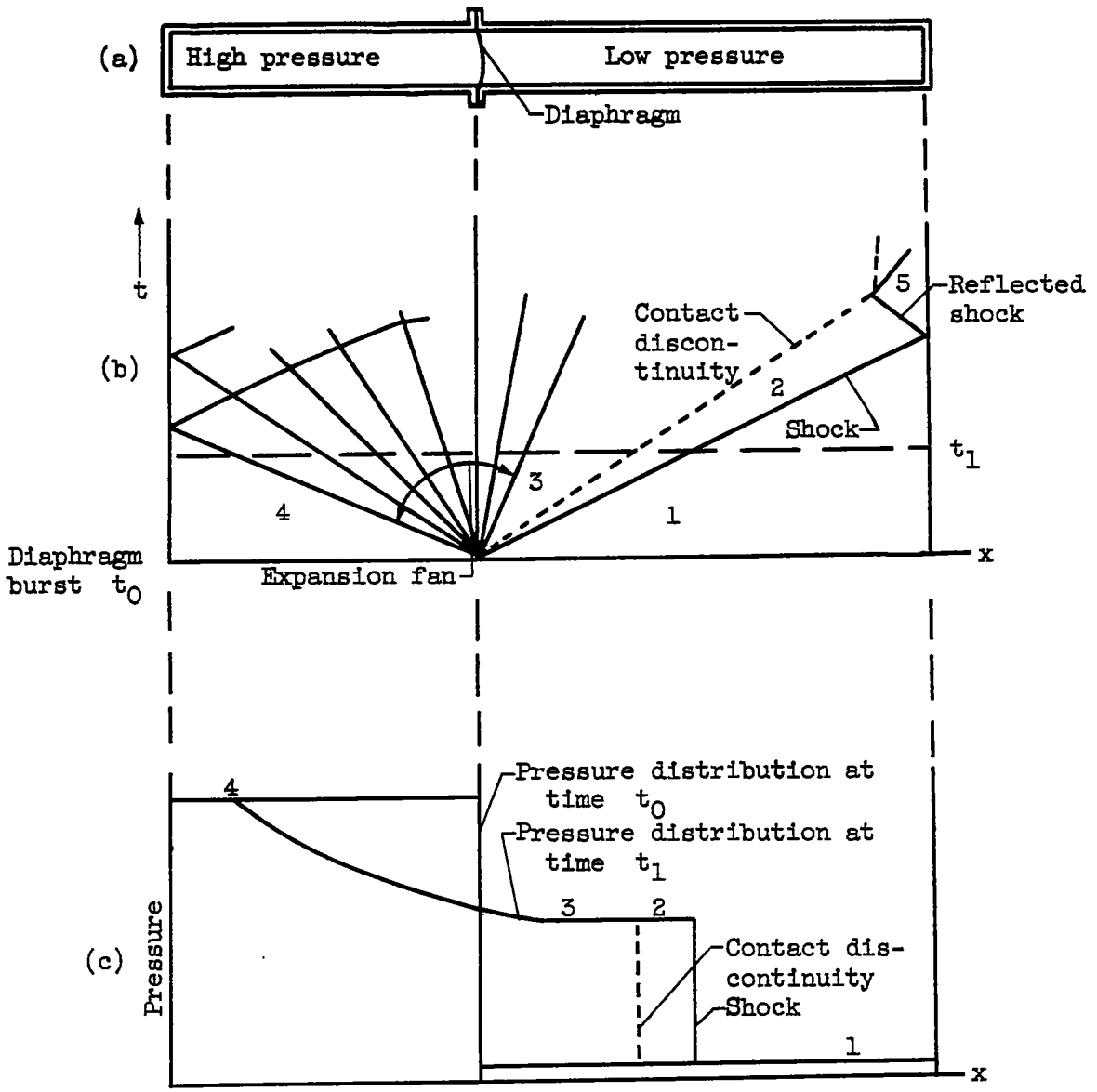

Figure 1. (a) Diagrammatic sketch of a shock tube. (b) An xt diagram of the sequence of events following diaphragm burst. (c) Pressure distribution at time $t_0 = 0$ and $t_1 > 0$.

Conservation of energy:

$$H_1 + \frac{1}{2} U_1^2 = H_2 + \frac{1}{2} (U_1 - u_2)^2 \tag{II-4}$$

where

U_1 shock speed

u_2 particle velocity in region 2 (with respect to the shock tube) 4785

$\rho_{1,2}$ densities in regions 1 and 2, respectively

H is the specific enthalpy and may be written (specific-heat ratio $\gamma = C_p/C_v$)

$$H = \frac{\gamma}{\gamma - 1} \frac{p}{\rho} \tag{II-5}$$

Combining equations (II-2), (II-3), (II-4), and (II-5) we can solve for p_2, ρ_2, and u_2 in terms of the quantities in region 1 and the speed of the shock U_1. The quantities behind the shock are most conveniently given as function of M_1 and are presented in reference 12, page 7. From reference 12 we have

$$M_{2,1}^2 = \frac{(\gamma - 1)M_{1,2}^2 + 2}{2\gamma M_{1,2}^2 - (\gamma - 1)} \tag{II-6}$$

$$\frac{p_2}{p_1} = \frac{2\gamma M_1^2 - (\gamma - 1)}{\gamma + 1} \tag{II-7}$$

$$\frac{\rho_2}{\rho_1} = \frac{(\gamma + 1)M_1^2}{(\gamma - 1)M_1^2 + 2} \tag{II-8}$$

$$\frac{T_2}{T_1} = \frac{a_2^2}{a_1^2} = \frac{\left[2\gamma M_1^2 - (\gamma - 1)\right]\left[(\gamma - 1)M_1^2 + 2\right]}{(\gamma + 1)^2 M_1^2} \tag{II-9}$$

The expansion from region 4 to region 3 is isentropic, and so it may be shown (ref. 13, p. 87) that

$$\frac{2a_4}{\gamma - 1} + u_4 = \frac{2a_3}{\gamma - 1} + u_3 \tag{II-10}$$

or since $u_4 = 0$, $p_3 = p_2$, and $u_3 = u_2$

$$\frac{p_4}{p_3} = \frac{p_4}{p_2} = \frac{1}{\left[1 - \frac{\gamma_4 - 1}{\gamma_1 + 1}\frac{a_1}{a_4}\left(M_1 - \frac{1}{M_1}\right)\right]^{\frac{2\gamma_4}{\gamma_4 - 1}}} \tag{II-11}$$

4785

Combining (II-7) and (II-11), we have

$$\frac{p_4}{p_1} = \left(\frac{2\gamma_1}{\gamma_1 + 1} M_1^2 - \frac{\gamma_1 - 1}{\gamma_1 + 1}\right) \frac{1}{\left[1 - \frac{\gamma_4 - 1}{\gamma_4 + 1}\frac{a_1}{a_4}\left(M_1 - \frac{1}{M_1}\right)\right]^{\frac{2\gamma_4}{\gamma_4 - 1}}} \tag{II-12}$$

CY-2

Thus, if the diaphragm pressure ratio p_4/p_1 is given and if γ is known for the low-pressure (1) and the high-pressure (4) gases, $M_1 (= U_1/a_1)$ is given by (II-12). This equation is plotted in figure 2(a) for $\gamma_1 = 5/3$, $\gamma_4 = 7/5$, and various ratios of a_4/a_1 and in figure 2(b) for specific driver (high-pressure) and driven (low-pressure) gas combinations. It is clear that the ratio of the sound speeds in the gases separated by the diaphragm is a most important parameter and (since $\frac{a_4}{a_1} \propto \sqrt{\frac{\mu_1}{\mu_4}}$; μ is the molecular weight of the gas) indicates that higher shock Mach numbers are obtainable at a given diaphragm pressure ratio by using a driver gas of lower molecular weight. The effect of lowering the molecular weight of the driver gas is shown specifically in figure 2(b) for various combinations of helium, hydrogen, argon, and air.

From the definition of M_2 and making use of equations (II-6) and (II-9), we may now write an expression for u_2, the velocity of the gas in region 2 with respect to the shock tube (i.e., the laboratory)

$$M_2 = \frac{U_1 - u_2}{a_2} = \left(\frac{U_1}{a_1}\frac{a_1}{a_2}\right) - \frac{u_2}{a_2} \tag{II-13}$$

4785

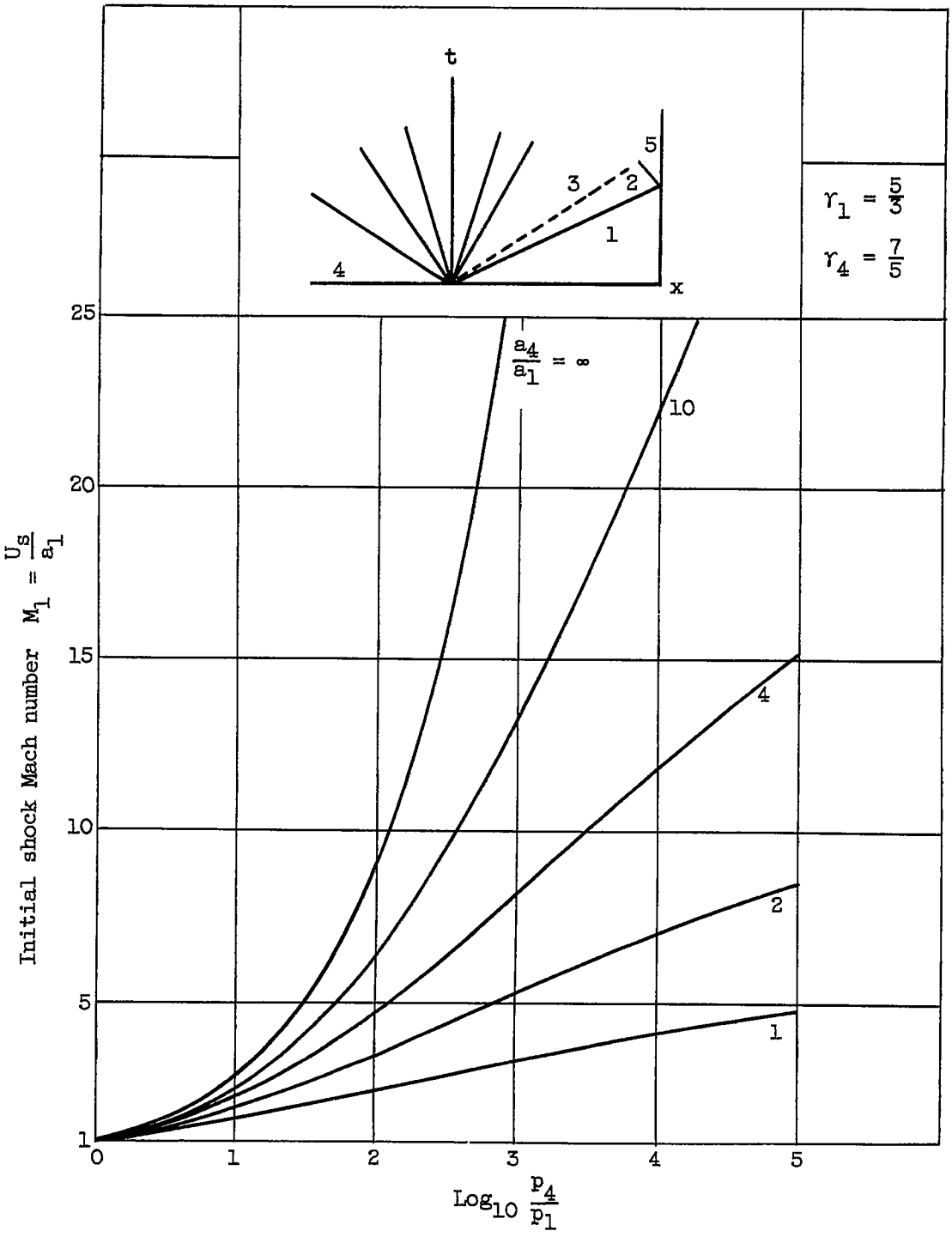

Figure 2. - (a) Relation between initial shock Mach number M_1 and diaphragm pressure ratio for several ratios of sound velocity in the high- and low-pressure gases.

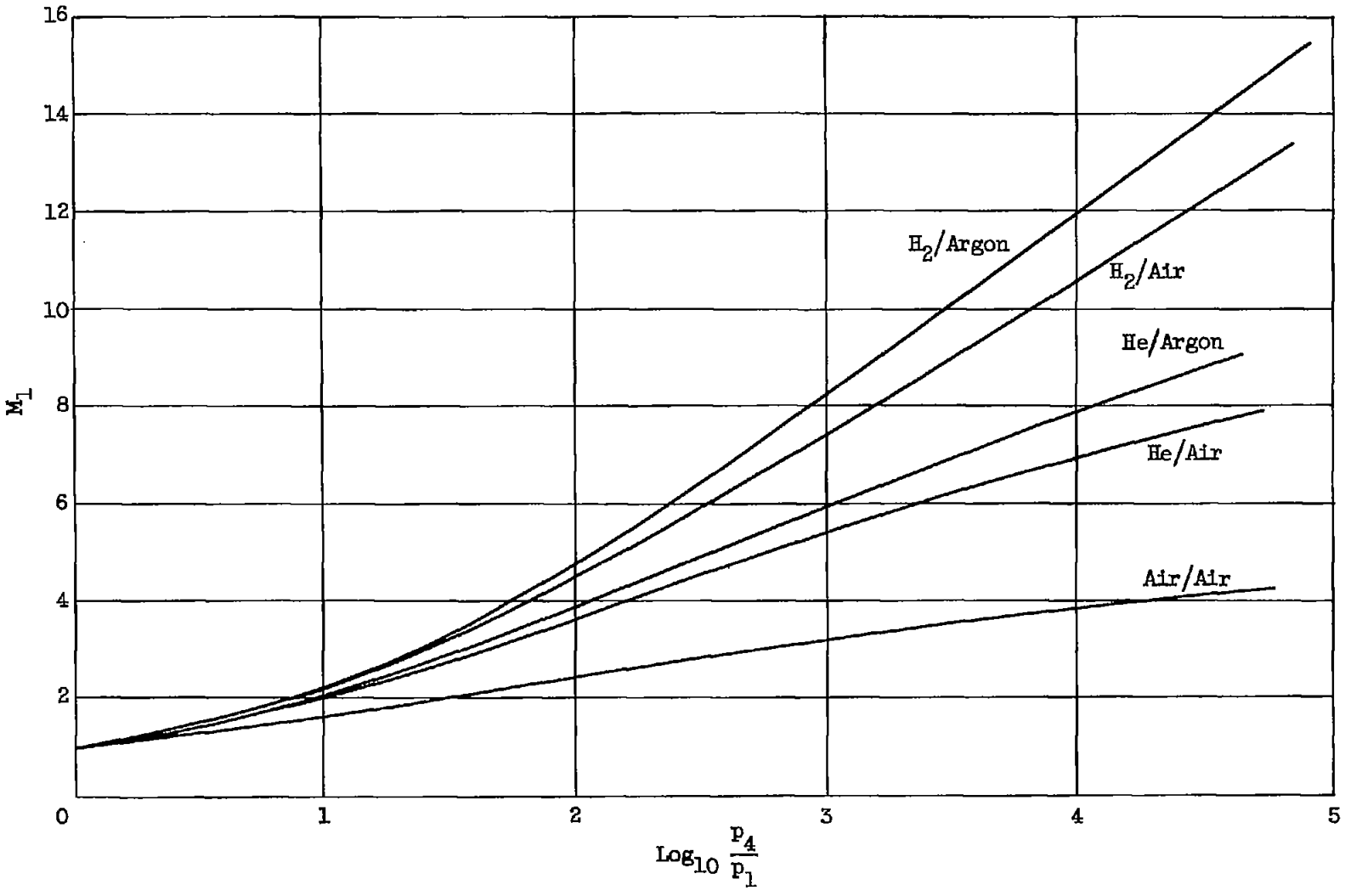

Figure 2. - Concluded. (b) Relation between shock Mach number M_1 and diaphragm pressure ratio for several specific high-pressure - low-pressure gas combinations.

Thus

$$\frac{u_2}{a_2} = M_1 \left\{ \frac{(\gamma + 1)^2 M_1^2}{\left[2\gamma M_1^2 - (\gamma - 1)\right]\left[(\gamma - 1)M_1^2 + 2\right]} \right\}^{\frac{1}{2}} - \left[\frac{(\gamma - 1)M_1^2 + 2}{2\gamma M_1^2 - (\gamma - 1)}\right]^{\frac{1}{2}} \tag{II-14}$$

which reduces to

$$\frac{u_2}{a_2} = \frac{2(M_1^2 - 1)}{\left\{\left[2\gamma M_1^2 - (\gamma - 1)\right]\left[(\gamma - 1)M_1^2 + 2\right]\right\}^{1/2}} \tag{II-15}$$

4785

It is interesting to note from (II-15) that the flow in the shock tube behind the initial shock is supersonic $(u_2 > a_2)$ if $M_1 > 2.068$ (for $\gamma = 1.4$). Also it is important to realize in using the shock tube as a wind tunnel that, no matter how strong the initial shock may be, the following flow is only slightly supersonic $(u_2/a_2 \approx 2$ in air for $M_1 = \infty)$. To use the shock tube as a hypersonic wind tunnel, modifications are required (ref. 14).

It is convenient to express u_2 in terms of the conditions ahead of the shock, thus

$$\frac{u_2}{a_1} = \frac{u_2}{a_2}\frac{a_2}{a_1} \tag{II-16}$$

and, with the aid of equations (II-9) and (II-15), this is

$$\frac{u_2}{a_1} = \frac{2(M_1^2 - 1)}{(\gamma + 1)M_1} \tag{II-17}$$

This expression for the velocity of the flow following the shock, in terms of the Mach number of the shock and the sound speed ahead of the shock, is true in general and gives the velocity of the following flow with respect to the laboratory coordinate system if the gas ahead of the shock is stationary. We will make use of this in a later section.

THE REFLECTED SHOCK WAVE

When the initial shock wave reaches the end of the tube, it is reflected (if the tube end is closed) as a shock wave which travels back up the tube and brings to rest the flow which has been accelerated

to u_2 by the initial shock wave. The condition that no fluid can pass through the closed end suggests that the velocity behind the reflected shock is zero and the statement previously made then follows. If, for convenience, we locate ourselves in a coordinate system moving with the reflected shock, we may write for M_3, the Mach number of the reflected shock:

$$M_3 = \frac{U_{rs} + u_2}{a_2} \tag{II-18}$$

4785

where U_{rs} is the speed of the reflected shock with respect to the laboratory, u_2 is the particle velocity of the flow behind the initial shock, and a_2 the sound speed of region 2. All the stationary shock relations of reference 10 are correct in this coordinate system and may be employed to relate M_3 to $M_5(= U_{rs}/a_5)$, and these will be used in subsequent discussion.

Now, in a coordinate system in which the reflected shock moves into a quiescent gas, we may write (from (II-17))

$$\frac{u_5}{a_2} = \frac{2}{\gamma + 1} \frac{(M_3^2 - 1)}{M_3} \tag{II-19}$$

where u_5 is the following flow velocity behind the reflected shock in this coordinate system. In the laboratory coordinate system we know that the flow behind the reflected shock is stationary and that the flow ahead of the reflected shock has velocity u_2. Thus, to shift the coordinate system to one in which the shock moves into a quiescent gas, we need only subtract (i.e., add in a negative direction) u_2 from the entire system. This gives us a quiescent zone ahead of the reflected shock, makes equation (II-19) valid in this system, and gives us a following velocity $u_5 = u_2$. We can then write from equation (II-19) and (II-17) that

$$u_2 = \frac{2a_1 (M_1^2 - 1)}{(\gamma + 1) M_1} = u_5 = \frac{2a_2 (M_3^2 - 1)}{(\gamma + 1) M_3} \tag{II-20}$$

Rewriting (II-20)

$$\frac{2}{\gamma + 1} \frac{(M_3^2 - 1)}{M_3} \frac{a_2}{a_1} = \frac{2}{\gamma + 1} \frac{(M_1^2 - 1)}{M_1} \tag{II-21}$$

and, using equation (II-9) for a_2/a_1, we have:

$$\frac{M_3^2 - 1}{M_3}\left\{\frac{\left[2\gamma M_1^2 - (\gamma - 1)\right]\left[(\gamma - 1)M_1^2 + 2\right]}{\left[(\gamma + 1)M_1\right]^2}\right\}^{\frac{1}{2}} = \frac{M_1^2 - 1}{M_1} \qquad \text{(II-22)}$$

Solving for M_3, we arrive finally at

$$M_3 = \left[\frac{2\gamma M_1^2 - (\gamma - 1)}{(\gamma - 1)M_1^2 + 2}\right]^{1/2} \qquad \text{(II-23)}$$

The expression (II-23) is useful in calculating the Mach number of the ideal reflected shock. It should be noted that the Mach number rises monotonically to a limiting value which depends only on γ.

$$\lim_{M_1 \to \infty} M_3 = \left(\frac{2\gamma}{\gamma - 1}\right)^{1/2} \qquad \text{(II-24)}$$

Thus

$$\lim_{M_1 \to \infty} M_3 = 2.645 \quad \text{for} \quad \gamma = 1.4$$

and

$$\lim_{M_1 \to \infty} M_3 = 2.235 \quad \text{for} \quad \gamma = 1.67$$

A very interesting relation may be obtained if we notice that the right-hand side of equation (II-23) is just the inverse of the expression for M_2 from equation (II-6). Thus we have

$$M_3 M_2 = 1 \qquad \text{(II-25)}$$

which is a very useful relation for M_3, the Mach number of the reflected shock, since M_2 is readily available in normal shock tables for given M_1.

In a form analogous to Prandtl's relation we may write (II-25) (multiplying through by a_2^2)

$$u_{3_r} u_{2_i} = a_2^2 \tag{II-26}$$

where

$$u_{3_r} = U_{rs} + u_2$$

$$u_{2_i} = U_1 - u_2$$

III - THE REFLECTED SHOCK WAVE IN A REAL SHOCK TUBE

THE LAMINAR BOUNDARY LAYER IN THE FLOW BEHIND THE INITIAL SHOCK WAVE

The flow following the initial shock wave is, of course, bounded by the walls of the tube, and therefore a boundary layer is established along the wall behind the initial shock. The flow problem to be solved is then nonstationary, viscous, and compressible and will involve heat transfer (fig. 3(a)).

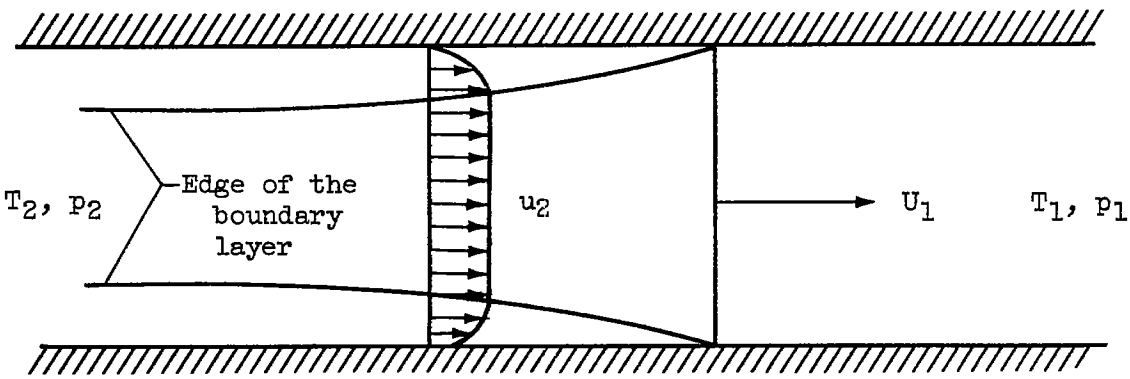

Figure 3(a).

The problem is generally handled by first transferring the entire picture to a coordinate system moving with the shock. This requires the superposition of velocity U_1 to the left in figure 3(a). In this new coordinate system the problem is steady (fig. 3(b)) and resembles the classical Blasius problem of viscous flow over a flat plate in a free stream.

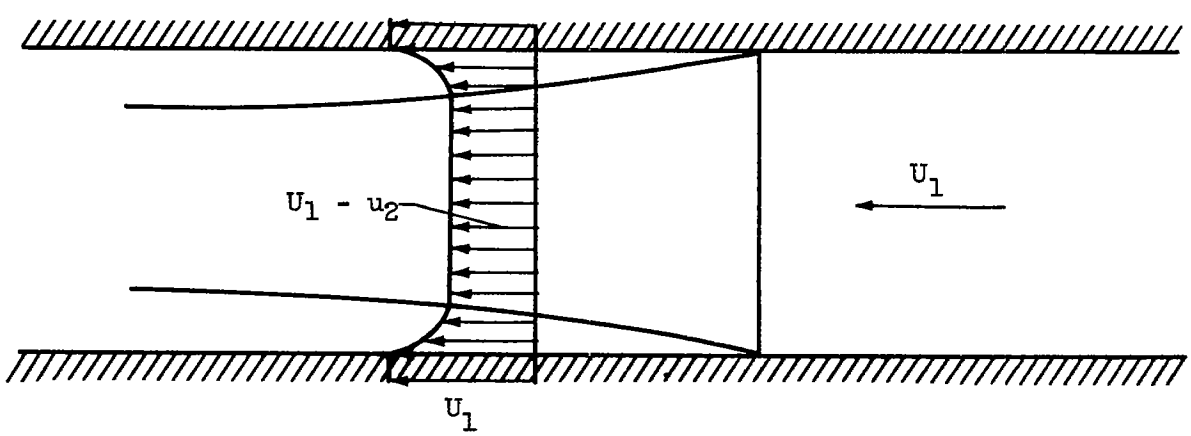

Figure 3(b).

There are, however, some important differences. First, there may be a pressure distribution along the tube. Second, the flow is compressible. Also, in this steady coordinate system, the plate itself (i.e., the wall) is moving. These differences must be considered.

In general the pressure variation along the tube is small, and so in the analysis the pressure is considered to be constant. The boundary-layer equations for the laminar compressible case may then be written:

4785

Continuity:

$$\frac{\partial(\rho u)}{\partial x} + \frac{\partial(\rho v)}{\partial y} = 0$$

Momentum:

$$u \frac{\partial u}{\partial x} + v \frac{\partial u}{\partial y} = \frac{1}{\rho} \frac{\partial}{\partial y}\left(\mu \frac{\partial u}{\partial y}\right)$$

CY-3

Energy:

$$\rho C_p \left(u \frac{\partial T}{\partial x} + v \frac{\partial T}{\partial y}\right) = \frac{\partial}{\partial y}\left(K \frac{\partial T}{\partial y}\right) + \mu\left(\frac{\partial u}{\partial y}\right)^2 \qquad \text{(III-1)}$$

where

x distance along wall behind the shock

y distance perpendicular to wall

u,v velocities in x and y directions, respectively

ρ density

C_p specific heat

K thermal conductivity

μ viscosity

T temperature

The boundary conditions are:

$$u(x, \text{wall}) = U_1 \qquad u(x, \text{mainstream}) = U_1 - u_2$$

$$v(x, \text{wall}) = 0 \qquad T(x, \text{mainstream}) = T_2$$

$$T(x, \text{wall}) = T_w$$

At this point we note that a stream function ψ exists which will satisfy the continuity relation of (III-1) if

$$\frac{\rho u}{\rho_0} = \frac{\partial\psi}{\partial y}; \frac{\rho v}{\rho_0} = -\frac{\partial\psi}{\partial x} \tag{III-3}$$

If it is assumed that the viscosity μ is proportional to the absolute temperature, it can be shown that the motion equation may be reduced to that for an incompressible case. By use of a Howarth-type transformation, we may find the relation between the independent variable for this imcompressible case Y and the physical variable y. Since there is no pressure gradient, this relation is written (see ref. 15)

4785

$$Y = \int_0^y \frac{T_w}{T}\, dy \tag{III-4}$$

or

$$Y = \int_0^y \frac{\rho}{\rho_w}\, dy \tag{III-5}$$

since pressure is constant across the boundary layer.

The equations we now have for an incompressible problem may be reduced to ordinary differential equations by use of Blasius' variable. So we write:

$$\eta = \sqrt{\frac{(U_1 - u_2)}{2x\nu_w}}\, Y; \; \psi = \sqrt{2(U_1 - u_2)x\nu_w}\, f(\eta) \tag{III-6}$$

The motion equation (III-1) becomes

$$f''' + ff'' = 0 \tag{III-7}$$

with boundary conditions

$$\left.\begin{aligned} f(0) &= 0 \\ f'(0) &= \frac{U_1}{U_1 - u_2} \\ f'(\infty) &= 1 \end{aligned}\right\} \tag{III-8}$$

This is the classical Blasius differential equation, but the problem differs from the classical problem in that the velocity at the wall is not zero (i.e., $f'(0) = U_1/U_1 - u_2$). In reference 7 this problem is solved numerically and the solution presented for the range of shock strengths; this is reproduced from reference 7 in figure 4. It should be noted that the velocity distribution in the boundary layer presented in this manner is affected only a small amount over the range of shock strengths.

4785

In reference 5 Rott and Hartunian, using the numerical solution of reference 7 with some modification, have solved the heat transfer problem. By expressing the heat transferred from the gas and into the wall in terms of the wall temperature, they are able to determine an expression for the wall temperature rise (after the shock passes by) as a fraction of the temperature rise across the shock. This is shown to be:

CY-3 back

$$\frac{\Delta T_w}{\Delta T_s} \approx \sqrt{\frac{(k\rho C_p)_{\text{gas at wall}}}{(k\rho C)_{\text{wall material}}}}$$

For air and steel walls this is $O(10^{-3})$. Thus we have the extremely important result that the wall temperature is essentially that of the original gas and tube in equilibrium before the passage of the shock. This result will be used in a later section in analyzing the behavior of the reflected shock.

ATTENUATION OF THE INITIAL SHOCK

As a result of the development of a boundary layer in the flow behind the initial shock in the real shock tube, the ideal picture of the shock propagating into the low-pressure gas must be modified. Although we might expect some change in the shock shape, this change in shape has been shown (ref. 4) to be confined to a very small portion of the shock near the wall; and actual photographs show (fig. 5) the initial shock to be not perceptibly modified from an ideal normal shock. It is found, however, that the actual speed of the shock is reduced somewhat from that calculated from equation (II-12) (fig. 6). This attenuation of the strength of the initial shock has been the subject for a number of analyses (for instance, refs. 6 and 8). For such an analysis it is usually assumed that the boundary layer is thin compared with the tube dimensions. Thus the flow is considered to be the ideal flow plus small perturbations due to the growth of the boundary layer. These perturbations are carried by waves assumed to be generated at the wall by the wall friction and heat transfer (ref. 6) and are integrated along the tube to determine the effect on the shock strength. In reference 8 these waves are assumed to be generated by vertical velocity at the edge

4785

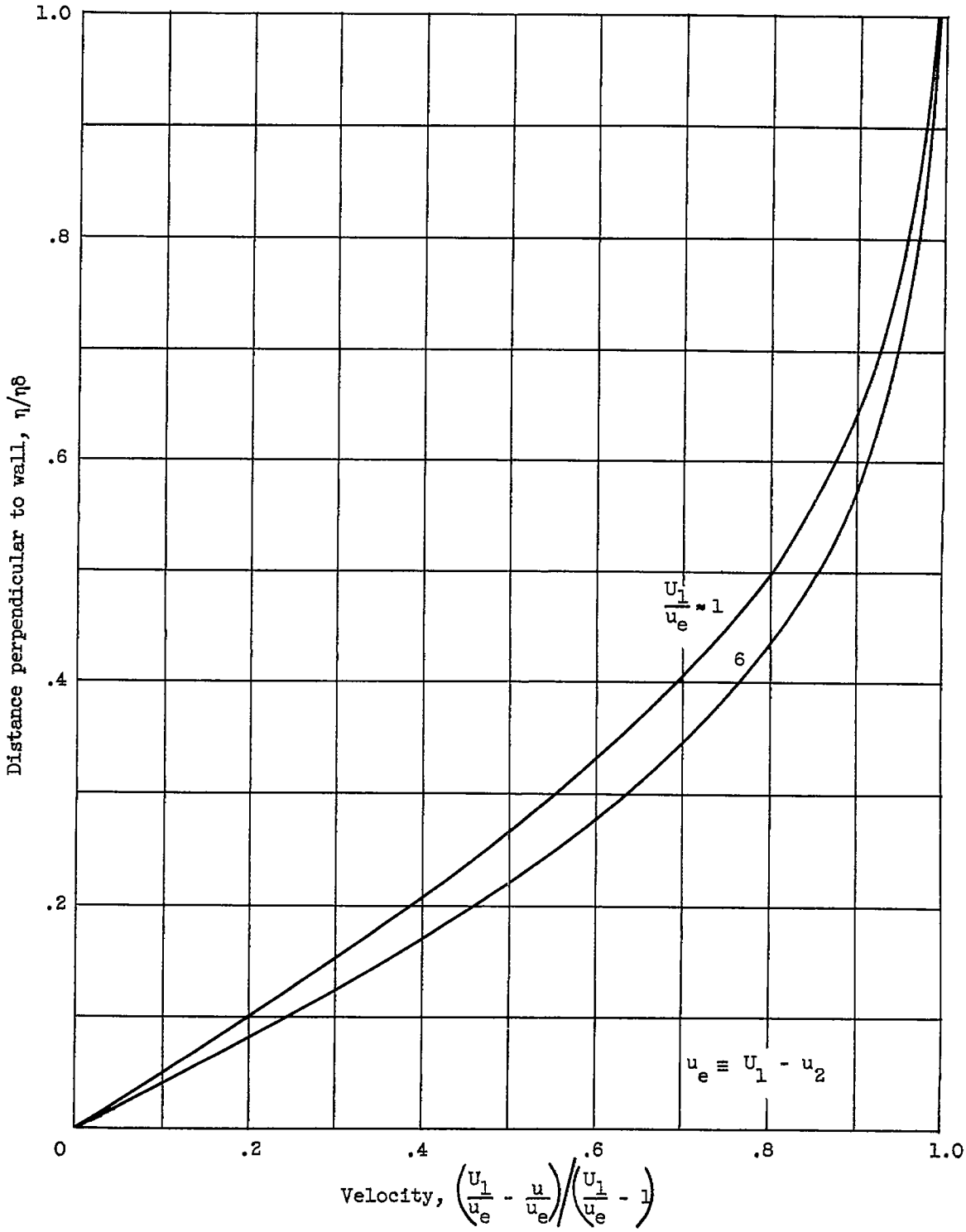

Figure 4. - Numerical solution for velocity in the boundary layer established by flow following initial shock (after ref. 7).

4785

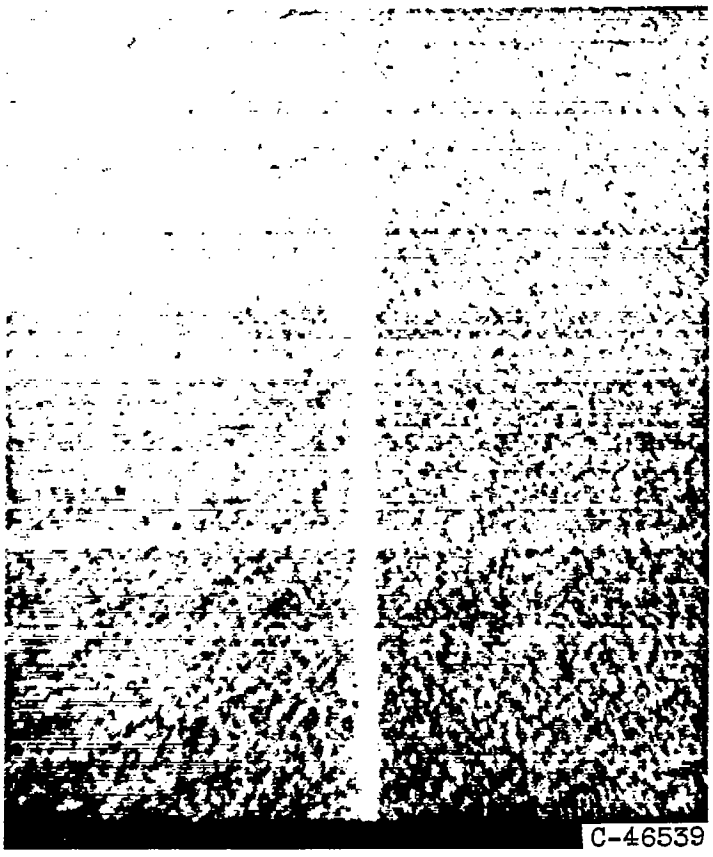

Figure 5. - Initial shock wave at $M_1 = 2.15$ and $p_1 = 1.0$ inch mercury absolute shortly before reflection.

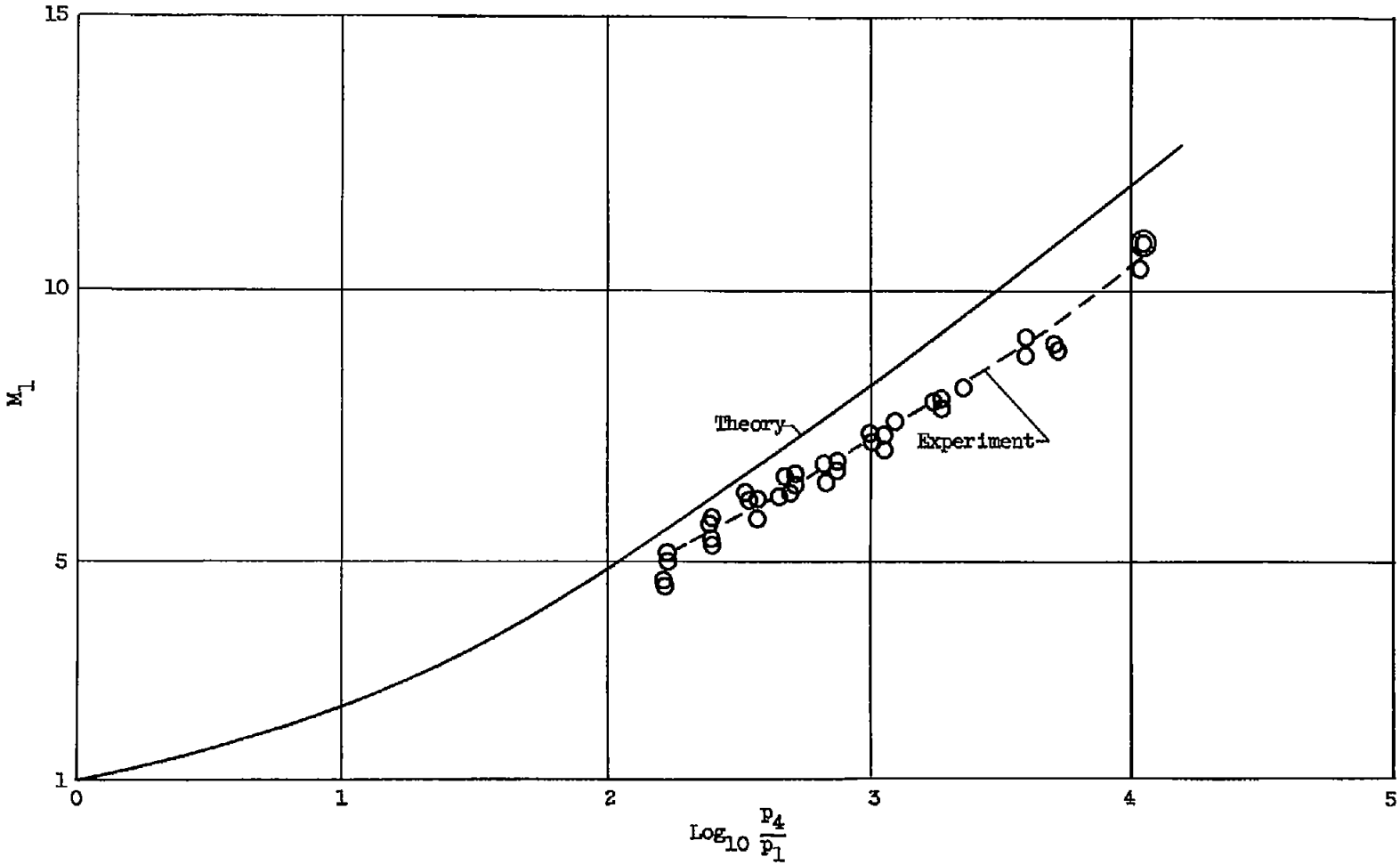

Figure 6. - Comparison of experimental values of initial shock Mach number with theoretical values of figure 2 (see ref. 16).

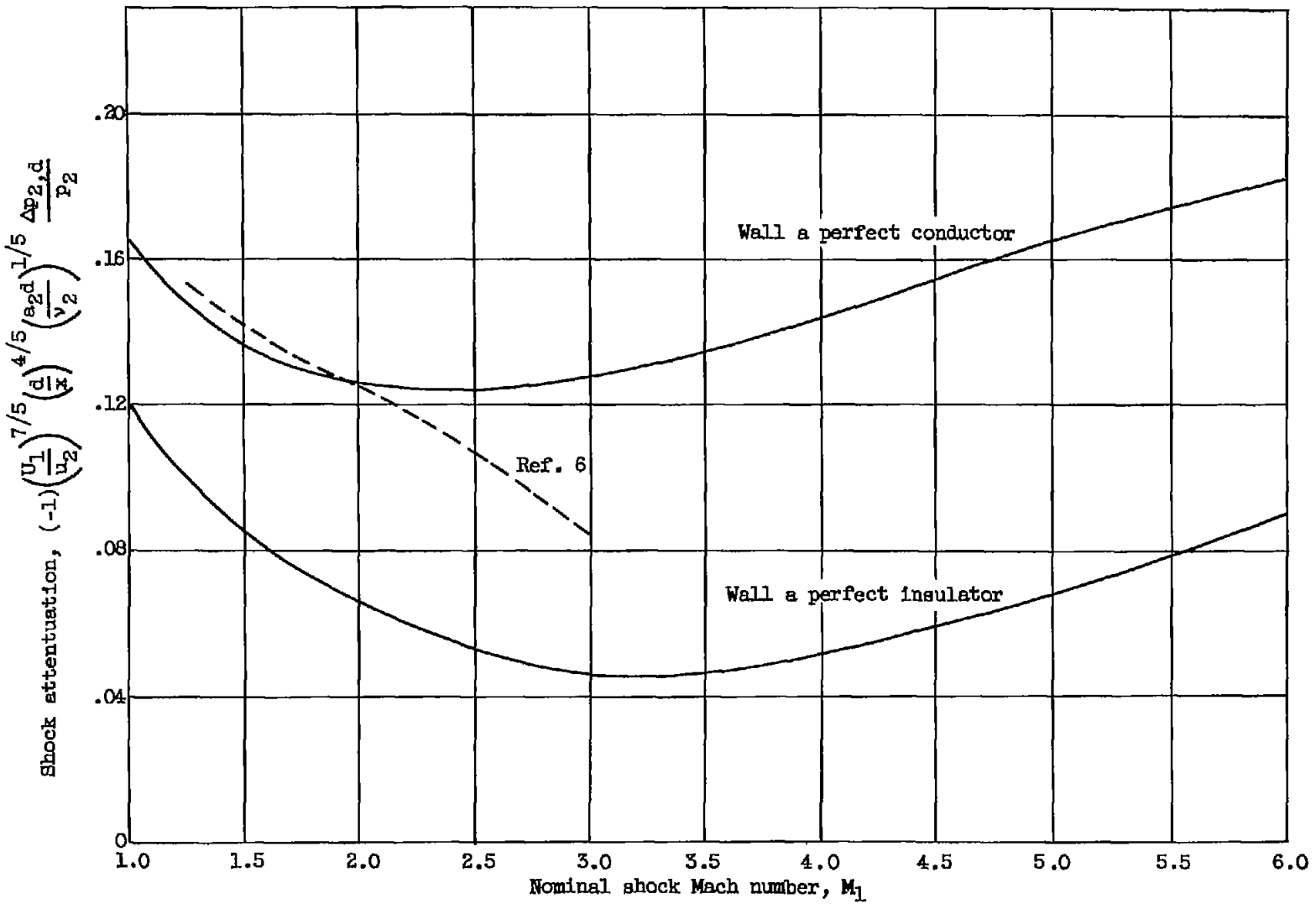

Figure 7. - Attentuation of initial shock as a function of nominal shock Mach number (ref. 8).

of the boundary layer. Both methods average the generating process at any station along the tube, and the waves thus generated are considered to be one-dimensional. Since the boundary layer generated behind the initial shock (calculated as previously discussed in the coordinate system moving with the shock) develops a negative displacement thickness in region 2, the vertical velocity at the edge of the boundary layer in region 2 is negative (away from the tube centerline) and tends to decelerate the shock. In the expansion between regions 3 and 4, the negative boundary-layer thickness is decreasing; this tends to accelerate the shock. Heat transfer to the wall tends to decelerate the shock. The net effect of all of the factors considered in references 6 and 8 is to decelerate the shock wave. The justification of the many assumptions involved in these analyses is not so much that they finally agree with each other, but rather that their results agree with experiment. In figure 7 is plotted the shock attenuation against nominal shock number (ref. 8), and these results will be used later in this report.

4785

THE INTERACTION OF THE REFLECTED SHOCK WITH THE BOUNDARY LAYER IN A REAL SHOCK TUBE

When the reflected shock leaves the closed end of the shock tube and starts to propagate back up the tube, it is confronted not only by the main flow following the initial shock, but also by the growing boundary layer developed in this flow near the walls. This boundary layer was described in THE LAMINAR-BOUNDARY LAYER IN THE FLOW BEHIND THE INITIAL SHOCK WAVE. If we examine the phenomenon in a coordinate system moving with the reflected shock, the situation encountered is represented in figure 8:

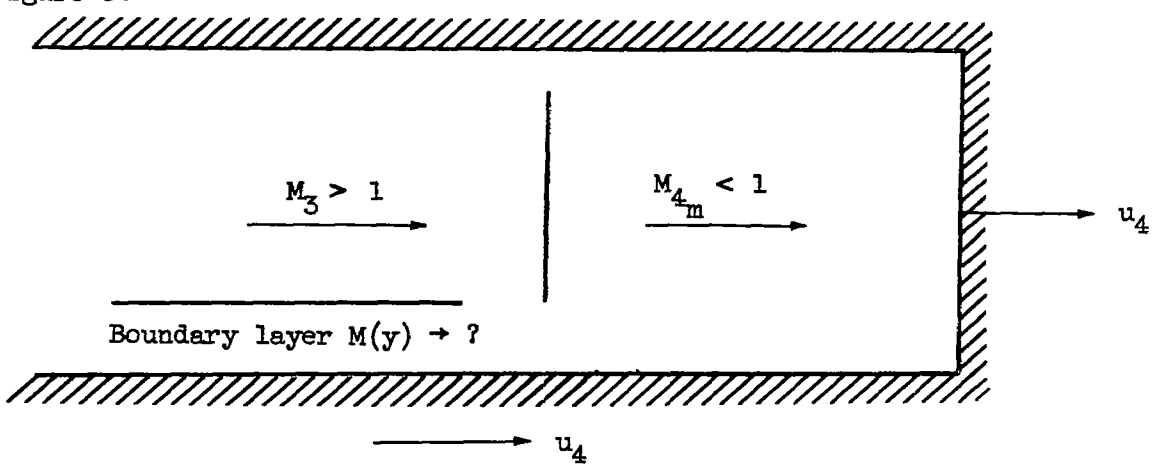

Figure 8.

To transfer the problem to this coordinate system from the laboratory system, it was necessary to add U_{rs}, the velocity of the returning shock

with respect to the laboratory, to all velocities in the laboratory system. Thus u_4, the velocity of the tube, is in this system

$$u_4 = 0 + U_{rs} = U_{rs} \tag{III-1}$$

and from (II-18):

$$M_3 = \frac{U_{rs} + u_2}{a_2}$$

4785

It was pointed out in section II that M_3 may be calculated from

$$M_3 = \left[\frac{2\gamma M_1^2 - (\gamma - 1)}{(\gamma - 1)M_1^2 + 2}\right]^{1/2} \tag{II-23}$$

or

$$M_3 M_2 = 1 \tag{II-25}$$

CI-4

The Mach number $M(y)$ in the boundary layer can also be determined (such a calculation has been made in appendix A for $M_1 = 2.24$, and a plot of $M(y)$ is shown in fig. 9); but a simplification in the picture will now be discussed. Since we want to determine what type of phenomenon can occur because of the falling off of the velocity in the boundary layer at the wall, we note that the difference between the main flow and the boundary-layer flow is greatest if we compare the main flow with a small layer of fluid near the wall. In the coordinate system of figure 8 (i.e., with the reflected shock stationary), the velocity of this small layer near the wall is u_4 (the wall velocity). The Mach number at the wall is also a minimum and is seen (fig. 9) to increase (at least for $M_{bl} < M_3$) to the mainstream value. We would expect then that whatever will occur to this small layer because of its velocity (and therefore energy) deficiency will occur subsequently, if at all, to the remainder (or a portion of the remainder) of the boundary layer. Thus, if we consider the entire boundary layer to be described by the stream tube closest to the wall, we are being conservative in looking for the effects of the energy deficiencies of the boundary layer. We are bound to find the widest limits for the regions in which phenomena resulting from boundary-layer energy deficiencies will occur. We will describe the boundary layer, then, as a jet of fluid of Mach number M_{bl} where

$$M_{bl} = \frac{u_4}{a_{\text{gas at wall temperature}}} \tag{III-2}$$

4785

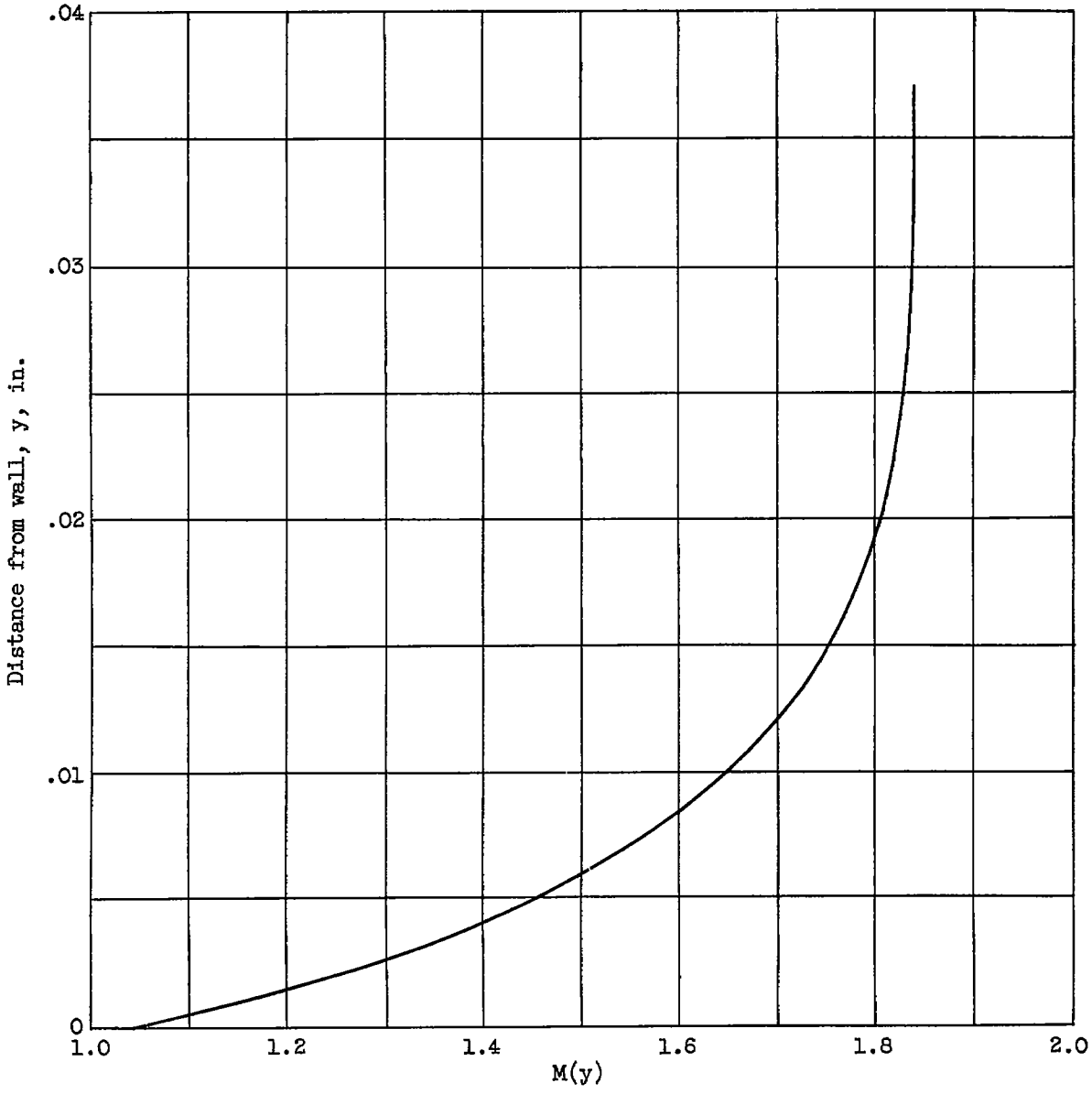

Figure 9. - Mach number distribution in boundary layer M(y) in coordinate system moving with reflected shock. $M_1^2 = 5$; $\gamma = 1.4$.

It has been noted in THE LAMINAR-BOUNDARY LAYER IN THE FLOW BEHIND THE INITIAL SHOCK WAVE that the wall temperature after the shock has passed is, to a very good approximation, the temperature of the gas and wall in equilibrium before the shock has passed, that is, $T_w \approx T_1$. Thus

$$M_{bl} = \frac{u_4}{a_1} \tag{III-3}$$

4785

To evaluate this in terms of M_1, the Mach number of the initial shock, we note that

$$M_{4_m} \equiv \frac{u_4}{a_4} \tag{III-4}$$

and from (II-6)

$$M_3 = \left[\frac{(\gamma - 1)M_{4_m}^2 + 2}{2\gamma M_{4_m}^2 - (\gamma - 1)}\right]^{1/2}$$

CY-4 back

Combining this with equation (II-23), eliminating M_3, and solving for M_{4_m}, we have

$$M_{4_m}^2 = \frac{2(\gamma - 1)M_1^2 + (3 - \gamma)}{(3\gamma - 1)M_1^2 - 2(\gamma - 1)} \tag{III-5}$$

Since we have

$$M_{bl} = \frac{u_4}{a_1} = \frac{u_4}{a_4}\frac{a_4}{a_2}\frac{a_2}{a_1}$$

we can write

$$M_{bl} = M_{4_m}\frac{a_4}{a_2}\frac{a_2}{a_1} \tag{III-6}$$

Substituting from equations (II-9), (II-23), and (III-5) into (III-6) and solving for M_{bl}, we obtain:

$$M_{bl} = \frac{2(\gamma - 1)M_1^2 + (3 - \gamma)}{(\gamma + 1)M_1} \tag{III-7}$$

We note then that $M_{bl} \neq M_3$ and is a function only of M_1 and γ. Presented in figure 10 is a plot of M_{bl} against M_1 for $\gamma = 1.4$ and 1.67. Also included in this figure are the curves for M_3, the reflected shock Mach number for $\gamma = 1.4$ and 1.67. Note that as M_1 takes large values and M_3 approaches an asymptotic value, M_{bl} approaches an asymptotic positive slope.

4785

$$\frac{dM_{bl}}{dM_1} = \frac{2(\gamma - 1)M_1^2 - (3 - \gamma)}{(\gamma + 1)M_1^2} \tag{III-8}$$

$$\lim_{M_1 \to \infty} \frac{dM_{bl}}{dM_1} = 2\left(\frac{\gamma - 1}{\gamma + 1}\right) \tag{III-9}$$

This limit is 1/3 for $\gamma = 1.4$, and 1/2 for $\gamma = 1.67$. It is apparent that the value of M_{bl}, which is originally lower than M_3, will eventually overtake and exceed M_3 and thus at this point (say M_1^*) divides the Mach number range into two regions. Below M_1^* the value of M_{bl} is always less than M_3. This is not surprising, as the fluid in the boundary layer is deficient in velocity, and such a situation is to be expected. However, because of the cooling effect of the wall, the Mach number of the fluid in the boundary layer (M_{bl}) rises as described and, at values of $M_1 > M_1^*$, exceeds M_3. It seems clear that the interaction phenomenon in the region where $M_{bl} < M_3$ may not even resemble the phenomenon encountered when $M_{bl} > M_3$. Certainly a more intricate interaction is to be expected in the former region ($M_1 < M_1^*$). Further investigation of these differences is indicated, and an argument suggested by Hess (ref. 17) for the interaction of shock waves with thermal boundary layers is extended for this purpose later in this section.

Since the asymptotic values for M_3 increase for decreasing γ and the asymptotic slopes of the curves for M_{bl} decrease with decreasing γ, the value of M_1 at which M_{bl} overtakes M_3 increases rapidly as γ falls. If we write

$$M_{bl} \approx 2\left(\frac{\gamma - 1}{\gamma + 1}\right) M_1 \tag{III-10}$$

4785

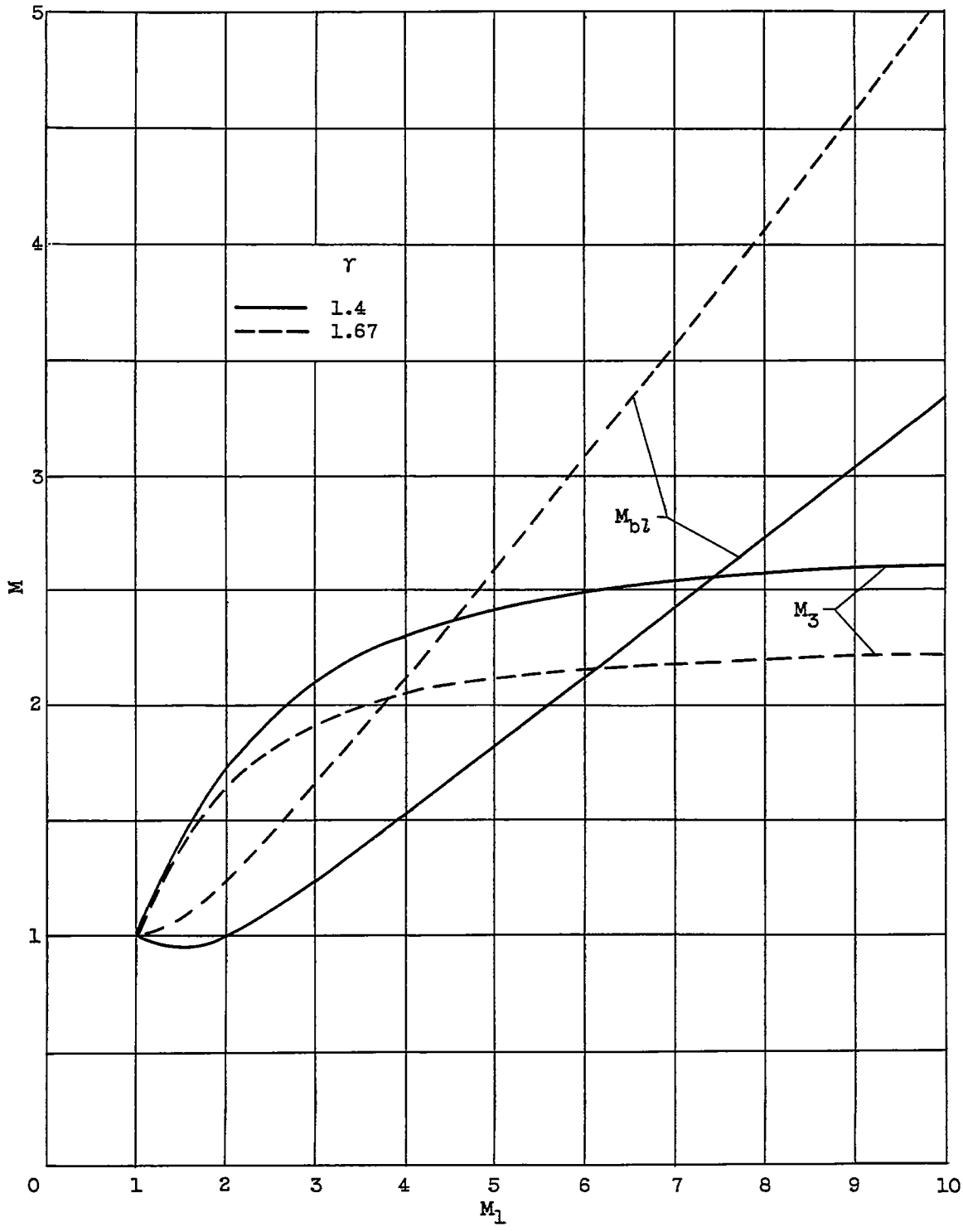

Figure 10. - Mach number of the main stream M_3 and Mach number of the boundary layer M_{bl}, as defined in coordinate system moving with reflected shock wave.

and from equation (II-24) we have

$$\lim_{M_1 \to \infty} M_3 = \left(\frac{2\gamma}{\gamma - 1}\right)^{1/2}$$

we find the crossover Mach number M_1^* may be written approximately as

$$M_1^* \approx \left(\frac{2\gamma}{\gamma - 1}\right)^{1/2} \left[\frac{\gamma + 1}{2(\gamma - 1)}\right] \tag{III-11}$$

and thus as γ falls, approaching the value 1, we find that

$$M_1^* \approx \sqrt{2}\ (\gamma - 1)^{-3/2} \tag{III-12}$$

Equation (III-12) indicates the rapid increase in the crossover Mach number with falling γ. This is an important effect and will be referred to in a later section.

It should be noted that for $\gamma = 1.4$, M_{bl} is at first (for low values of M_1) subsonic, and does not become supersonic until $M_1 = 2.0$. It is clear that M_{bl} will be subsonic at first for all gases except monatomic gases since (from (III-8) or by weak shock approximation) (see appendix B)

$$\left.\frac{dM_{bl}}{dM_1}\right]_{M_1=1} = \frac{3\gamma - 5}{\gamma + 1} \tag{III-13}$$

We now have two adjacent streams (the main stream at M_3, and the boundary layer at $M_{bl} \neq M_3$) about to interact with the reflected shock. The reflected shock is stationary in this coordinate system and the situation is as in figure 11.

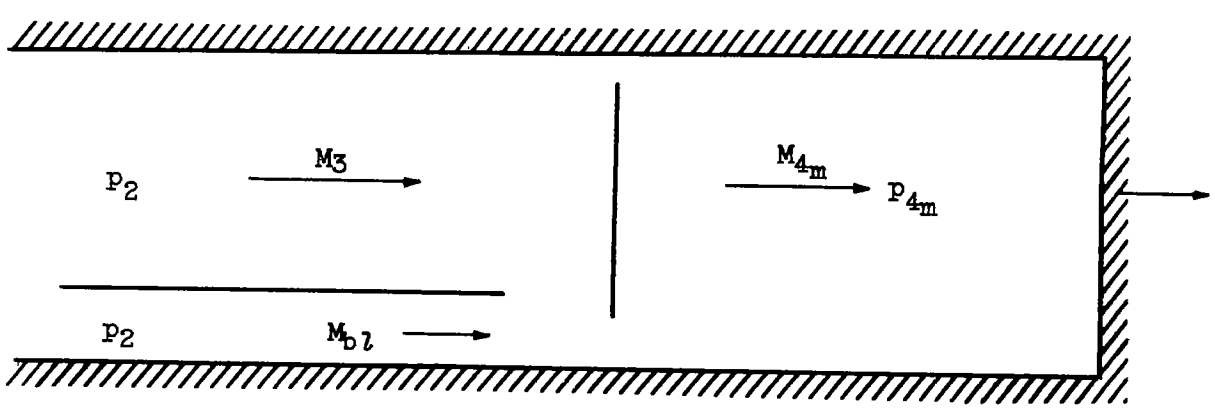

Figure 11.

The pressure in the main stream p_{4_m} behind a stationary, undisturbed shock wave may be immediately calculated from Rankine-Hugoniot relations (eq. (II-7)).

$$\frac{p_{4_m}}{p_2} = \frac{2\gamma}{\gamma + 1} M_3^2 - \frac{\gamma - 1}{\gamma + 1} \tag{III-14}$$

Since M_3 is a function of M_1 and γ, this pressure ratio may be plotted against M_1 and is so plotted in figure 12 for various values of γ. The question now arises: Is it at all possible for the lower energy fluid at M_{bl} to maneuver this pressure rise and enter the region behind the shock where the pressure is now p_{4_m}. To find the limit of this possibility, we examine the stagnation pressure of the fluid at M_{bl}.

$$\frac{p_{stag_{bl}}}{p_2} = \left(1 + \frac{\gamma - 1}{2} M_{bl}^2\right)^{\frac{\gamma}{\gamma-1}} \tag{III-15}$$

for $M_{bl} < 1$.

This, too, is shown in figure 12 plotted against M_1. At $M_1 = 1$, $p_{stag_{bl}}$ is greater than p_{4_m} but, as M_1 is increased, p_{4_m} rises rapidly in this range and soon exceeds $p_{stag_{bl}}$. This occurs when

$$\frac{p_{4_m}}{p_2} = \frac{2\gamma}{\gamma + 1}\left[\frac{2\gamma M_1^2 - (\gamma - 1)}{(\gamma - 1)M_1^2 + 2}\right] - \left(\frac{\gamma - 1}{\gamma + 1}\right) = \frac{p_{stag_{bl}}}{p_2} =$$

$$\left\{1 + \frac{\gamma - 1}{2}\left[\frac{2(\gamma - 1)M_1^2 + (3 - \gamma)}{(\gamma + 1)M_1}\right]^2\right\}^{\frac{\gamma}{\gamma-1}} \tag{III-16}$$

At this point (the first pressure crossover) $M_1 = 1.33$ for $\gamma = 1.4$, and $M_1 = 1.57$ for $\gamma = 1.67$. As we continue to higher values of M_1 (we assume that the boundary-layer compression is preceded by a shock when $M_{bl} > 1$), p_{4_m} exceeds $p_{stag_{bl}}$ until we arrive at the second

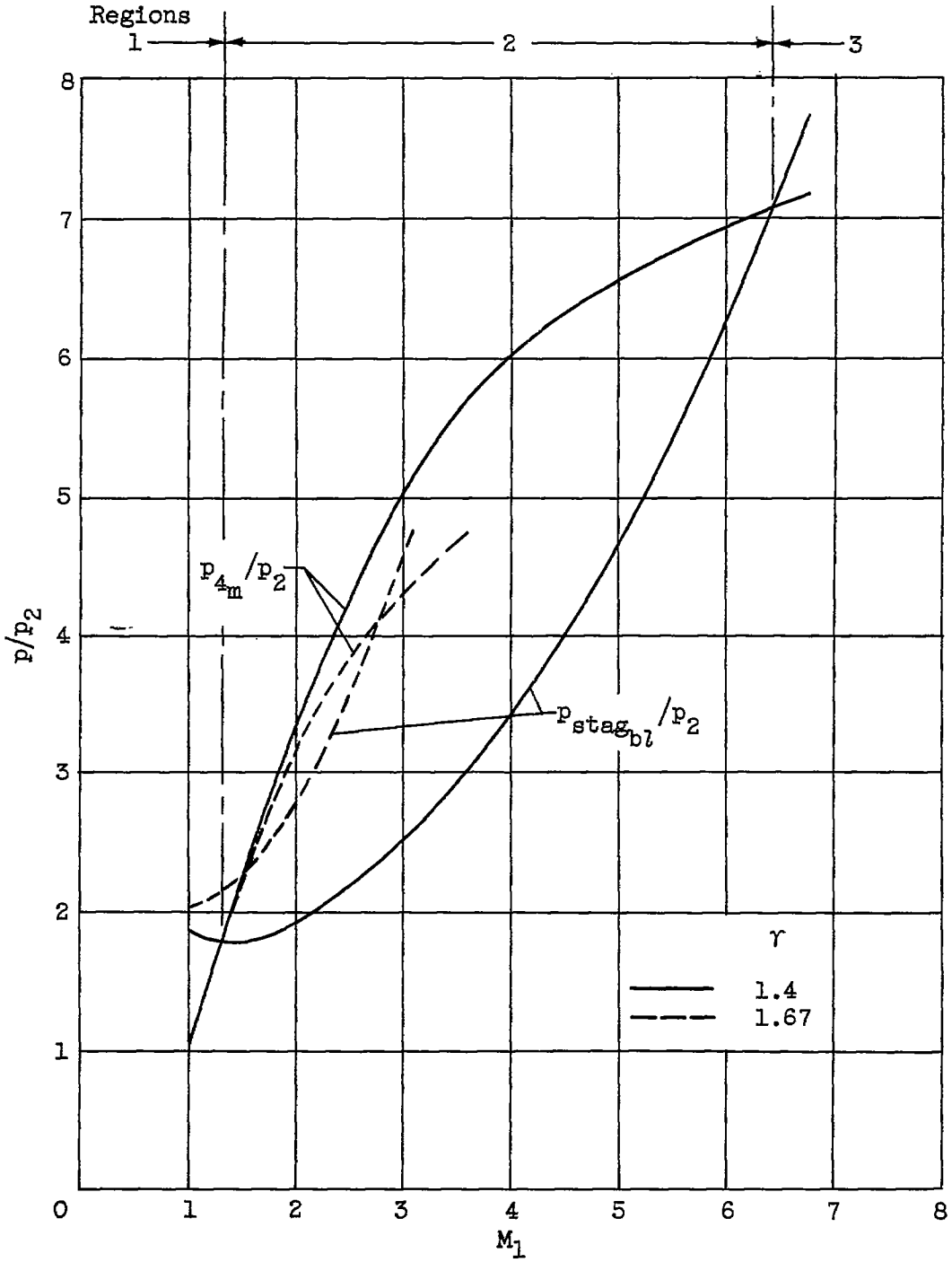

Figure 12. - Pressure ratio across normal shock at M_3 and pressure-rise ratio in boundary layer described by M_{bl}, both plotted against M_1.

4785

pressure crossover. At this point $p_{stag_{bl}}$ overtakes p_{4_m} and exceeds the pressure behind the undisturbed shock for all higher values of M_1. This occurs when

$$\frac{2\gamma}{\gamma + 1}\left[\frac{2\gamma M_1^2 - (\gamma - 1)}{(\gamma - 1)M_1^2 + 2}\right] - \left(\frac{\gamma - 1}{\gamma + 1}\right) = \frac{\left\{\frac{\gamma + 1}{2}\left[\frac{2(\gamma - 1)M_1^2 + (3 - \gamma)}{(\gamma + 1)M_1}\right]^2\right\}^{\frac{\gamma}{\gamma-1}}}{\left\{\frac{2\gamma}{\gamma + 1}\left[\frac{2(\gamma - 1)M_1^2 + (3 - \gamma)}{(\gamma + 1)M_1}\right]^2 - \left(\frac{\gamma - 1}{\gamma + 1}\right)\right\}^{\frac{1}{\gamma-1}}} \qquad \text{(III-17)}$$

4785

At this point (the second pressure crossover) we find that $M_1 = 6.45$ for $\gamma = 1.4$, and $M_1 = 2.8$ for $\gamma = 1.67$. These curves are shown in figure 12. We note that the two crossover points divide the Mach number range into three regions, which we have called regions 1, 2, and 3 on the figure. In regions 1 and 3 the stagnation pressure of the boundary layer exceeds the pressure behind the undisturbed shock. Thus we can expect the boundary layer to pass continuously under the foot of the shock and into the region behind reflection. Although the boundary layer is actually growing in thickness ($\propto \sqrt{\nu t}$), this growth is slow and will not essentially change the picture in this region. We are suggesting therefore that, at least in considering the problem of outlining the regions for the different interaction possibilities, we will disregard this growth. In region 2 in figure 12 we are confronted with an entirely different situation from that in regions 1 and 3. The stagnation pressure of the energy-deficient fluid in the boundary layer is exceeded throughout this region by the pressure behind the undisturbed shock. Recall that the width of this region on the Mach number plot was calculated by taking a conservative view of the boundary layer, and this would give the widest range for its occurrence. Whether or not this is quantitatively pessimistic (assuming that whatever occurs is undesirable) might be questioned, but this does not concern us now. We are concerned right now only with the fact that such a region exists, that it has upper and lower limits for its appearance, and with the question of what might occur when the boundary layer, by compressing even to stagnation pressure, cannot match the pressure in the region behind the reflected shock. At this point we can only say we would not expect a steady through flow of this energy-deficient boundary-layer fluid into the region behind the undisturbed shock. Rather we would expect a gathering up of this fluid in a region adjacent to the foot of the shock. Qualitatively we can imagine a quasi-steady picture of a ball of fluid, sitting next to the

CY-5

foot of the shock and unable to pass into the higher pressure region behind the shock, growing in some manner with time. For the details of the interaction picture, that is, the effect of this growing ball on the main flow, on the shock itself, and on the flow in the region behind the shock, it was necessary to resort to experiments. Fortunately the experiments which were made added enough information to allow a model for the phenomenon to be projected, and the analysis could then continue ultimately to a complete picture of this interaction phenomenon. We will proceed now to a description of the experiments and will pick up this discussion after some of the results of the experiments have been presented.

4785

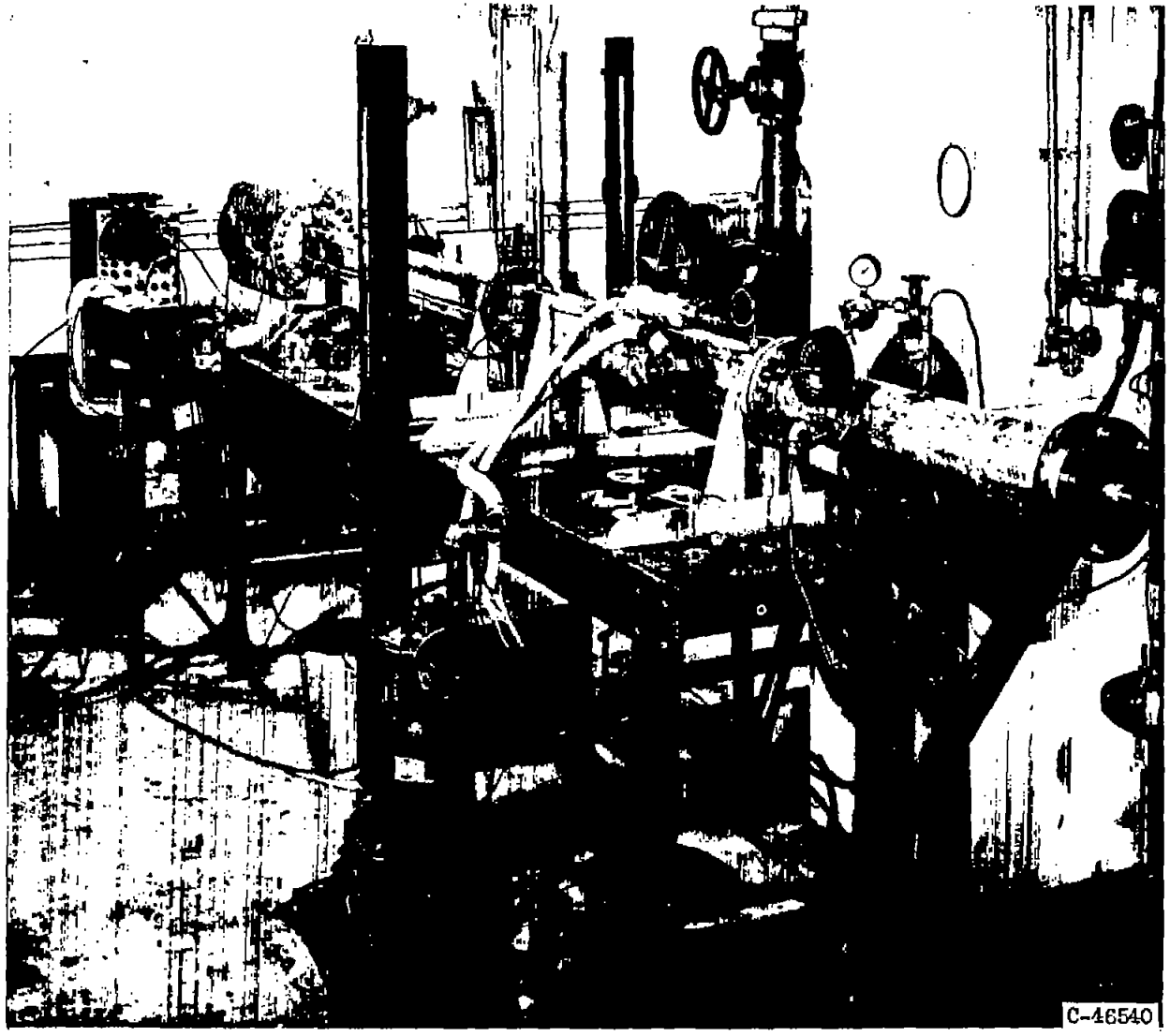

Figure 13. - The 2- by 4-inch shock tube.

IV - EXPERIMENTAL DETERMINATIONS

DESCRIPTION OF THE EXPERIMENTAL SETUP AND EQUIPMENT

The Shock Tube

The shock tube (fig. 13) consisted of a five-inch-diameter circular heavy-walled steel pipe 33 inches long, connected at the diaphragm section to a rectangular welded-steel wall tube, 2 by 4 inches in cross section and 142 inches long. The shorter high-pressure circular tube had an internal transition section which brought the cross section from circular to rectangular at the diaphragm station. At this station the two sections were held together by 1-inch-thick flanges between which the celluloid diaphragm was pressed. Seal was effected by O-rings of slightly different diameters, one on each side of the diaphragm, and the flanges were held together by six 3/4-inch bolts. Diaphragms of commercial cellulose acetate sheet were employed and, depending on the pressure in the high-pressure chamber (which was varied from slightly below atmospheric to 60 lb/sq in. gage), diaphragm thicknesses of 0.005 to 0.025 inch were used. A brass lance was mounted in the high-pressure section and was fitted with a 3-sided steel arrow-barb for puncturing the diaphragm. The use of an arrowhead reduced considerably the criticalness of diaphragm thickness for proper puncture characteristics. Fastened at the end of the longer low-pressure chamber was the test section. It consisted of two 2-inch-square aluminum blocks 24 inches long squeezed between 1-inch-thick glass plates which were themselves squeezed by an outer-support casting (fig. 14). Seal was obtained between glass and

4785

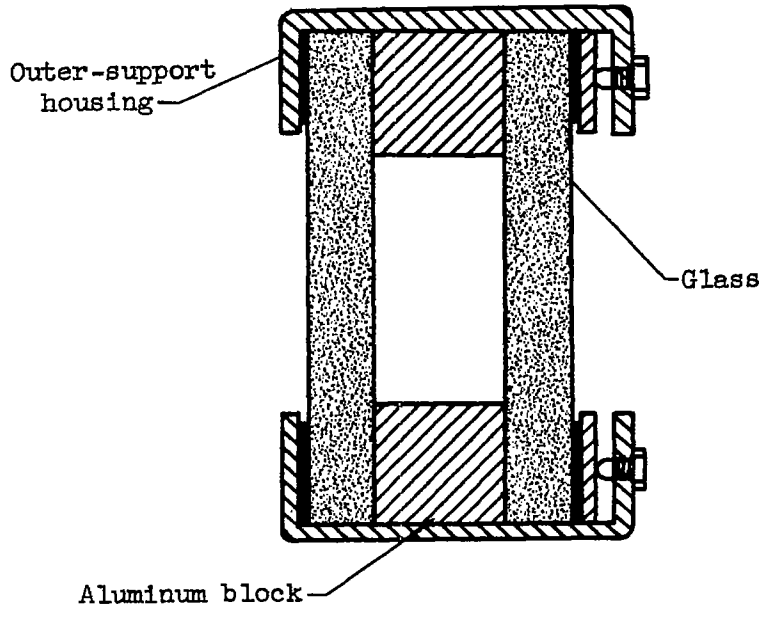

Figure 14. - Cross-sectional view through test section.

aluminum by use of a special glass to aluminum cement (Hy-Sol Company, Olean, N.Y.) of the epoxy-resin variety. The test section was sealed at one end to the steel tube by squeezing between the flanges of the outer-support housing and the steel tube flanges, a gasket-like strip of lucite in which O-ring channels had been cut. An end plate was sealed to the test section in a similar manner. The test section was 24 inches long and through the glass a length of 15 inches of the flow passage was made visible from upper to lower wall. The problem of sealing all of these surfaces was a formidable one, but with a Kinney vacuum pump
4785 it was possible to evacuate the low-pressure chamber and test section to pressures of 0.08 inch mercury absolute in about 15 minutes. The high-pressure section was of course fitted to be supplied with air from the laboratory air supply, or could be supplied alternately from helium or hydrogen tanks. The pressure in the high-pressure chamber was read on a 4-inch-face 30-inch - 100-pound-per-square-inch Lonergan vacuum-pressure gage. Mounted on the low-pressure section was a small tank 2 inches in diameter and 6 inches long which could be filled with gas from a supply tank, and whose contents could be measured and then dumped into the low-pressure chamber. The pressure in the low-pressure chamber was measured on a 60-inch mercury manometer which could be read to 0.01 of an inch. The entire shock tube was mounted on a rollable table so that it could be moved into proper alinement with the schlieren system.

The Spark Schlieren System and Photographic Techniques

The schlieren system used was the double mirror system and is discussed in detail in reference 18. In this system light passes from a source to a concave mirror and then through the test section. If the light source is located at the focus of the mirror, the light reflected from this mirror will be a parallel beam of rays as it passes through the test section. After traversing the test section, this light is brought to another concave mirror (preferably of the same focal length as the first) and is again brought to focus. Introduction of a knife edge at this second focus will permit schlieren photographs to be made when the light passing the knife edge is allowed to fall on a photographic plate. In the actual system used, Porro-Abbé prisms were located at the two foci; one to bring the light from the primary source to the first mirror, and the second to bring the light from the second mirror to the lens of the plate-holder. The mirrors were 4 feet in focal length and 12 inches in diameter. The pictures were made on 4 by 5 inch Royal Pan Film (ASA-200; this could be increased to 800 by overdeveloping). Since it was necessary to stop shock waves moving at thousands of feet per second, the light source for this schlieren system had to be of very short duration (≈ 1 μsecond). No such light system was available commercially, and so one had to be built. The requirements of such a system, then, dictated that it be capable of producing a very short time duration flash, sufficiently bright to expose the film satisfactorily.

In discharging a condenser through a gap to produce a spark, we may be guided by the theoretical solution for the behavior of such a circuit in choosing the components and the operating values. For an LRC circuit (i.e., discharging a condenser through an inductance and a resistor), we know that

$$Q = Q_0 e^{-\frac{Rt}{2L}} \left(\cos qt + \frac{R}{2Lq} \sin qt\right) \qquad \text{(IV-1)}$$

where Q is the charge, R the resistance, L the inductance, C the capacitance, t the time, and $q = \sqrt{\frac{1}{LC} - \frac{R^2}{4L^2}}$.

4785

Thus for a spark of short duration it is desirable to have very small inductance (R is essentially the resistance of the gap). For a high intensity spark we need as high an initial charge as possible (Q_0). This latter suggests high voltage as well as high capacitance. The compromise then (once the voltage has been fixed) is between decreasing the capacitance to obtain small inductance and increasing the capacitance to obtain good storage value, at the expense of increasing the inductance, which will increase with the physical size of the condenser and thus increase the decay time. The smallest possible condenser which could operate at 10,000 volts was chosen. It had capacitance $C = 0.5$ μfd and estimated inductance of $L = 0.1$ μH. The resistance of the gap was also estimated at 1 ohm. This gave the hope of a decay time (to $1/e$ the value of initial charge) of

$$t = \frac{2L}{R} = \frac{2 \times 10^{-7}}{1} \text{ seconds}$$

with an initial charge of

$$Q_0 = CV_0 = 0.5 \times 10{,}000 \times 10^{-6} = 5000 \ \mu\text{coulombs}$$

If 2000 μcoulombs flow for one μsecond, the wattage in the spark will be roughly 10^7 watts. Thus the above values for C and V_0 deemed sufficient to produce satisfactory exposures on Royal Pan film. In the actual experiment this spark light source not only exposed the film very satisfactorily but stopped very clearly the reflected shock phenomena. Even the faster initial shocks could be stopped satisfactorily (up to $M_1 = 4$). The actual spark electrodes were made of brass rod 7/8 inch in diameter, hollowed out to leave 1/8-inch wall, and tapered 60° down to the spark gap (fig. 15). A 1/8-inch hole was drilled through the sparking point of each electrode so that, looking down through the hollow electrode, the spark could be seen filling the 1/8-inch hole whenever the discharge was triggered. This spot of light could then be focused by a small lens on a rectangular slot mounted on the Porro-Abbé prism at the focus of the first concave mirror, the rectangular slot thus acting as a secondary

light source for the schlieren system. The whole system operated with amazing consistency, but the problem of triggering the spark at the proper moment had yet to be resolved.

4785

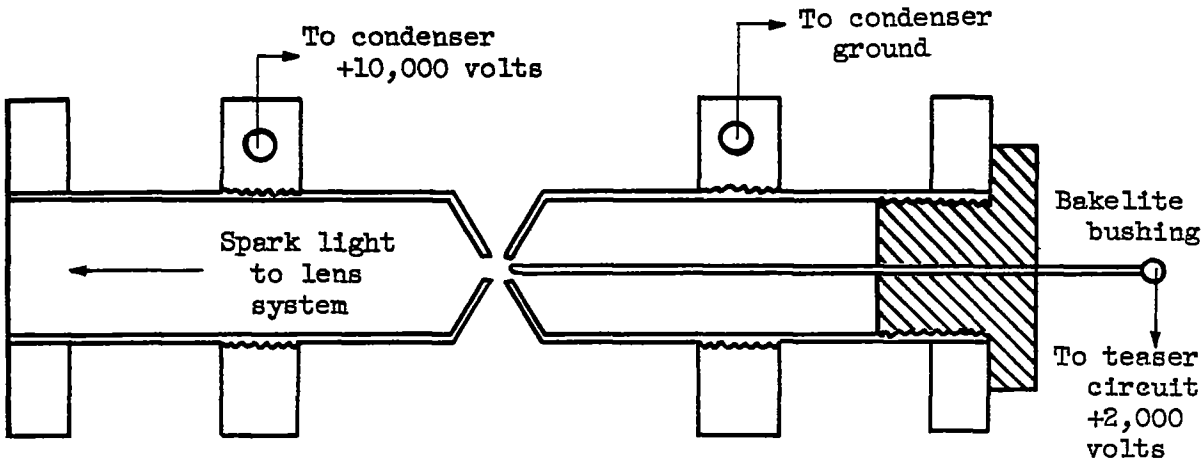

Figure 15. - Spark assembly.

The Spark-Triggering System

The primary requirement of the spark-triggering system was to cause the condenser (which was maintained at 10,000 volts) to discharge through the spark gap, and provide a light source for schlieren photography at precisely the moment of interest. In the design of this system a great deal of time was spent devising a satisfactory pickup or signal generator, that is, a transducer of some sort to convert a signal from the shock into an electrical impulse to signal the spark-trigger system. Several types of pickups were tried but proved unsuccessful for various reasons. At first an attempt was made to design a very fast-acting mechanical switch, located in the wall of the low-pressure chamber, which would close rapidly when confronted suddenly by the increased pressure behind the shock wave. Although the diaphragm was made of the thinnest available rubber sheet that would stand up, and the switch itself was made of aluminum foil (0.005 in.), this switch required 2 to 4 milliseconds to close at the operating pressure ratios. This was generally above the minimum intrinsic time delay allowable but was not the most serious difficulty with this method. It was necessary to be able to photograph within 100 microseconds for proper observation of the interesting phenomena. This required an almost constant time delay, whatever the time delay might be. In the case of the mechanical pressure switch the delay was sometimes acceptable but varied as much as 1000 to 2000 microseconds, and was thus unsuitable for our program. Next a hot-wire signal generator was built and tested. This consisted of a heated coil (actually a "glow" ignition plug) which would be cooled by the flow behind the shock wave and, because of changing resistance with cooling, generate a signal in a series resistance. This method was actually

satisfactory and gave dependable and accurate trigger signals. It had to be discontinued, however, since the type of hot-wire used would only last for two or three firings of the shock tube. Pieces of diaphragm hurtling down the tube would strike the hot wire and break it, and it thus required constant replacement. The pickup finally adopted consisted of a piezoelectric crystal encased in a metal bellows and mounted in the wall of the shock tube. When the diaphragm was punctured, the "sound" of the explosion of the diaphragm would travel down the steel wall of the shock tube itself and energize the crystal mounted in the wall. This sytem worked very well and very consistently. The only difficulty involved was the low strength of the signal (2 millivolts). This was easily handled by amplifying the signal 200 times to bring it to a useful value. 4785

The Tektronix oscilloscope model 512 could be triggered to sweep by a signal of approximately a half-volt, and could be adjusted to emit a 50-volt signal at any time (up to 1 sec in 10 μsec intervals) after the start of a sweep. This 50-volt signal was then sent to the trigger teaser (fig. 16). In the trigger teaser a 1 μfd condenser charged to ≈2000 volts was immediately discharged upon receipt of a signal through a secondary spark gap of about 0.001 inch located within the volume of the main spark gap. The discharge through this teaser spark precipitated the discharge of the main spark and thus exposed the plate at the proper instant.

This entire system, once adjusted, operated with good dependability and essentially reduced the problem of making exposures at the proper time to adjusting the time delay at the oscilloscope. Although theoretical values for the time delay (calculated from theoretical speed of the shock) were a great aid in determining the proper time delay, the last adjustment for exact location had always to be made empirically. Once, however, the time delay was determined for a given Mach number (in a given gas), adjustment of the entire system was seldom necessary.

Description of Experimental Methods

Many of the experiments were made with air as the medium for the shock-wave travel. In this case the low-pressure chamber was evacuated to the proper pressure while the high-pressure side was filled with driver gas to the required pressure. The time delay for the spark discharge was set on the Tektronix oscilloscope from calibration tests previously made, and the schlieren system was adjusted previously with the aid of a bright constant-point light source substituted for the spark. The main and teaser condensers were already charged to 10,000 and 2,000 volts, respectively, with gaps adjusted, so that at these voltages the entire system was just on the verge of firing and would discharge immediately on signal. The room was then darkened and the

4785

CY-8

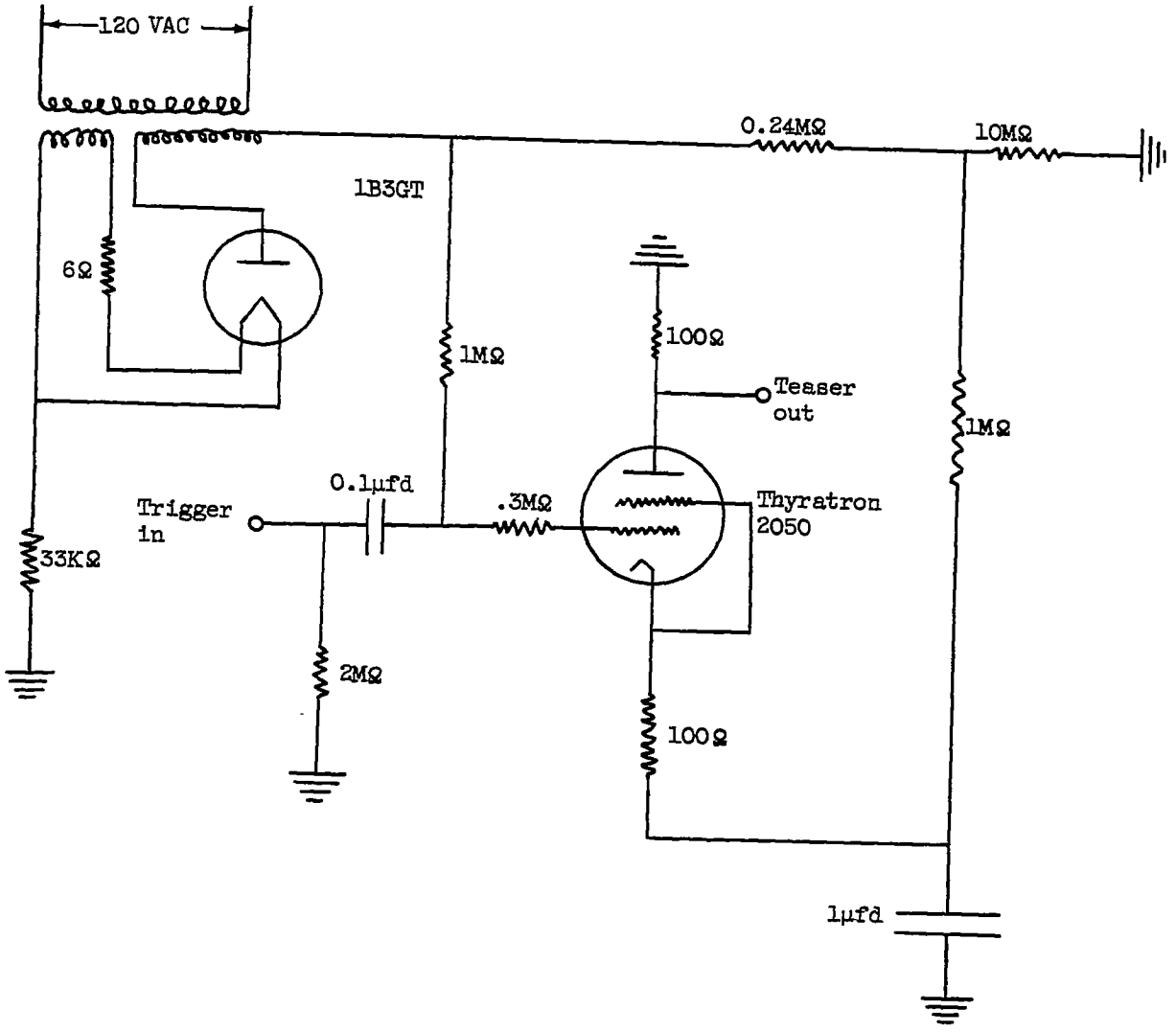

Figure 16. - Trigger teaser diagram.

camera opened. With the lance driven home, the diaphragm would burst, and this was sufficient signal to the pickup in the shock tube wall to start the train of events ending a few thousand microseconds later with the discharge of the main spark and exposure of the film at the exact instant of interest. Great care had to be taken to shield the entire electrical system so that no stray signal would trigger the spark and expose the film before the firing of the shock tube. With sufficient shielding, however, the entire system was quite dependable and gave usable results without extraordinary difficulties. When using hydrogen as a driver gas (with air in the low-pressure chamber) an explosion would usually occur when the contact surface (hydrogen) would hit the heated air behind the reflected shock. This occurred, however, after the instant of interest and did not affect the photograph already made, as the light from the flash of the explosion was not focused on the plate. After every run the tube was opened at both ends, cleaned, flushed with air, and then reassembled in preparation for the following run.

4785

When argon (or any gas other than air) was to be the medium for shock travel, the system of operation had to be modified. In this case the low-pressure chamber was evacuated as before, and the high-pressure chamber filled with driver gas to the required pressure. Then with the time delay, trigger, spark, and schlieren readied as before, the small tank located on the low-pressure chamber was filled to a certain pressure with argon. The small tank pressure required was determined previously, and was of such a value that when the argon contained in the small tank was emptied into the low-pressure chamber of the shock tube, the final pressure of argon in the low-pressure chamber was the desired value (the value which gave the correct diaphragm pressure ratio for the required Mach number of the test). These machinations were necessary because the low-pressure side of the shock tube could not be perfectly sealed; and, without a perfect seal, air could leak into the chamber under vacuum. When air was the shock-travel medium, no contamination was involved. However, when any other gas was used, air leaking in would dilute the gas and invalidate the results. Although the air leak was very slow, it was deemed necessary to resort to the method described to give the leak the minimum time to contaminate the gas in the low-pressure side. Thus, with the low-pressure chamber evacuated to as low a pressure as possible, the argon in the small tank was emptied into the shock tube, and a few seconds later the shock tube was fired. This system required great care in setting because any deviation in small tank pressure would give a deviation in the low-pressure chamber value. This would modify the diaphragm pressure ratio and change the Mach number and, therefore, the speed of the shock wave. With everything preset for timing, it was easy to miss the shock entirely in the photographs. However, given proper attention, the system operated satisfactorily (i.e., within the normal laboratory patience), and many clarifying photographs were made using argon and other gases as the shock wave medium.

4785

CY-6 back

DISCUSSION OF EXPERIMENTAL RESULTS AND THE PROPOSED MODEL FOR INTERACTION IN REGION 2 (fig. 12)

Variation of Shock Mach Number

The first series of tests was made in an attempt to verify the calculation and assumptions of section III. Recall that the analysis of section III predicted the existence of three regions of shock - boundary-layer interaction which would depend on the initial shock Mach number. Values of the Mach number at the boundaries of these interaction regions were also predicted, and were shown to depend on the ratio of specific heats γ for the gas in which the shock traveled. In the first series of tests, then, schlieren photographs were made of the interaction phenomena to verify the existence of the three regions and also, if these regions did exist, to ascertain whether the analysis would properly predict the Mach number boundaries for these regions. Since the analysis suggested something unusual would occur in region 2 (which up to this point could only be guessed), it could be expected that such a series of photographs would also show the nature of the phenomenon in this region. Once this would be determined, perhaps a clarification of the flow in the region behind the reflected shock would be possible.

With these points in mind a series of photographs was made using air ($\gamma = 1.4$) as the medium for shock travel and varying the Mach number of the initial shock over the range of interest. A convenient pressure level was chosen ($p_1 = 0.5 - 1.0$ in. Hg abs). In region 1 ($1 < M_1 < 1.33$) photographs were made at $M_1 = 1.16$. These photographs indicated that almost no deviation from the ideal normal reflected shock occurred until the shock had traveled quite a distance from the reflecting wall (fig. 17). That is, there was no noticeable effect until the shock was traveling into the flow with a boundary layer that had grown to a thickness of several millimeters, thus reducing the channel width by several percent (about 14 in. after reflection). Even at this point the effect was limited to a slight curvature of the shock. (In fig. 18 we include, for comparison, a picture of the initial shock shortly before reflection; note that the pressure gradient, being in the opposite direction, causes the initial shock to appear as a lit pressure ridge, while the reflected shock always appears as a shaded pressure ridge.) As the Mach number of the initial shock was increased, no change in structure could be detected until a value of $M_1 = 1.5$ was obtained (fig. 19). In this photograph there appears a small but definite reaching forward of the shock near the wall. At $M_1 = 1.6$, this reaching forward at the wall is accompanied by what seems to be a small tail originating at the point of intersection of the shock and the wall and extending for some distance into the region behind the reflected shock (fig. 20). It is not clear

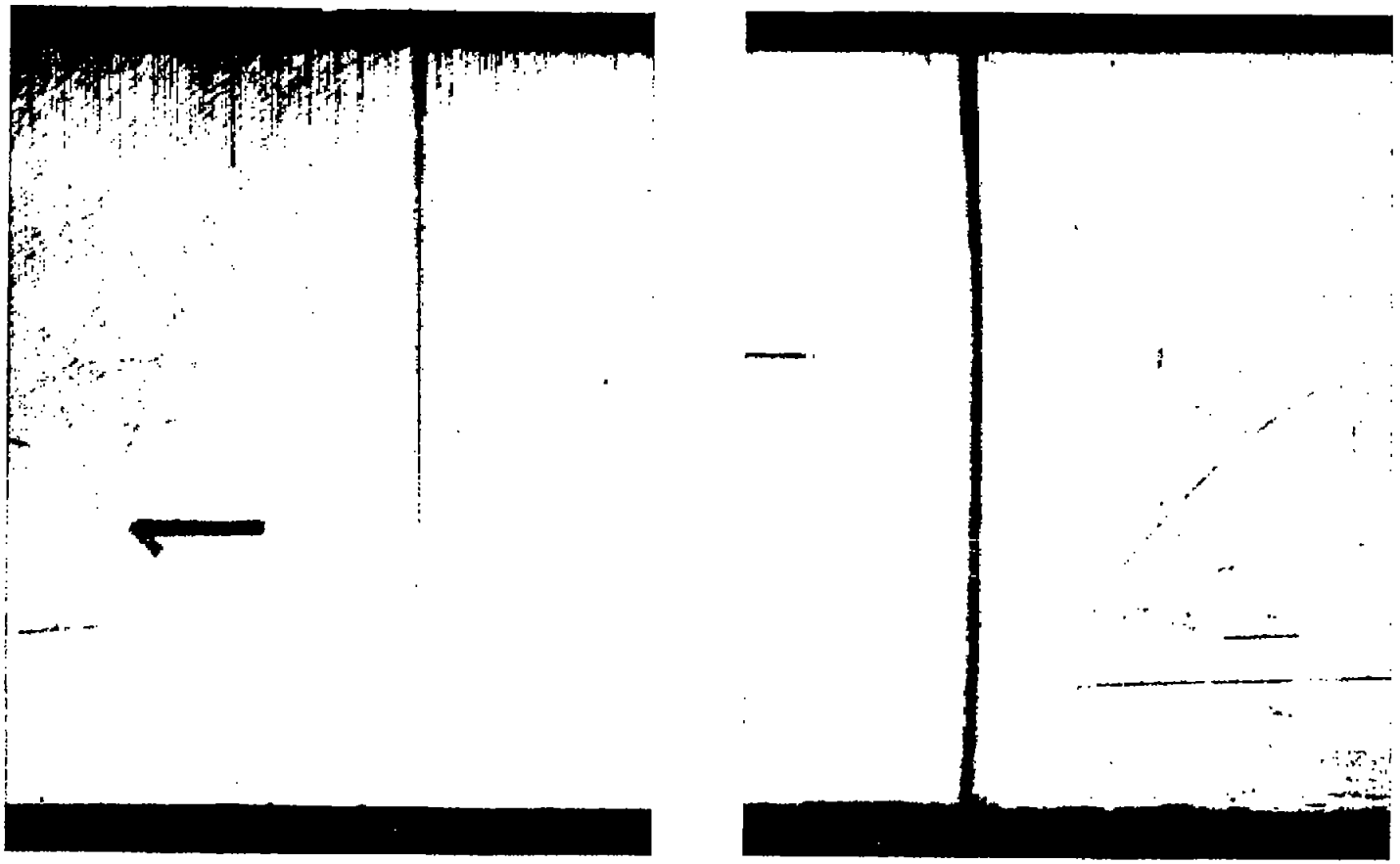

C-46544

(a) 3 Inches after reflection.

(b) 14 Inches after reflection.

Figure 17. - Reflected shock wave in air ($\gamma = 1.4$) at $M_1 = 1.16$.

4785

Figure 18. - Initial shock wave at $M_1 = 2.15$ shortly before reflection.

4785

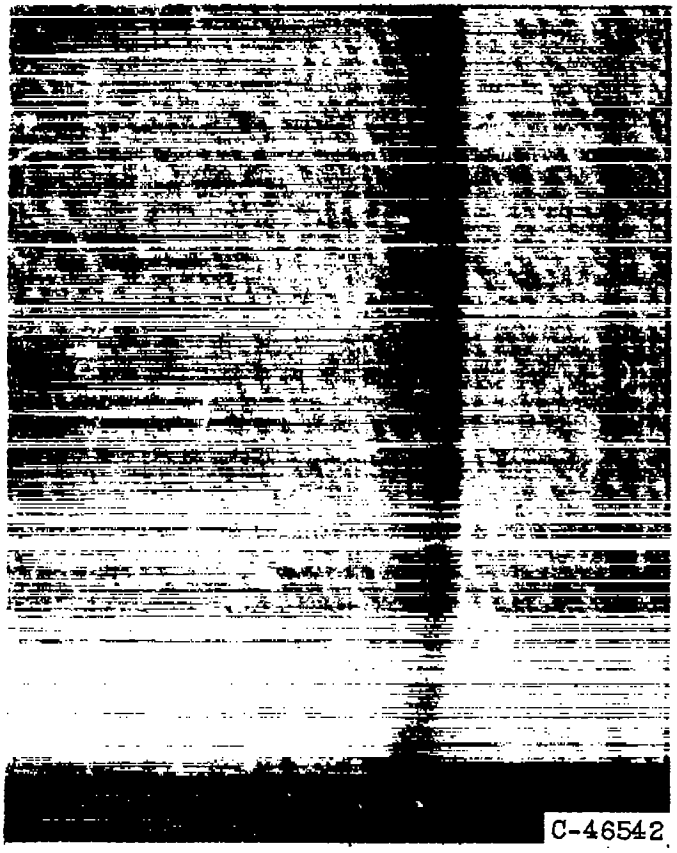

Figure 19. - Reflected shock wave in air ($\gamma = 1.4$) at $M_1 = 1.5$, 2.75 inches after reflection; $p_1 = 0.9$ inch mercury absolute.

4785

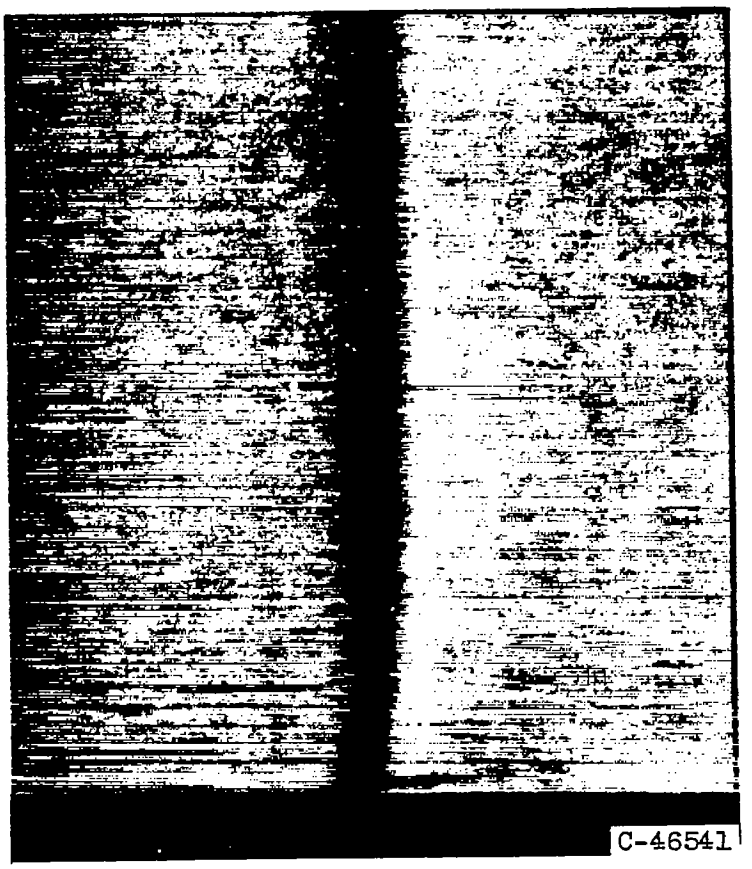

Figure 20. - Reflected shock wave in air ($\gamma = 1.4$) at $M_1 = 1.6$, 2.75 inches after reflection; $p_1 = 0.9$ inch mercury absolute.

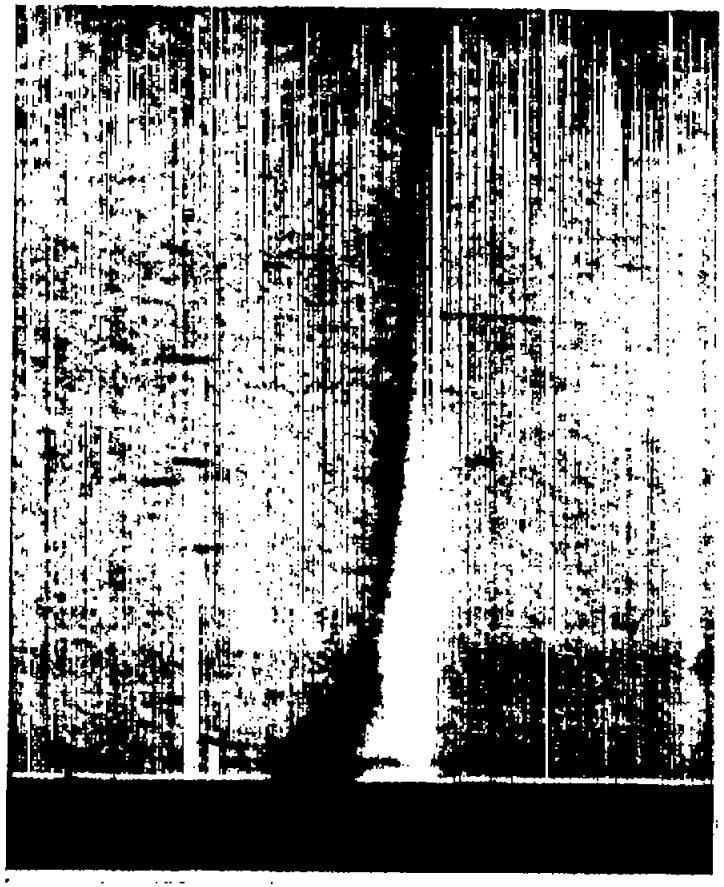

(a) 2.75 Inches after reflection;
p_1 = 0.9 inch mercury absolute.

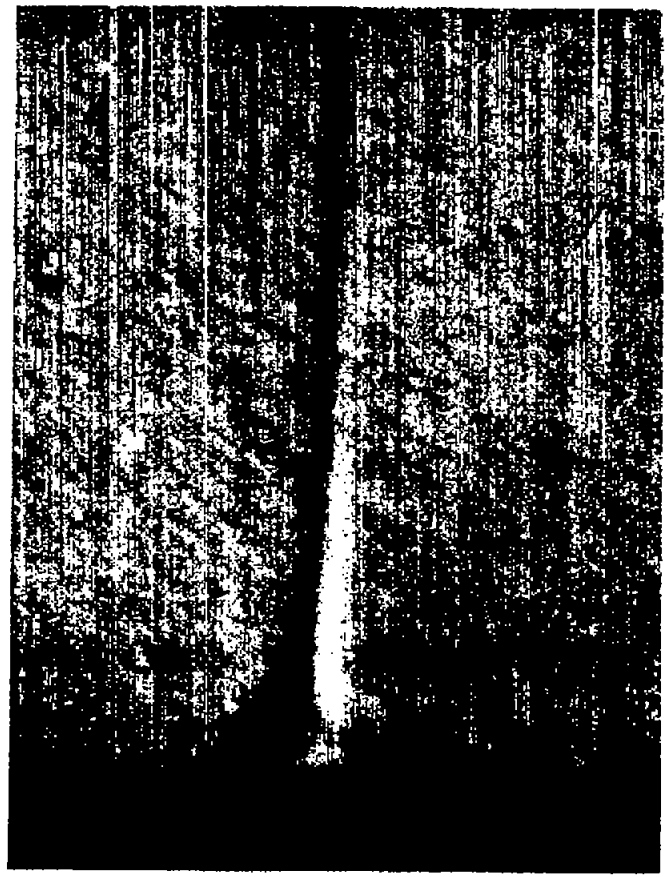

C-46545

(b) 2.75 Inches after reflection;
p_1 = 1.0 inch mercury absolute.

Figure 21. - Reflected shock wave in air (γ = 1.4) at M_1 = 1.8.

4785

CY-7

(c) 4 Inches after reflection; p_1 = 0.9 inch mercury absolute.

Figure 21. - Concluded. Reflected shock wave in air (γ = 1.4) at M_1 = 1.8.

4785

Figure 22. - Reflected shock wave in air ($\gamma = 1.4$) at $M_1 = 2.15$, 2.75 inches after reflection; $p_1 = 0.9$ inch mercury absolute.

4785

CY-7, back

Figure 23. - Reflected shock wave in air ($\gamma = 1.4$) at $M_1 = 2.15$, 2.9 inches after reflection; $p_1 = 0.9$ inch mercury absolute.

at this point what role this tail plays in the interaction but a look at figure 21 ($M_1 = 1.8$) soon gives the answer. In this photo it is apparent that the "tail" of figure 20 is actually the bottom side of a small triangular pattern which has appeared near the wall at the base of the shock. The height of this triangle (perpendicular to the wall) is ≈20 times the thickness of the boundary layer at this point (about 4 in. from the reflecting wall) and, moreover, the leading edge of the triangle is leading the main shock front. We are now well within region 2 of figure 12, and a picture of the interaction phenomenon in this region is developing. In figures 21(b) and (c) are two more photos of the reflected shock (at $M_1 = 1.8$) which show the pattern clearly, but in these the rearward leg of the triangle seems to have a slightly modified relation to the forward and bottom legs. Actually, these two rearward legs are not the same part of the phenomenon, and which rearward leg is visible depends on the schlieren sensitivity. An explanation for the difference between them had to wait until more pictures were made. In figure 22 ($M_1 = 2.15$) both rear legs are visible (the most rearward is very faint), but it was not until the picture in figure 23 was made ($M_1 = 3.0$) that the difference was clear. In this photo, unfortunately, the bottom leg is not visible, but taking the relevant information from each photo makes it possible to describe the entire phenomenon. In figure 23 we can see clearly the most rearward leg. It appears to be a little tail originating at the intersection of the forward leg of the triangular pattern and the main shock. The line which sometimes appears as a rearward leg of the pattern (in fig. 22, for instance) is clearly a fold in the shock sheet. This may be explained as follows: The phenomenon which exists at the wall boundary certainly exists on the glass boundary. Instead of seeing it in cross section (as we do at the bottom wall), we see a bottom view of it on the glass. Presumably, then, the picture (without corner effects) should look like the sketch in figure 24, the shaded area being the other view of the interaction of the shock wave and

4785

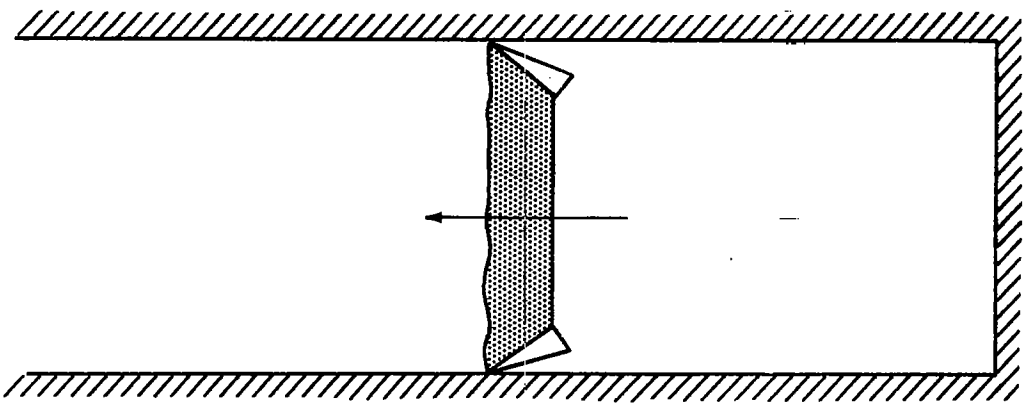

Figure 24.

4785

(a) 2.9 Inches after reflection.

Figure 25. - Reflected shock wave in air ($\gamma = 1.4$) at $M_1 = 3.0$; $p_1 = 0.9$ inch mercury absolute.

4785

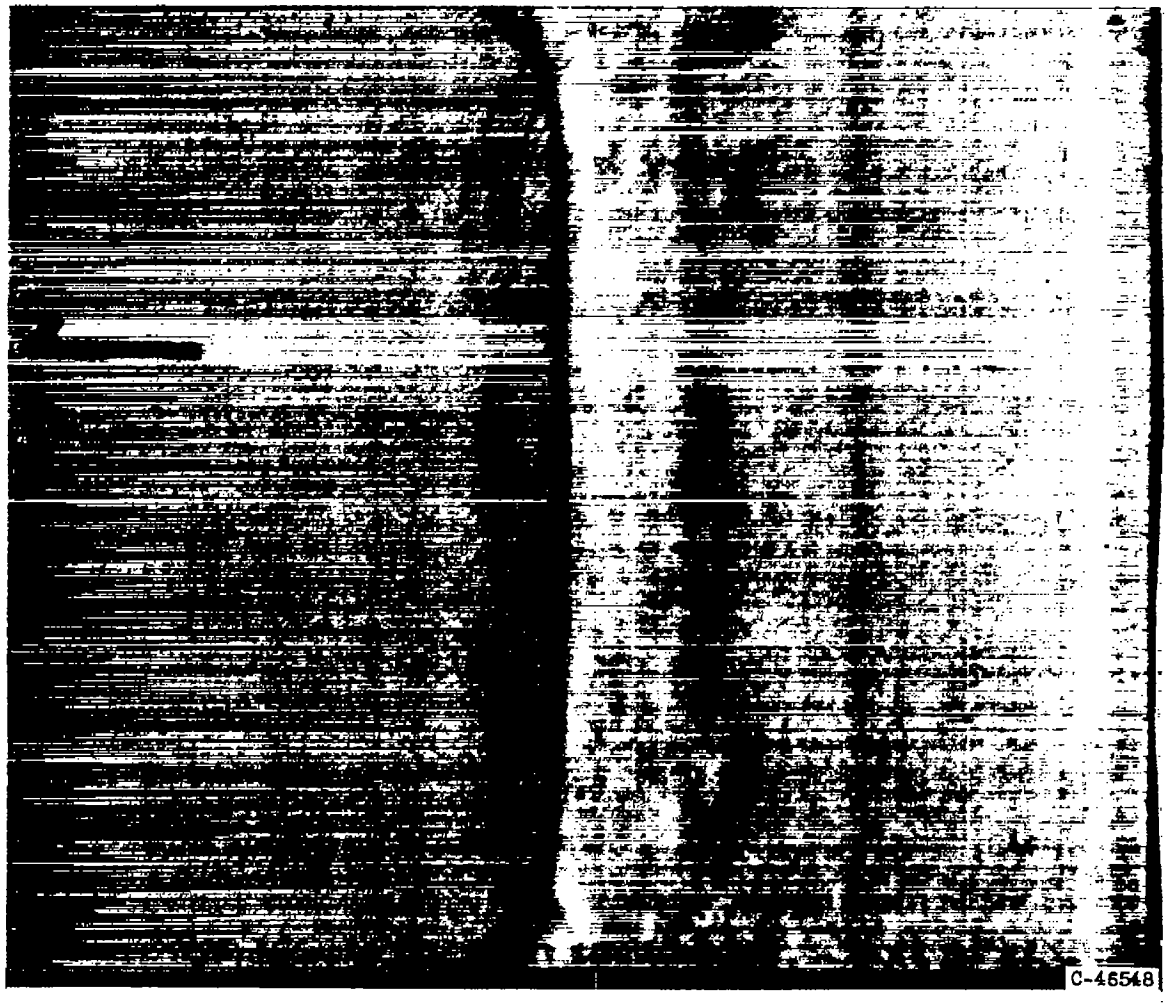

(b) 2.5 Inches after reflection.

Figure 25. - Concluded. Reflected shock wave in air ($\gamma = 1.4$) at $M_1 = 3.0$; $p_1 = 0.9$ inch mercury absolute.

the fluid boundary layer on the glass (see also fig. 25). However, due to the presence of the corner where the glass and wall meet, the shock sheet is apparently bent back in the corner, and the photos of figures 23 and 25 show this folding back quite clearly. Thus, in describing the interaction two-dimensionally, this fold must be neglected whenever it appears. Also clearly visible in figures 25(a) and (b) is a light region behind the shock wave, which runs the entire height of the tube. This light area ends abruptly some distance behind the shock in a slightly darker vertical swath, and the field thereafter up to the reflecting wall seems relatively undisturbed. This latter part of the phenomenon will be discussed later, after presentation of the photographs which gave the clue to its meaning.

4785

Unfortunately the relevant pieces of the phenomenon do not all appear perfectly put together in any one photograph. The entire phenomenon was of such a nature that, if the schlieren system was adjusted to make certain parts visible, other parts were lost. It was necessary, therefore, to piece together the relevant bits of information from all the photographs. Because of slight misalignments, three-dimensional effects, corner effects and so forth, extraneous material would appear and had to be disregarded. However, compiling the relevant information obtained, it is possible to make a sketch of what we have observed so far, and this sketch appears in figure 26(a).

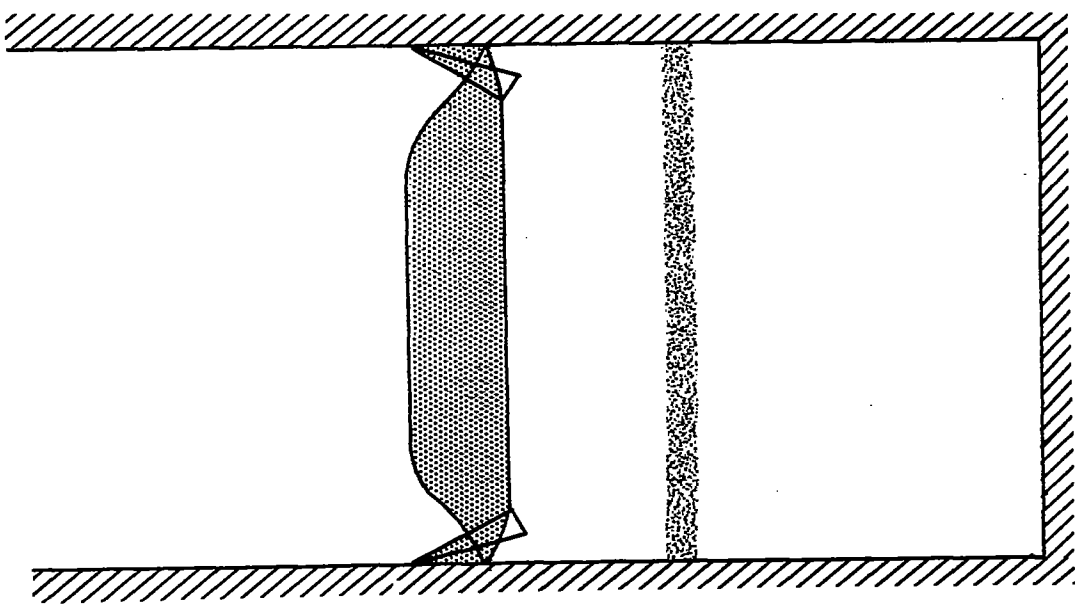

Figure 26(a).

An enlarged view of the region of interest is presented for discussion (fig. 26(b)):

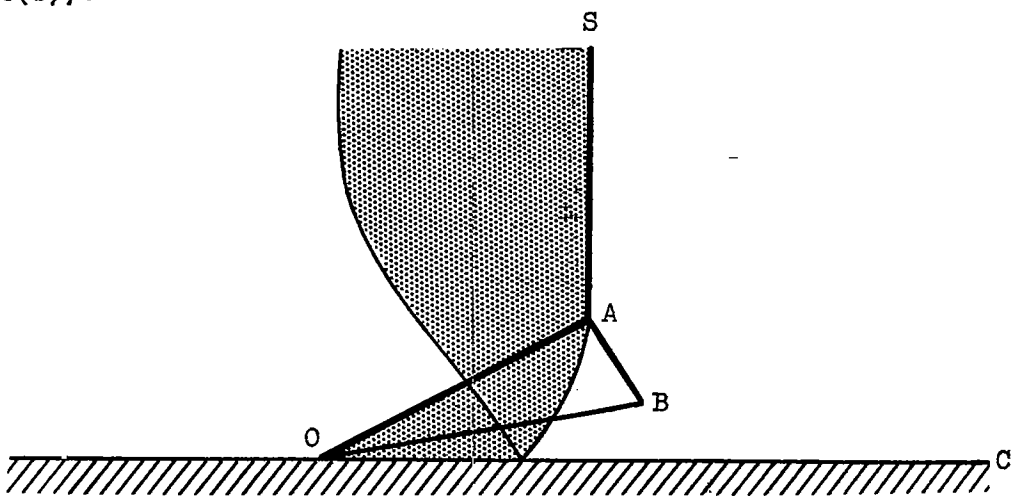

Figure 26(b).

4785

With this picture of the actual phenomenon, it was possible to suggest a mechanism by which the interaction was taking place. With the model thus proposed and the assumptions it would involve, the shape of the interaction might then be calculated for any initial Mach number (within region 2 of fig. 12) and these calculations compared with measured values from the photographs for verification of the model. The following model was proposed.

Let us suppose OA (in fig. 26(b)) is an oblique shock which turns a supersonic flow through an angle COB. This immediately implies that the flow being turned is not boundary-layer fluid, since the boundary-layer Mach number $M_{bl} < 1$ until $M_1 \geq 2$ and the phenomenon in question is already quite developed at $M_1 = 1.8$. The boundary-layer fluid then must be passing under OB. It is concluded that OB is a streamline of the flow separating boundary-layer fluid from mainstream fluid, visible to the schlieren because of strongly varying temperature profile of the boundary layer. The pressure is thus continuous across OB. If this is so, then the pressure in region OAB is the same as that of the boundary-layer fluid under OB. To determine this pressure let us redraw the picture of figure 26(b) in the coordinate system moving with the reflected shock, and modify the picture to be consistent with the discussion above (fig. 27).

4785

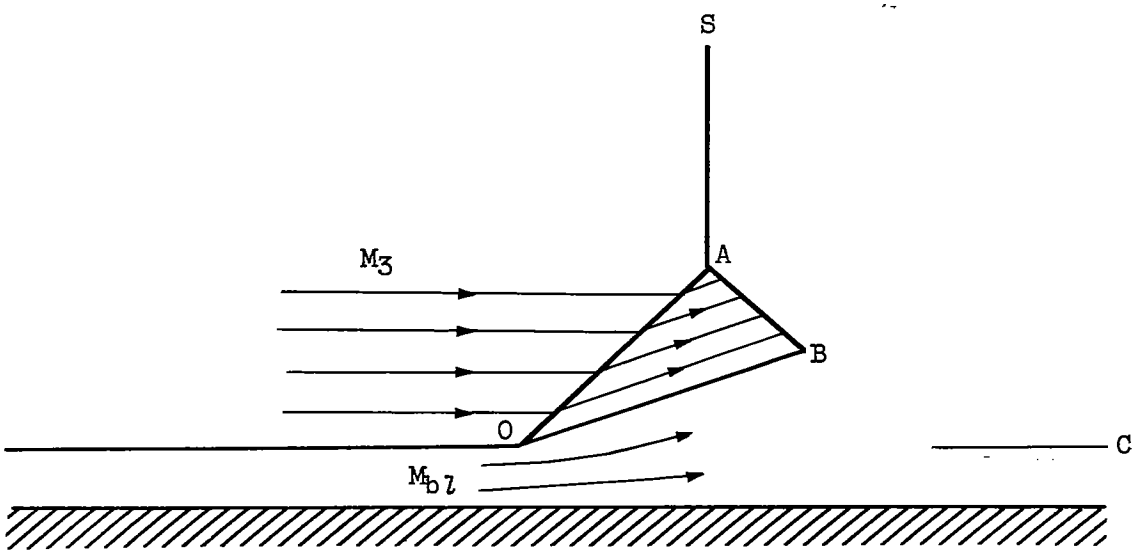

Figure 27.

CY-8

In region 2 (fig. 12) the boundary layer cannot enter the region behind the undisturbed shock, even at stagnation pressure. Let us say, then, that the boundary-layer fluid compresses under OB subsonically to the stagnation pressure associated with M_{bl}. We then have a method for calculating the pressure in region OAB. If we extrapolate this model into region 2 for values of M_1 where $M_{bl} > 1$, we can calculate the angles COA and COB for the entire region 2, since these are determined by M_3 (which is known), the oblique shock relations, and the pressure of region OAB. Using this model and the oblique shock relations, these calculations were made (see appendix C) and are presented as the solid lines in figures 28 (for COA against M_1) and 29 (for COB against M_1). Superimposed on these figures are measured values. Within the accuracy of measurement of such quantities from the photographs, the check between the measured and theoretical values is quite good, suggesting that the model for the interaction is quite a satisfactory one. The experimental data are slightly high at low values of M_1 and slightly low at high values of M_1. These discrepancies arise from the assumptions involved in the calculation. The high values at low M_1 can be accounted for in the assumption that the entire boundary layer is a jet described by M_{bl}. This is actually not true, and thus the calculation will give a stagnation pressure (and therefore a wave angle) lower than measured. At higher values of M_1, the assumption that the pressure below OB has reached stagnation pressure is questionable, and thus the calculation gives higher pressures (and therefore larger wave angles) than the measured values. Over-all, however, the predicted values for wave and

4785

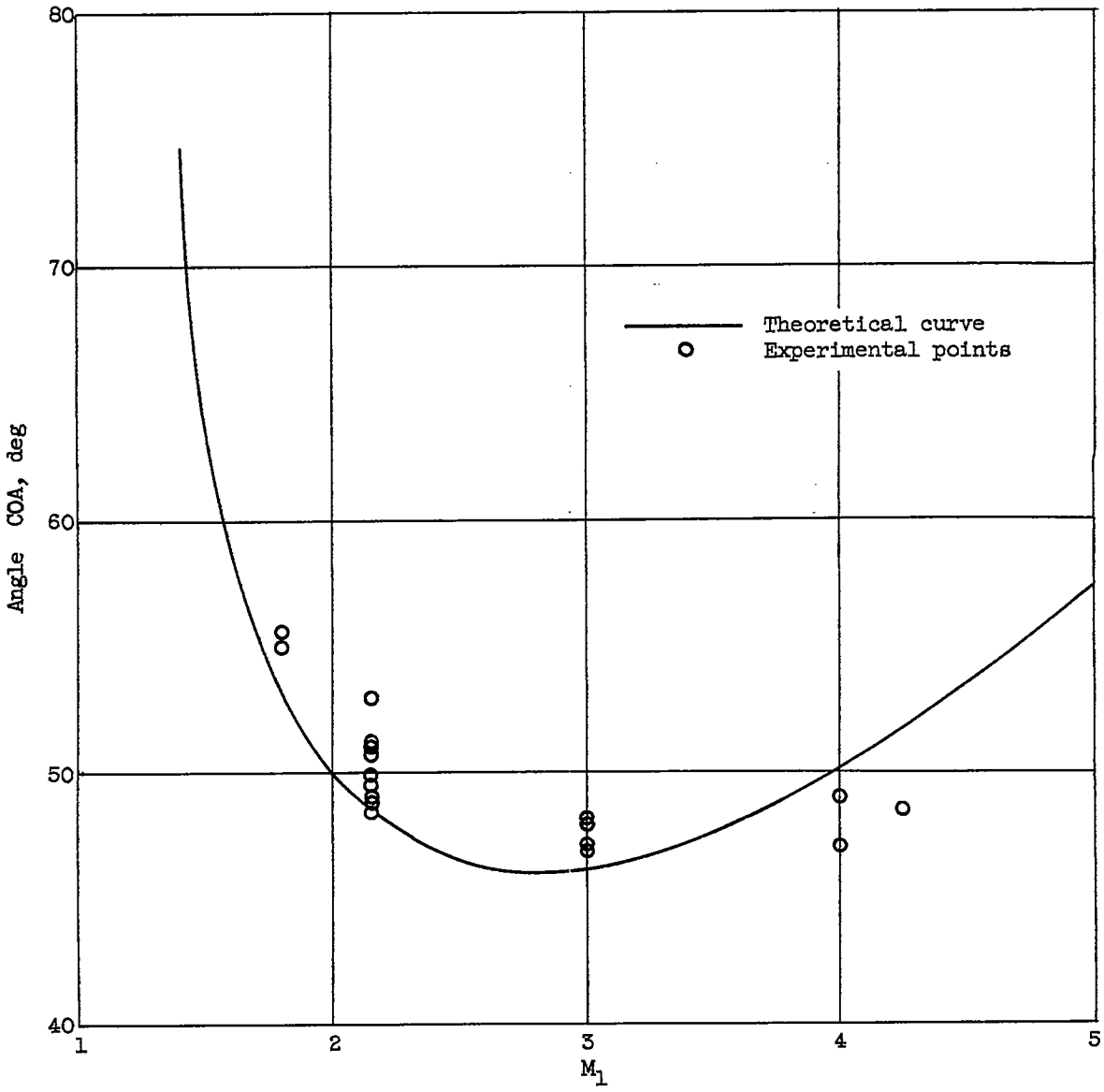

Figure 28. - Angle of the leading "foot" of region 2 shock-wave - boundary-layer interaction in air (γ = 1.4) plotted against Mach number of initial shock. Experimental points are included for comparison.

4785

CY-8 back

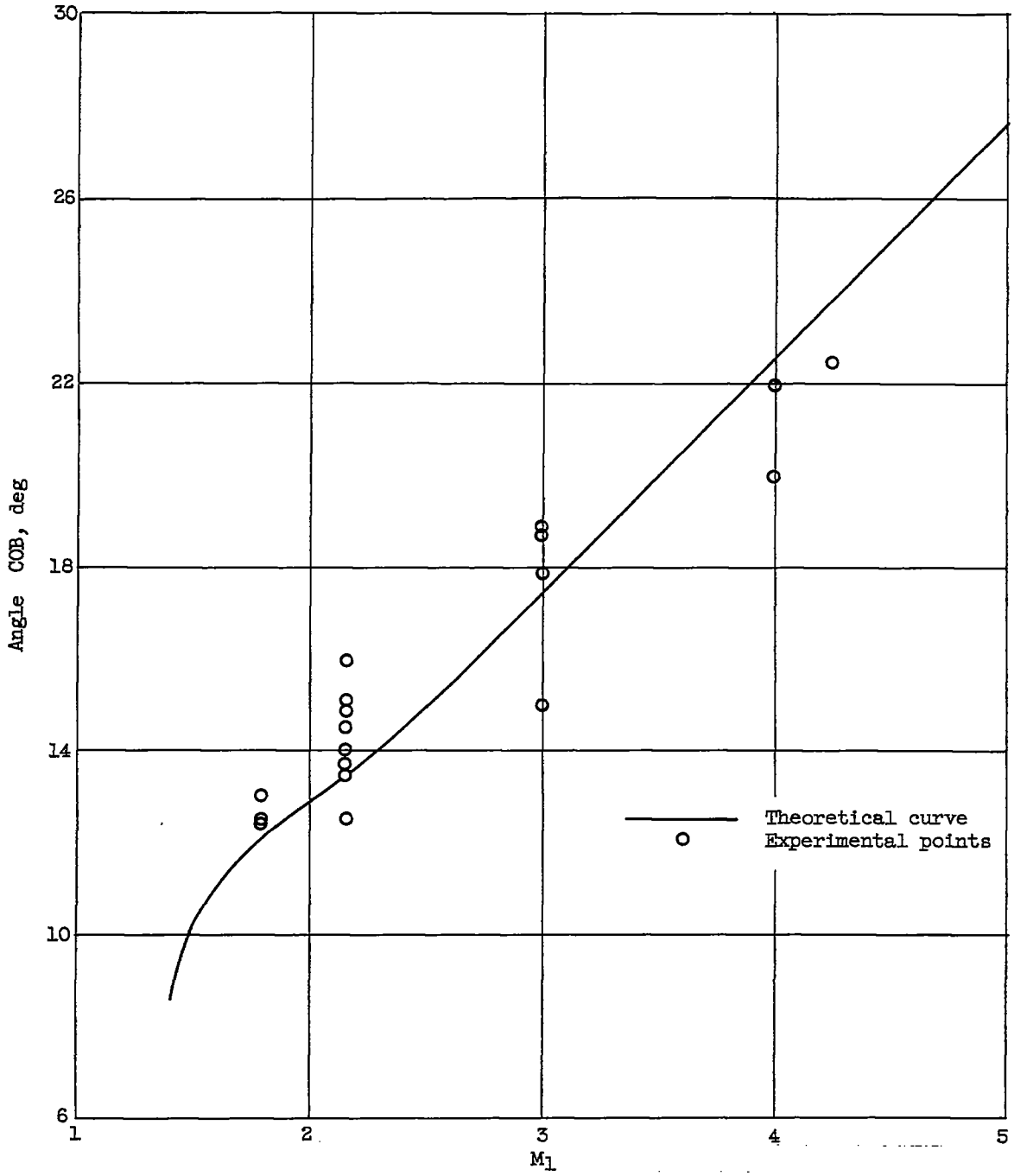

Figure 29. - Angle of streamline bounding the compression of fluid at M_{bl} in air ($\gamma = 1.4$) plotted against M_1.

deflection angles (COA and COB) are good and, at intermediate values of M_1, are close to the measured values. Perhaps we should note here that the effects of the two strong assumptions we have made act very fortuitously, over much of the Mach number range, in such a way as to reduce the over-all quantitative error. Thus the extreme assumption that we have stagnation pressure in the boundary layer couples with the conservative description of the boundary layer by M_{bl} to give a rather good quantitative picture of the interaction.

We have a start now in describing the phenomena occurring in region 2, but still have not shown that there is an upper bound (the second pressure crossover), as predicted by the analysis of section III. Missing, too, is an explanation of the light region behind the reflected shock followed by the darker swath which appears in the photos of figure 25. The second of these problems was resolved by a group of extremely fortunate pictures presented in figures 30 to 33. These pictures were made at an initial Mach number of 2.15 and, of hundreds of pictures made, were the only ones to give the small piece of added information necessary. Examining these pictures (figs. 30 to 33) carefully, one can notice in all of them a line leading from the triple point back to the reflecting wall. This line is identified as the locus of all particles that have passed through the triple point (the point of intersection of the two oblique shocks with the main shock) and, as such, divides the main flow into two parts. The part of the main flow above this line has passed through the single undisturbed shock. The part of the main flow under this line (i.e., between this line and the wall) has passed through the two oblique shocks. This dividing line is visible to the schlieren because of the entropy difference arising between the two portions of the main fluid having different histories. Notice that as we move back along this line from the shock to the reflecting wall it takes a sharp dip in towards the wall boundary, and that this dip coincides with the dark swath running the height of the channel; that is, since the same phenomenon occurs in the interaction between the shock and the fluid boundary layer on the glass, we see it as a swath in the other view. Also faintly visible between this line and the wall (particularly in fig. 32) is another small region, presumably the ball of boundary-layer fluid which collects behind the foot of the shock. This smaller region is quite clearly outlined in two photographs made at Cornell Aeronautical Laboratory in Buffalo[1] (figs. 34 and 35). It is clear, then, that the dip in the outer main flow occurs in conjunction with the termination of the rearward motion of the fluid in the boundary-layer stagnation-pressure bubble. The dark vertical swath we see could be this ending of the bubble, or it could be an indication of a compression (since it is dark) of the fluid in the inner and outer main flow. It is now possible

4785

[1]The author is indebted to Cornell Aeronautical Laboratory for making these photographs available.

4785

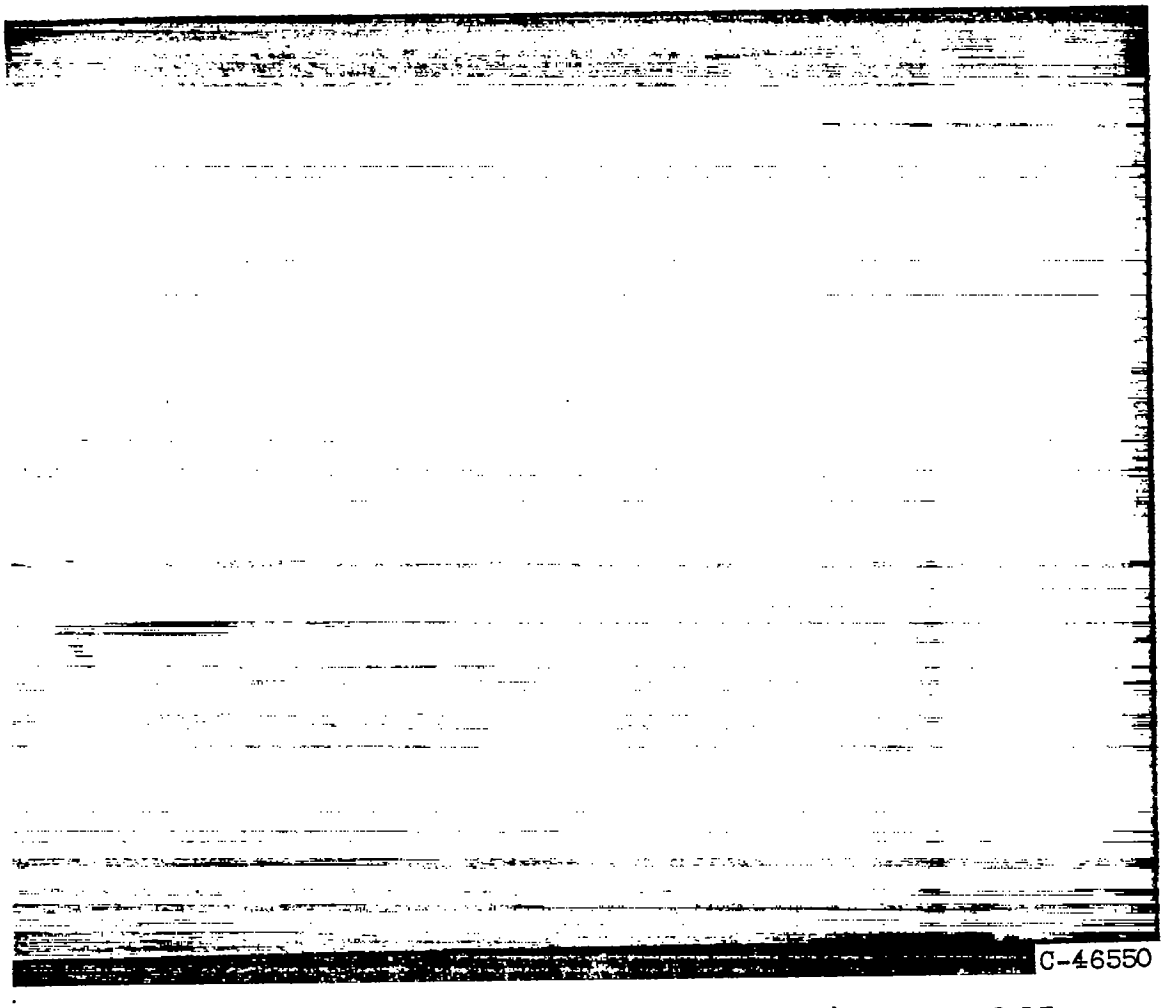

Figure 30. Reflected shock wave in air ($\gamma = 1.4$) at $M_1 = 2.15$, 0.9 inches after reflection; $p_1 = 1.8$ inches mercury absolute.

4785

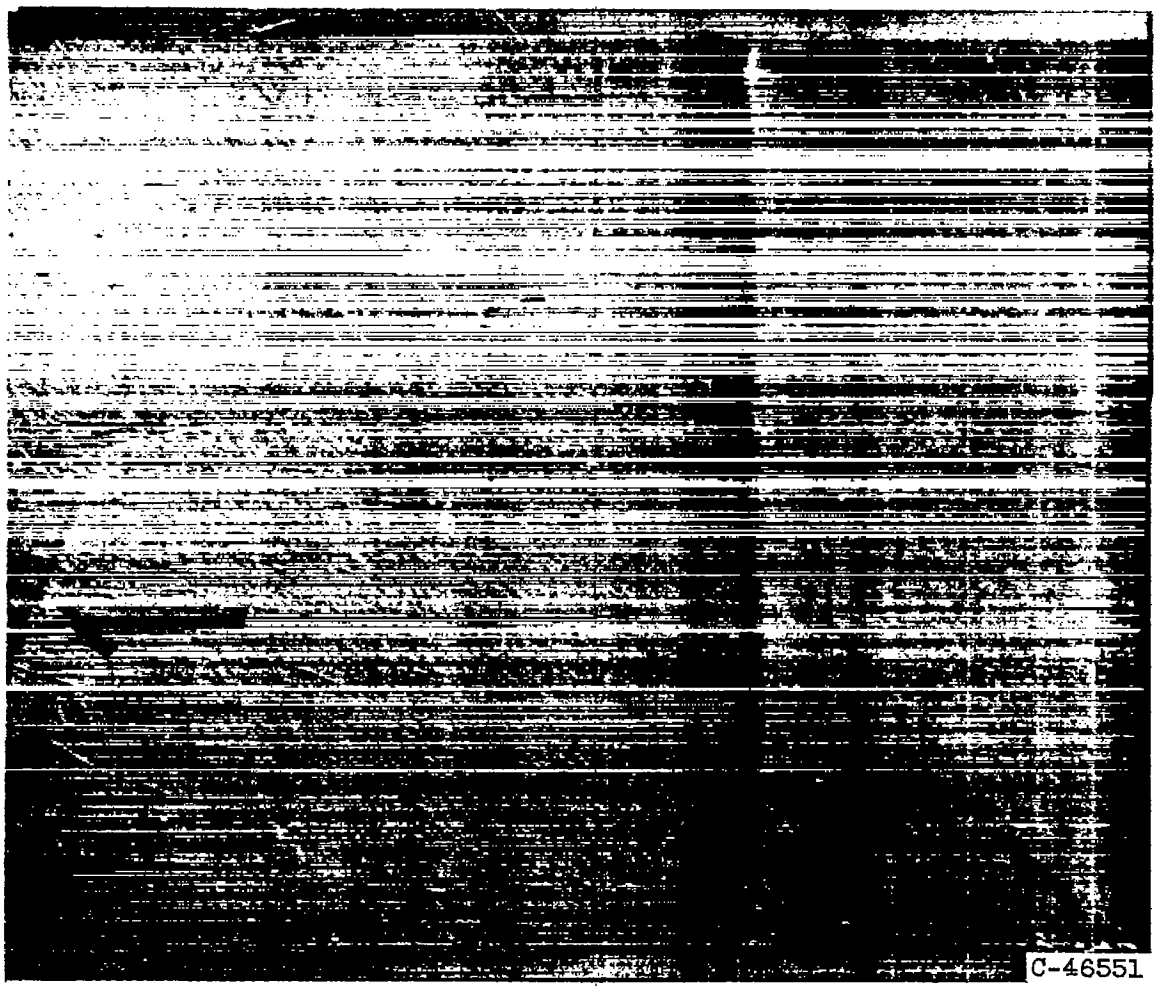

Figure 31. - Reflected shock wave in air ($\gamma = 1.4$) at $M_1 = 2.15$, 1.75 inches after reflection; $p_1 = 1.8$ inches mercury absolute.

4785

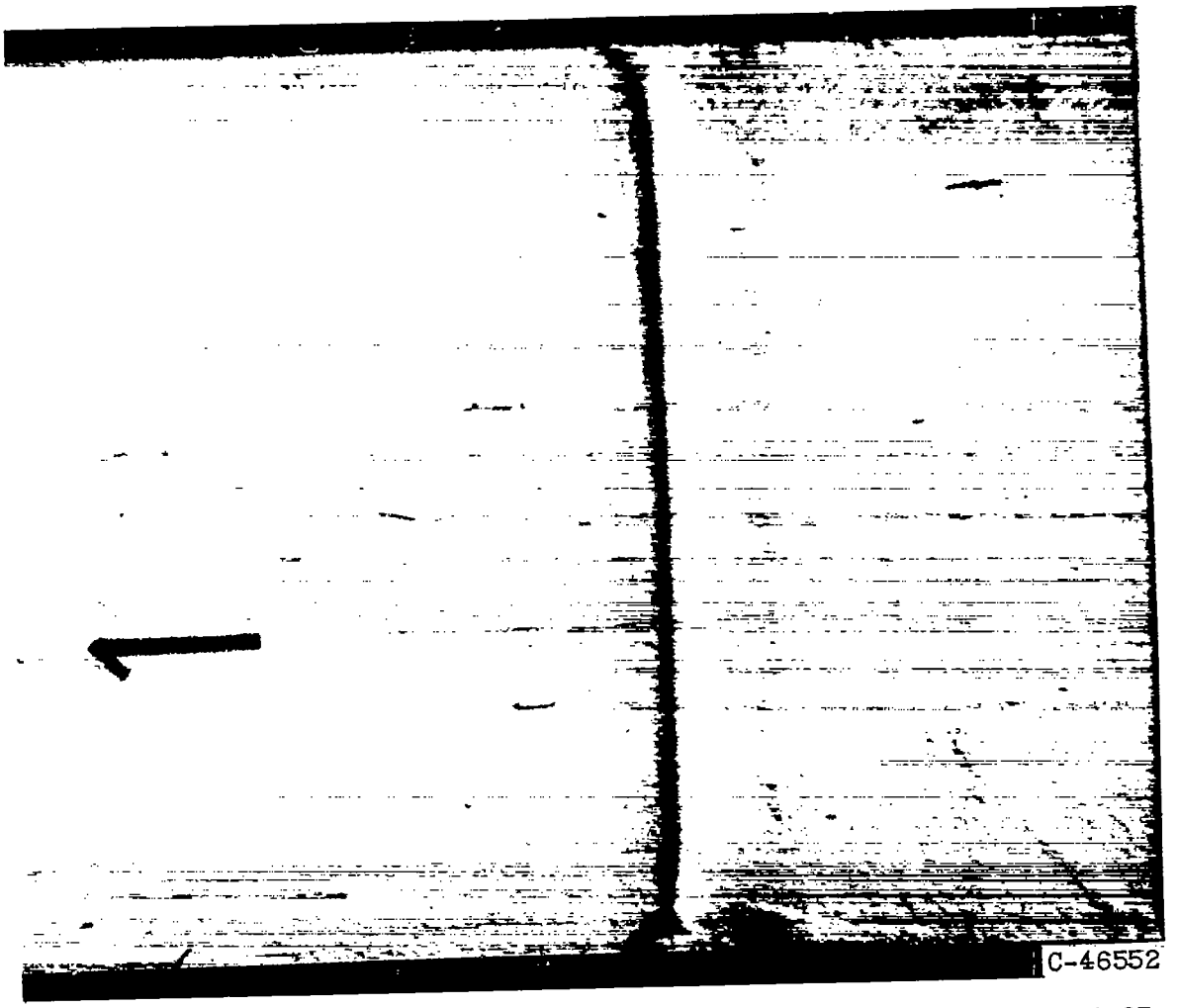

Figure 32. - Reflected shock wave in air ($\gamma = 1.4$) at $M_1 = 2.15$, 2.25 inches after reflection; $p_1 = 1.8$ inches mercury absolute.

4785

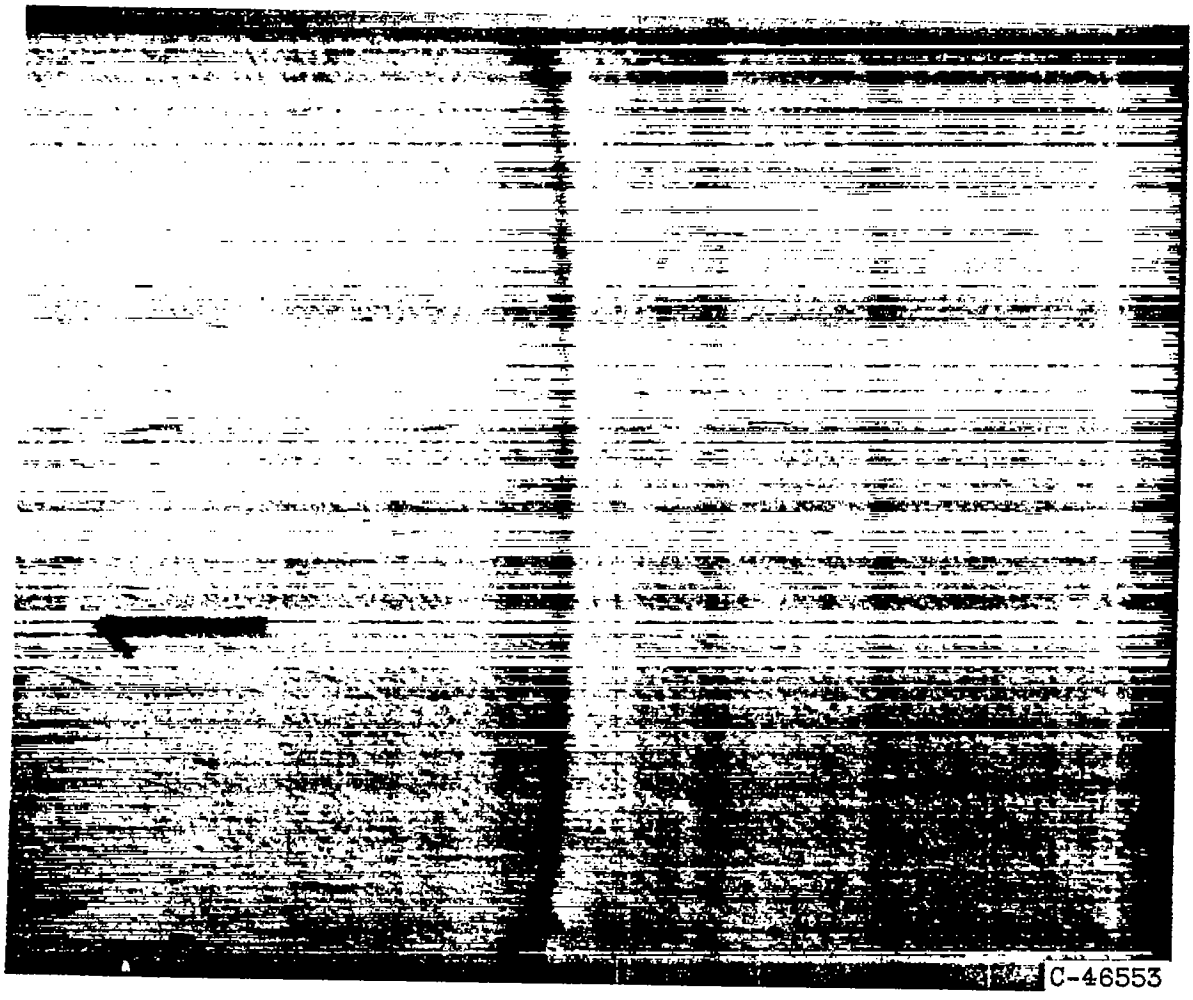

Figure 33. - Reflected shock wave in air ($\gamma = 1.4$) at $M_1 = 2.15$, 2.75 inches after reflection; $p_1 = 1.8$ inches mercury absolute.

4785

CY-9

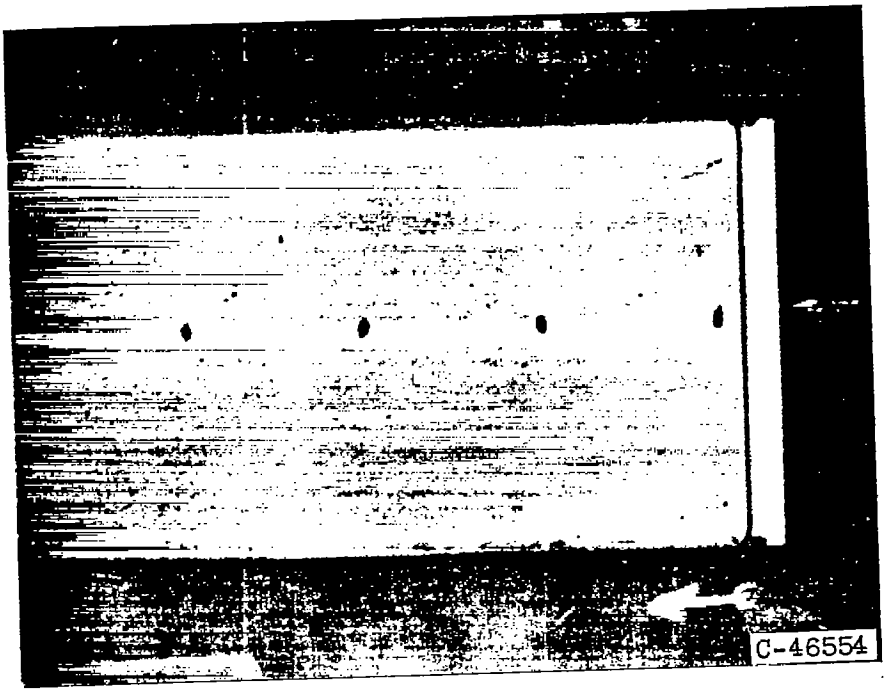

Figure 34. - Reflected shock wave in air ($\gamma = 1.4$) in 2 1/2- by 1 1/2-inch shock tube at $M_1 \approx 6.0$, shortly after reflection; $p_1 = 10$ millimeters mercury absolute (courtesy Cornell Aeronautical Laboratory).

4785

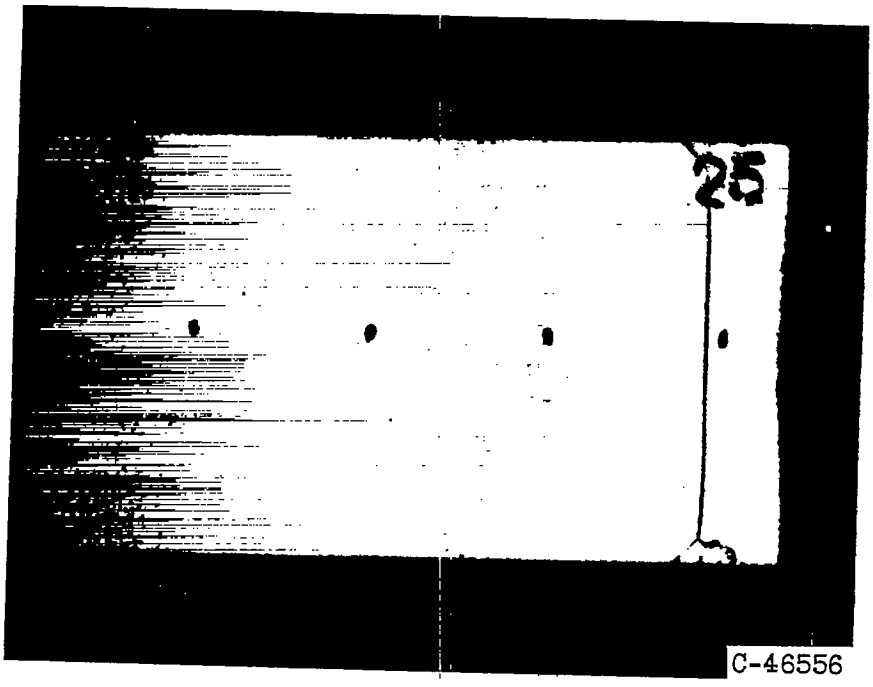

Figure 35. - Reflected shock wave in air ($\gamma = 1.4$) in 2 1/2- by 1 1/2-inch shock tube at $M_1 \approx 6.0$, approximately 1/2 inch after reflection, showing inner ball of boundary-layer fluid; $p_1 = 10$ millimeters mercury absolute (courtesy Cornell Aeronautical Laboratory).

to make more complete the picture of the interaction phenomenon, and this is presented in figure 36.

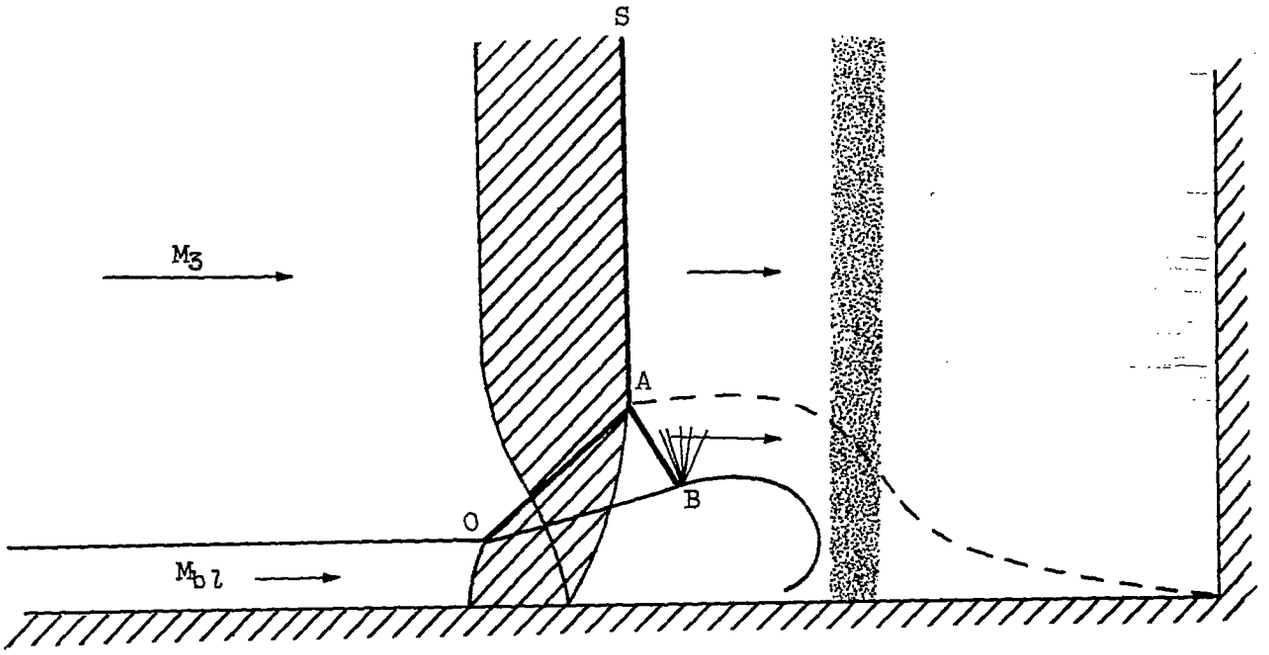

Figure 36. - Interaction in region 2.

We have included two extra features of the flow in figure 36 not heretofore noted. First, we have suggested that an expansion takes place in the portion of the main flow that has passed through the bifurcation. This is required by the fact that at point B the pressure is nearly the stagnation pressure of the boundary layer and, when the secondary shock AB reaches the free boundary of the bubble, an expansion is reflected from this surface. This is seen clearly as the light region in figure 32. Perhaps there are other shocks and expansions in this flow as the fluid travels over the bubble, but this is not clear. What is probable, however, is that this fluid of higher total pressure than the boundary-layer bubble cannot come to stagnation at the wall together with the bubble fluid. Thus, the stagnation point for this fluid will be somewhat to the rear of the end of the bubble, and some of this fluid may enter under the bubble. This is suggested schematically in figure 36.

The interaction of region 2 (fig. 36) appears quite consistently in air when the Mach number of the initial shock has a value within region 2 of figure 12 (section III). Several additional pictures at Mach numbers up to 5 are presented (fig. 37). The problem now is to show that this interaction disappears when the Mach number for air ($\gamma = 1.4$) is

4785
CY-9 back

4785

(a) $M_1 = 4.24$.

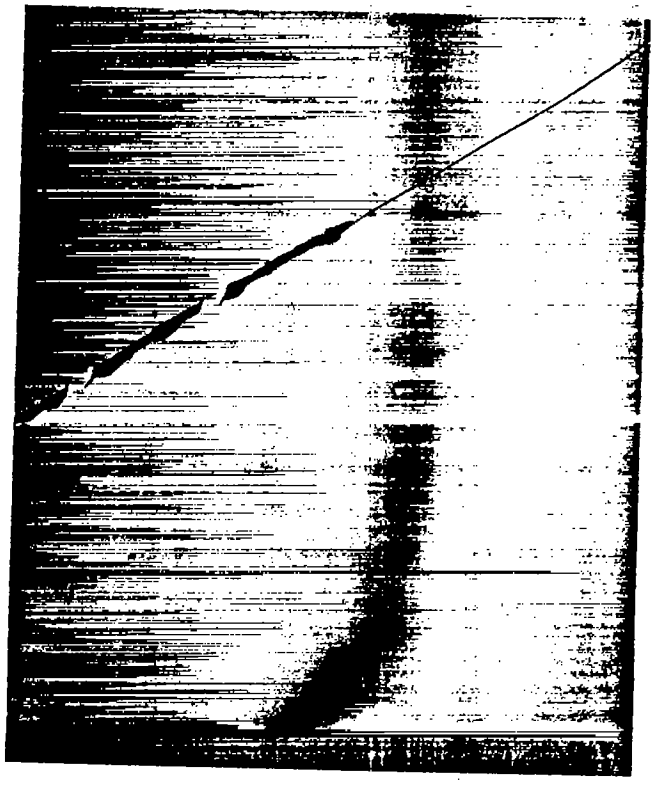

C-46557

(b) $M_1 \approx 5.0$.

Figure 37. - Reflected shock wave in air ($\gamma = 1.4$) shortly after reflection; $p_1 = 0.9$ inch mercury absolute.

increased above 6.45, as is predicted. This turned out to be impossible, and the value 6.45 for the second pressure crossover was never checked. The reason for this follows from the discussion of section III, where it was pointed out that decreasing the value of γ for the gas rapidly increased the crossover Mach number. Thus, as the initial shock Mach number is increased towards 6.45 and γ for air falls to approximately 1.2, the crossover Mach number increases from 6.45 (at $\gamma = 1.4$) to approximately 16. Some alternative method had to be devised to verify the existence of an upper Mach number boundary to region 2. The solution
4785 to this problem lay in using a monatomic gas for the shock-travel medium. Since a monatomic gas has a constant specific heat and also has a higher γ than does a diatomic gas, both difficulties encountered, using air as the shock medium, in trying to verify the existence of an upper Mach number boundary to region 2 could be avoided. Not only is the value for the second pressure crossover Mach number lower ($M_1 = 2.8$ for $\gamma = 1.67$) than for diatomic gas, but also it will remain constant at this Mach number level; and an accurate check of the upper bound Mach number should be possible. Unfortunately a new difficulty arose.

Examining figure 12, in which the undisturbed pressure behind the shock as well as the boundary-layer stagnation pressure are plotted against M_1 for $\gamma = 1.67$, we notice that the change in γ has changed the pressure crossover points considerably. The curve for p_{4_m} has been lowered, and that for $p_{stag_{bl}}$ has been raised. This, of course, moves the crossover points closer together than in the case for $\gamma = 1.4$. The first crossover point has been raised to $M_1 = 1.57$, and the second has been lowered to $M_1 = 2.8$. However, although we have a well-defined region 2 (where the stagnation pressure of the boundary layer is lower than the pressure behind the undisturbed shock), the ratio of $p_{stag_{bl}}$ to p_{4_m} is never less than 0.9. If we examine the case for air ($\gamma = 1.4$), we notice that this ratio ($p_{stag_{bl}}/p_{4_m}$) falls as low as 0.5 (at $M_1 =$ 2.15 - 3.25). Most important to note is that, in trying to locate the first pressure crossover for $\gamma = 1.4$ experimentally (analytically $M_1 = 1.33$), it was not possible to obtain a really noticeable effect until the initial Mach number was raised to $M_1 = 1.5$. At this value of M_1 the ratio of the boundary-layer stagnation pressure to the pressure behind the undisturbed shock has fallen to ≈ 0.8. If we take this as an experimental limit (at least for our experiment), this indicates that much above the value 0.8 for this pressure ratio the interaction between the boundary layer and the shock wave will be so small that it (the interaction) and its effects will not be detectable until a

relatively long time after reflection. This makes impossible an exact check of the crossover values as predicted from the analysis, but still allows a check to be made. To obtain an experimental value for the second pressure crossover, it is necessary to obtain the interaction of region 2 at some Mach number below the predicted value, and then increase the Mach number M_1 until this interaction disappears (if it disappears). Since the ratio of boundary-layer stagnation pressure to p_{4_m} is never less than 0.9 for $\gamma = 1.67$, it is always well above the experimentally determined limit value of 0.8 for this ratio and the region 2 interaction, and its effects will never be visible in pure argon[1]. To make the experimental verification of the second pressure crossover and to verify the existence of a region 3 in which the flow is relatively undisturbed (again as in region 1), a compromise must be made between two effects of the change in γ of the shock-travel medium. The first effect of raising γ is to reduce the value for the second pressure crossover. The second effect of raising γ is to decrease the pressure difference between p_{4_m} and $p_{stag_{bl}}$ in region 2. Thus an intermediate value of γ is desirable. That is, a value of γ should be chosen which will reduce the Mach number of the second pressure crossover to a convenient value while not lowering the difference between p_{4_m} and $p_{stag_{bl}}$ below a value which will allow good photographs to be made of the region 2 interaction. The value decided upon for γ was $\gamma = 1.62$. Gas with this value of γ was obtained by diluting argon with air and calculating γ for the mixtures from the following relation

$$\gamma_{mix} = \frac{\sum_n C_{p_n} f_n}{\sum_n C_{v_n} f_n}$$

where f_n is the fraction of mixture of component n.

Thus $\sum_n f_n = 1$.

At a mixture of 92 percent argon and 8 percent air we obtain a γ for the mixture of 1.62, and curves similar to those for $\gamma = 1.4$ and 1.67 of figure 12 are plotted in figure 38 for $\gamma = 1.62$. Note that the lower pressure crossover is at $M_1 = 1.5$, while the second pressure

[1]Photographs were taken in pure argon, and this proved to be the case. The interaction in region 2 for pure argon was so small as to be almost invisible. A later reference will be made to this matter in discussing the experimental work of R. Strehlow.

4785

4785

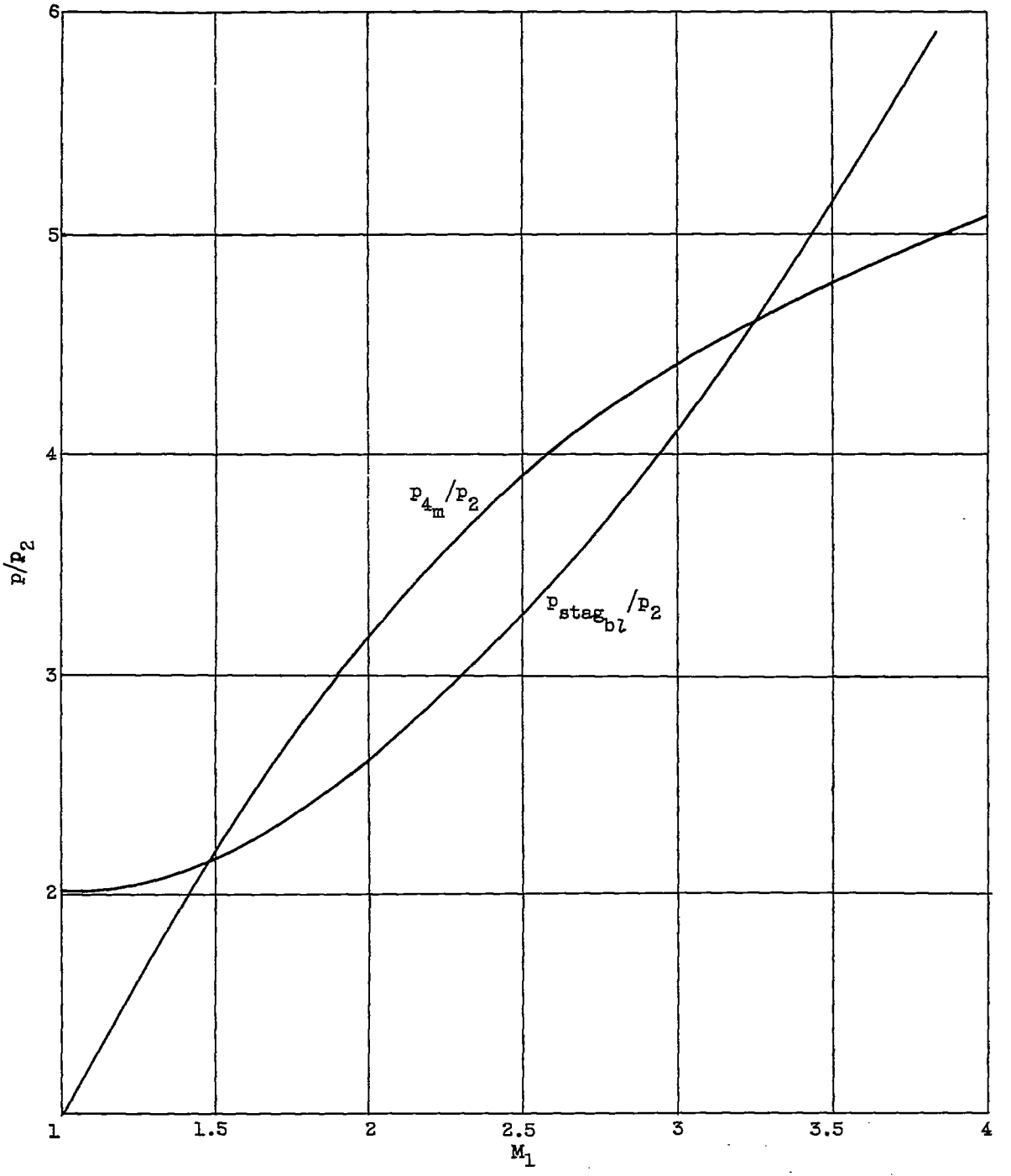

Figure 38. - Pressure ratio across normal shock at M_3 and pressure-rise ratio in boundary layer described by M_{bl}, plotted as a function of M_1 for a gas of $\gamma = 1.62$.

crossover has been lowered to $M_1 = 3.27$. This has been accomplished at the expense of raising the ratio of $p_{stag_{bl}}/p_{4_m}$ to a minimum value of ≈ 0.8 (from a min. value of 0.5 at $\gamma = 1.4$), but at this value we can expect that the region 2 interaction will be visible in the photographs. In figure 39 are shown several photographs of the interaction in this gas ($\gamma = 1.62$) at $M_1 = 2.2$. Note that the interaction of region 2 is clearly discernible in these photos. The characteristic triangular pattern is present exactly as before (as for air), but now we are in an excellent position to check the second pressure crossover at 3.27, since the value for γ will remain almost constant for this gas mixture in this Mach number range. As pointed out before, no exact check of this value is possible, since our experiment is limited in defining a boundary to region 2 by the maximum ratio of $p_{stag_{bl}}/p_{4_m}$ of approximately 0.8 and the boundary is calculated for $p_{stag_{bl}}/p_{4_m} = 1.0$. However, we can at least bracket the calculated value of the second pressure crossover with the experiment and show that the relatively undisturbed shock interaction of region 1 reappears above the calculated second pressure crossover. To this end photographs were made at an initial Mach number of 3.6, and in figure 40 is presented a photo of the interaction in this region. It is clear from this figure that the interaction of region 2 is not present (as shown in fig. 39), and we have an almost undisturbed reflected shock as in region 1 (this is more clearly discernible in the original photographs). Thus we have obtained the region 2 interaction at a Mach number below the calculated second pressure crossover and a relatively undisturbed shock interaction at a Mach number above this value. We have determined an upper limit to the interaction of region 2 and have bracketed the calculated value of the second pressure crossover.

Reynolds Number Effects

In the work done so far, it has been assumed that the shock interacts with a laminar boundary layer. However, at some point behind the initial shock the boundary layer will become turbulent, and it is reasonable to expect that this transition to turbulence of the boundary layer will be accompanied by a change in the interaction of region 2. Unfortunately, it is not possible at the present time to predict the conditions under which the boundary layer in a shock tube becomes turbulent. However, it seemed possible that an experiment could be devised, without too much difficulty, in which we could attempt to observe the effect of transition to turbulence of the boundary layer on the shock-wave - boundary-layer interaction. For such a study the most desirable information would be a high-speed motion picture record of the behavior of the phenomenon from the moment of reflection of the shock to the time of arrival of the contact surface. Such a study would have required, however, considerable expansion of the equipment, and it was felt that a series of instantaneous pictures, properly spaced

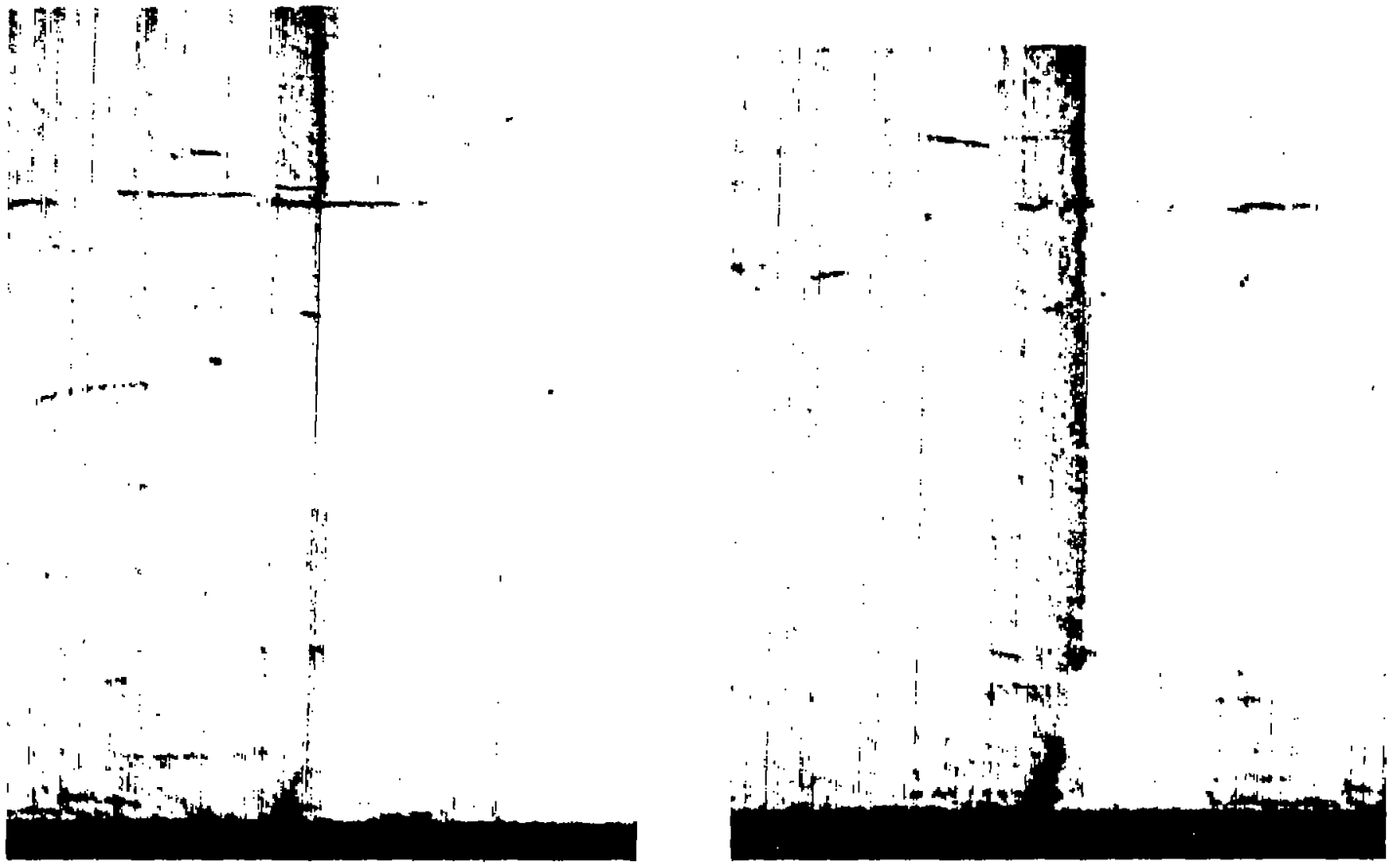

C-46558

(a) 1.25 Inches after reflection.

(b) 1.5 Inches after reflection.

Figure 39. - Reflected shock wave in gas of $\gamma = 1.62$ showing the region 2 (fig. 12) interaction at $M_1 = 2.2$.

4785

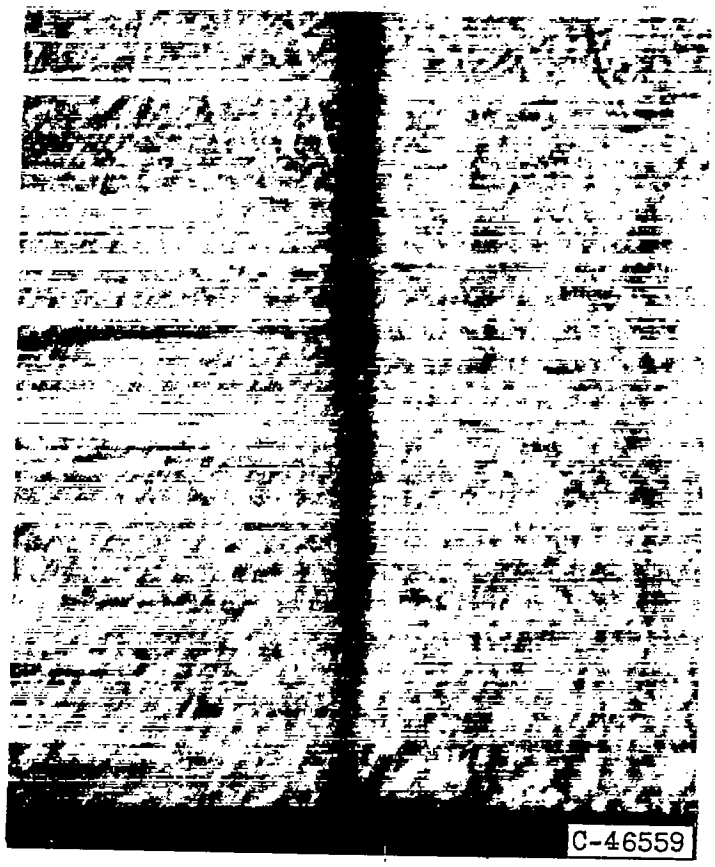

Figure 40. - Reflected shock wave in gas of $\gamma = 1.62$ at $M_1 = 3.6$, 1.5 inches after reflection.

over the time of interest, would show quite satisfactorily any of the interesting effects detectable by the schlieren system. Although it was not quite possible with the equipment available to obtain such a series of photos in a single experiment, it was possible to simulate such a time sequence by repeating the experiment a number of times and exposing the film at increasing time after reflection. Maintaining all variables constant, such a series of experiments was made at $M_1 = 2.15$ in air ($p_1 = 0.9$ in. Hg abs), and the simulated sequence was obtained. These pictures are presented in figure 41. In these photos the reflected shock is moving (as indicated by the arrow) from right to left. We note that the interaction (clearly that of region 2) grows with time but remains similar to itself in figures 41(a) to (f). This growth is discussed further in the next section. From figure 41(g) on, it is to be noted that the line of high density gradient which forms the bottom line of the triangular pattern, and which presumably is the boundary between the cold boundary layer fluid and the hot main fluid, begins to shorten. Finally in figure 41(k), it is no longer visible and is not present in any subsequent pictures. We take the shortening and final disappearance of this boundary to be the manifestation in the interaction phenomenon of the transition of the boundary layer from a laminar to a turbulent state. Certainly, as the boundary layer becomes turbulent, the phenomenon as proposed for the laminar case will become less and less necessary. The energy transferred from the main stream to the boundary-layer fluid by turbulent transfer obviates the difficulties encountered by the low-energy boundary layer in the laminar case. The shortening of the line dividing the main fluid from the boundary-layer fluid in the series of pictures of figure 41 is the indication of the onset of this turbulent mixing effect. The final disappearance indicates that turbulent mixing has been completely substituted for the laminar interaction. Perhaps this laminar interaction still occurs at a much smaller scale for an extremely thin laminar sublayer, but this is so small as to be invisible in the photographs, and we can only surmise, as in the case of the steady shock-wave boundary-layer interaction (ref. 19) that such an interaction exists.

It would be of value here if we could define a Reynolds number with which to characterize the flow. To do this, we have tried to make somewhat of an analogy between the flow in the shock tube and the flow over a flat plate in an airstream. The Reynolds number in the latter case may be defined as

$$Re \equiv \frac{\rho_w U_\infty x}{\mu_w}$$

where ρ_w and μ_w are the density and viscosity calculated for the conditions at the wall. U_∞ is the undisturbed free-stream velocity and x

4785

CY-10 back

4785

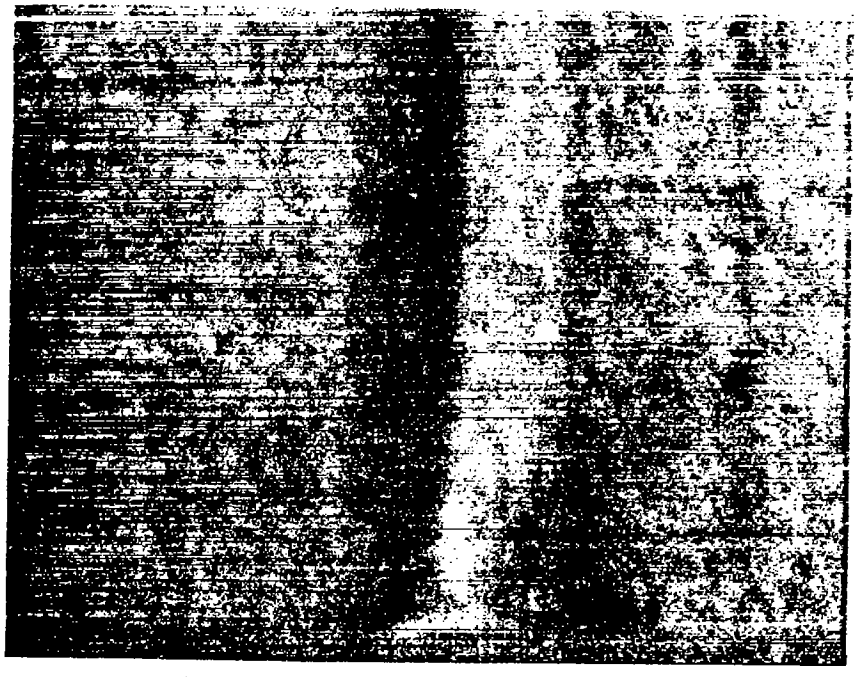

(a) 1.35 Inches after reflection.

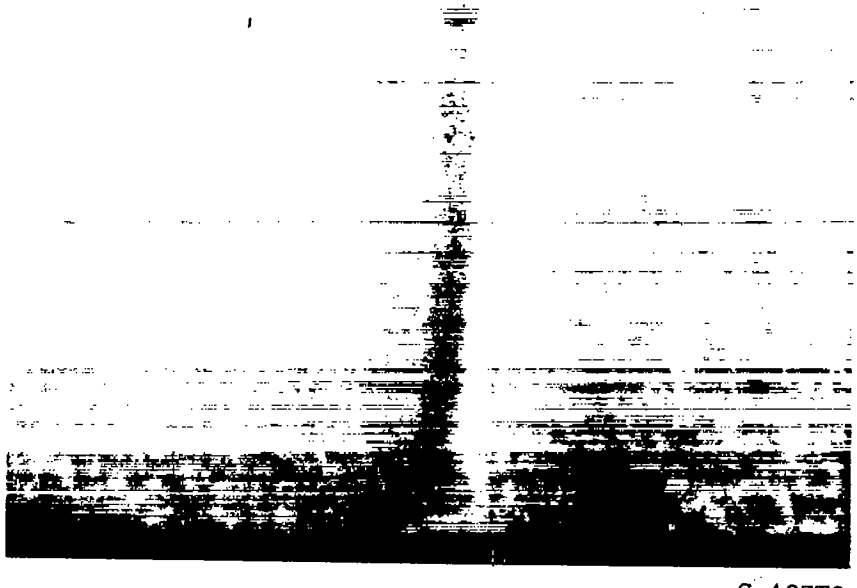

C-46576

(b) 1.65 Inches after reflection.

Figure 41. - Reflected shock wave in air ($\gamma = 1.4$) at $M_1 = 2.15$, $p_1 = 0.9$ inch mercury absolute, at increasing time after reflection.

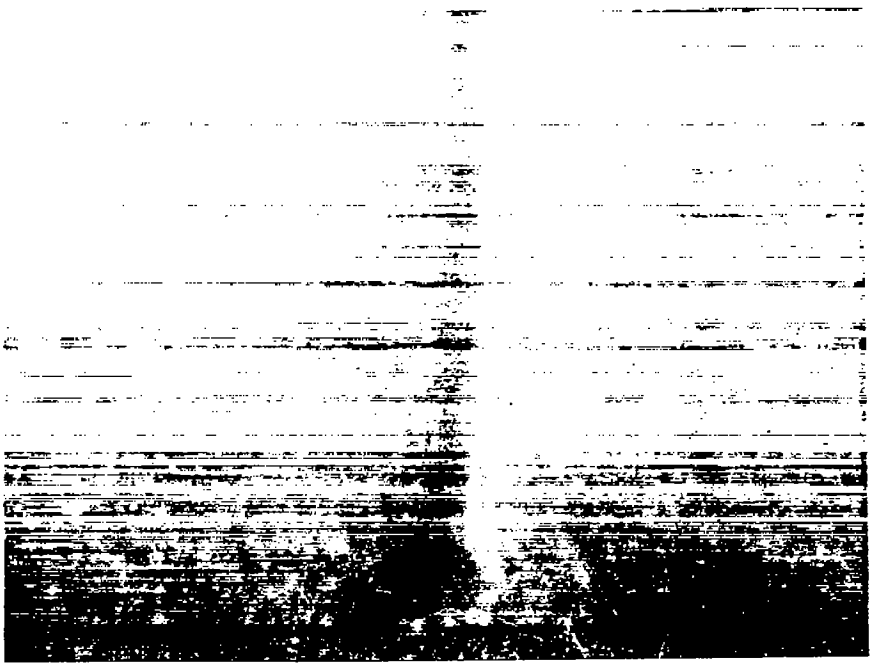

(c) 2.0 Inches after reflection.

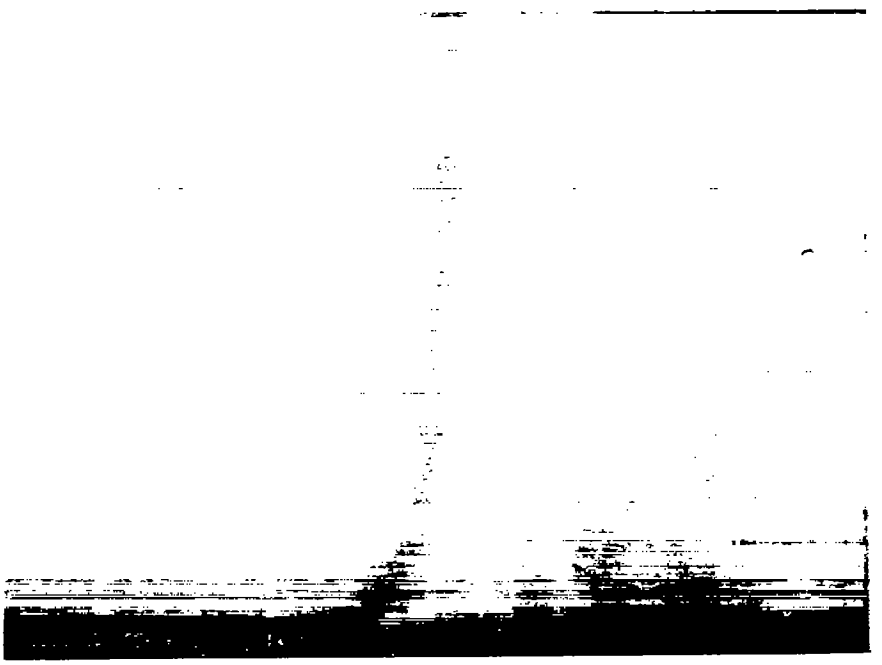

C-46560

(d) 2.05 Inches after reflection.

Figure 41. - Continued. Reflected shock wave in air ($\gamma = 1.4$) at $M_1 = 2.15$, $p_1 = 0.9$ inch mercury absolute, at increasing time after reflection.

4785

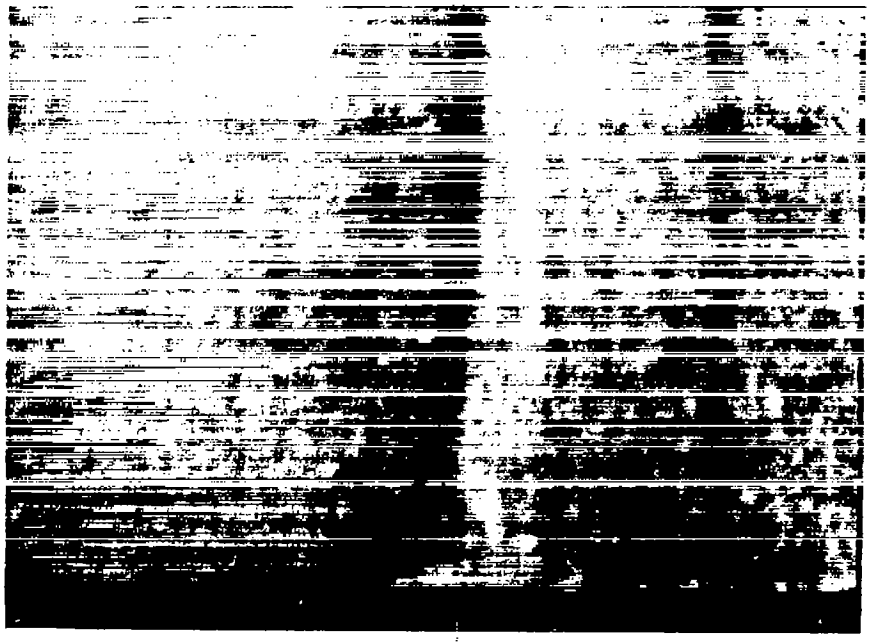

(e) 2.4 Inches after reflection.

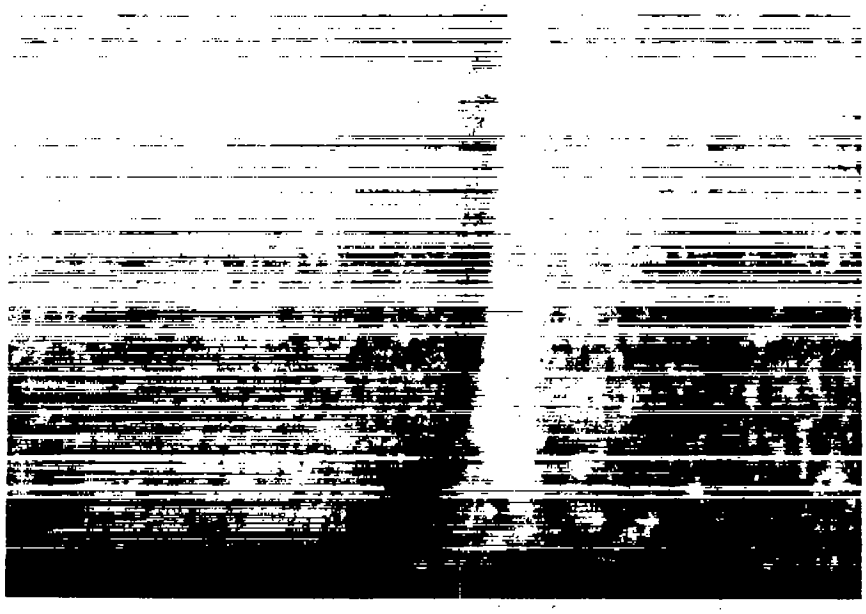

C-46561

(f) 2.6 Inches after reflection.

Figure 41. - Continued. Reflected shock wave in air ($\gamma = 1.4$) at $M_1 = 2.15$, $p_1 = 0.9$ inch mercury absolute, at increasing time after reflection.

4785

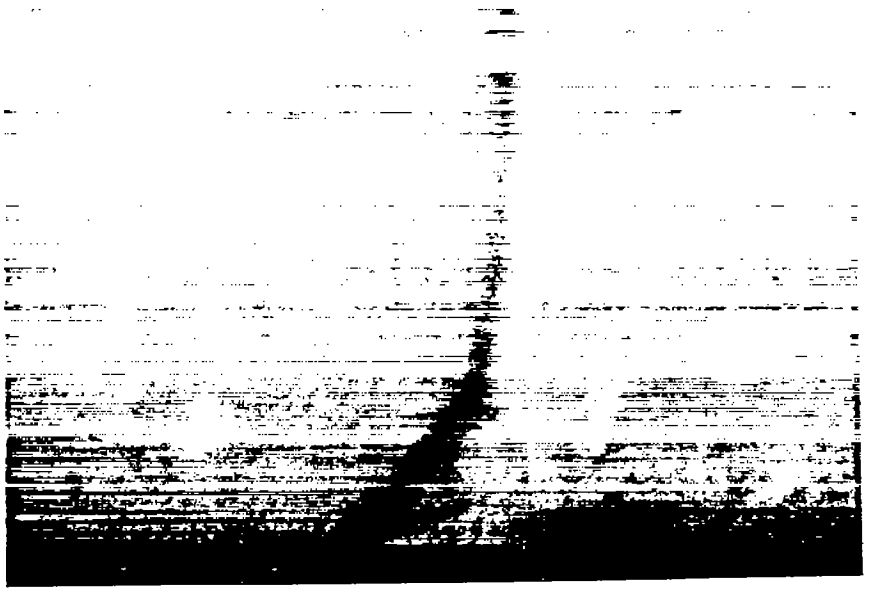

(g) 2.7 Inches after reflection.

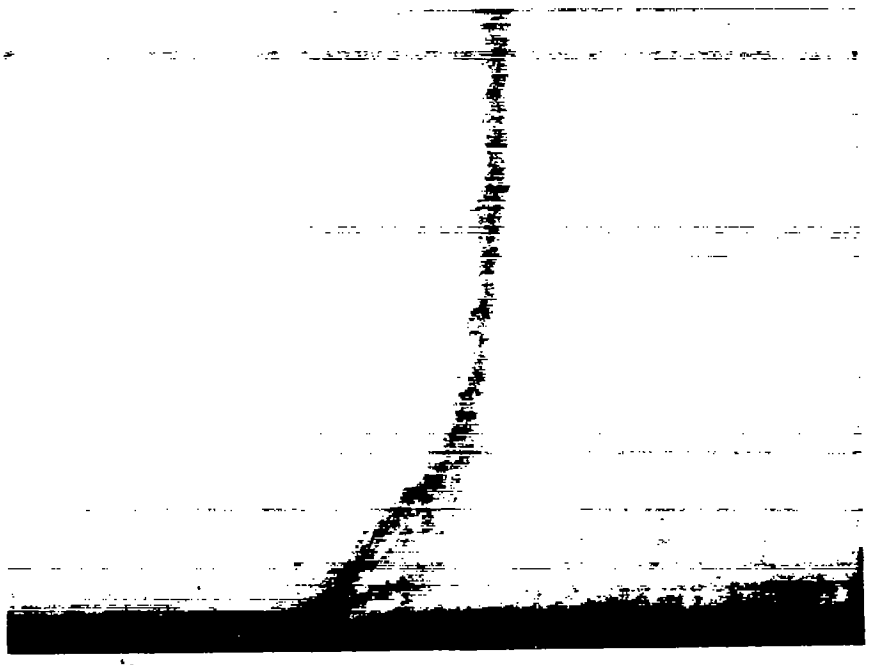

C-46562

(h) 3.1 Inches after reflection.

Figure 41. - Continued. Reflected shock wave in air ($\gamma = 1.4$) at $M_1 = 2.15$, $p_1 = 0.9$ inch mercury absolute, at increasing time after reflection.

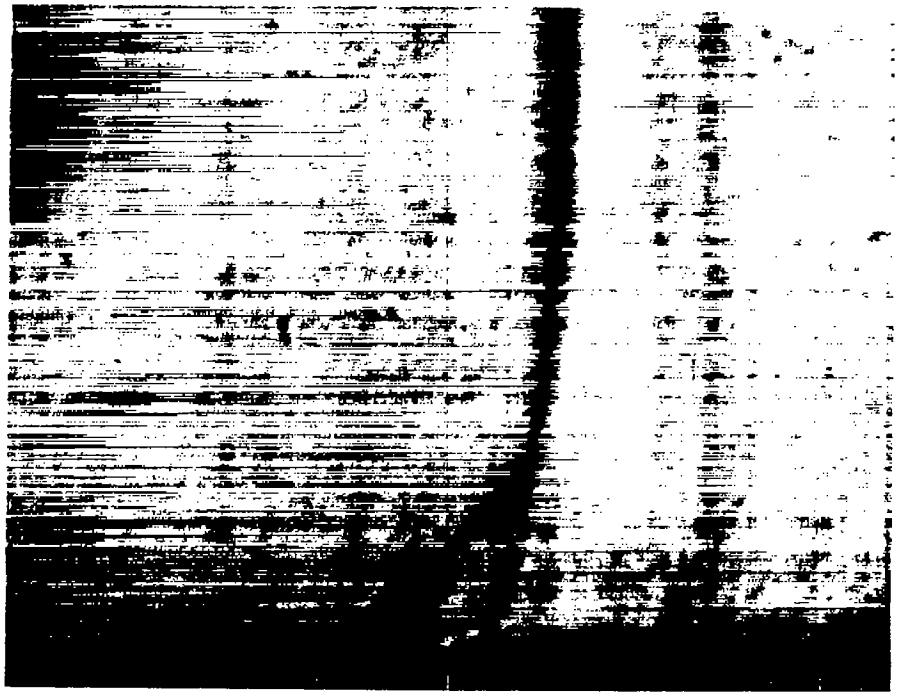

(i) 3.6 Inches after reflection.

C-46563

(j) 3.7 Inches after reflection.

Figure 41. - Continued. Reflected shock wave in air ($\gamma = 1.4$) at $M_1 = 2.15$, $p_1 = 0.9$ inch mercury absolute, at increasing time after reflection.

4785

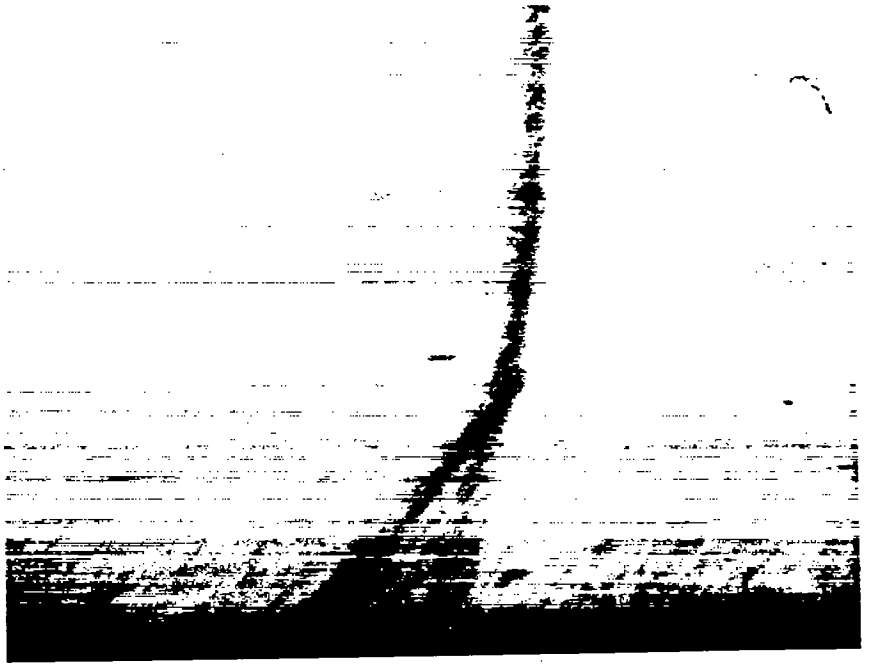

(k) 4.2 Inches after reflection.

CY-11

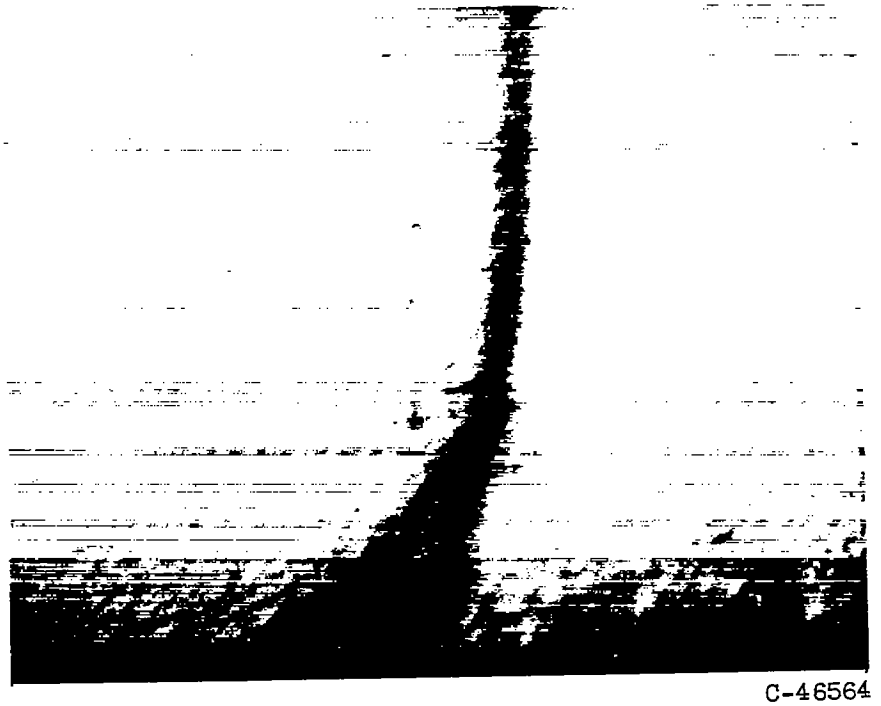

C-46564

(l) 4.3 Inches after reflection.

Figure 41. - Continued. Reflected shock wave in air ($\gamma = 1.4$) at $M_1 = 2.15$, $p_1 = 0.9$ inch mercury absolute, at increasing time after reflection.

4785

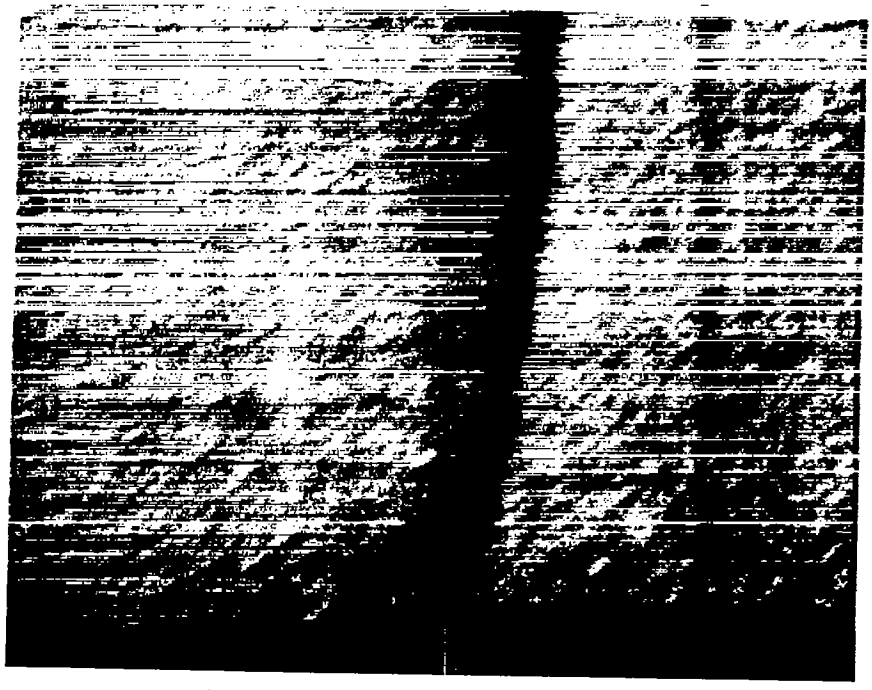

(m) 5.6 Inches after reflection.

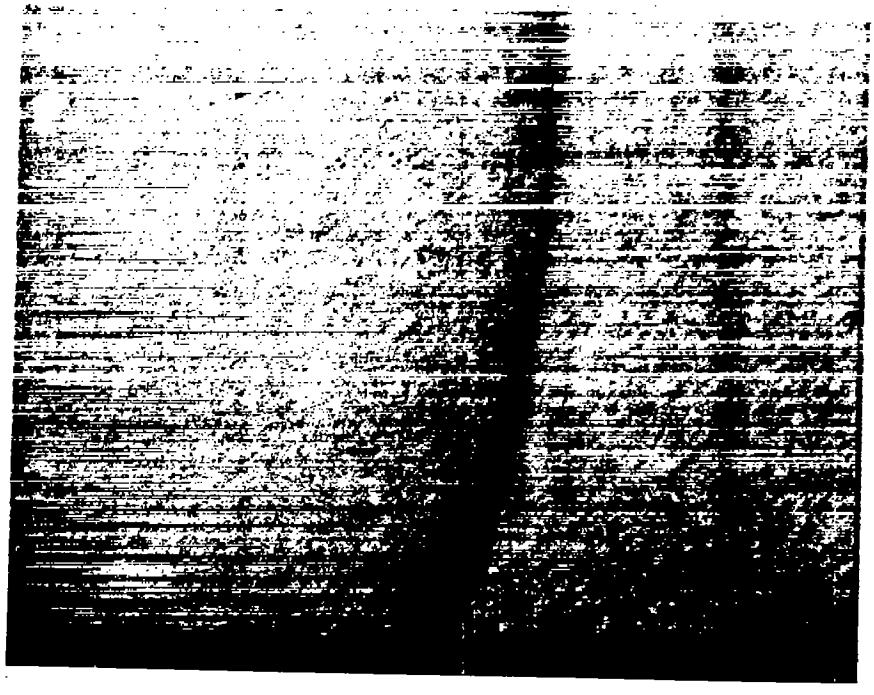

C-46565

(n) 6.0 Inches after reflection.

Figure 41. - Continued. Reflected shock wave in air ($\gamma = 1.4$) at $M_1 = 2.15$, $p_1 = 0.9$ inch mercury absolute, at increasing time after reflection.

4785

CY-11 back

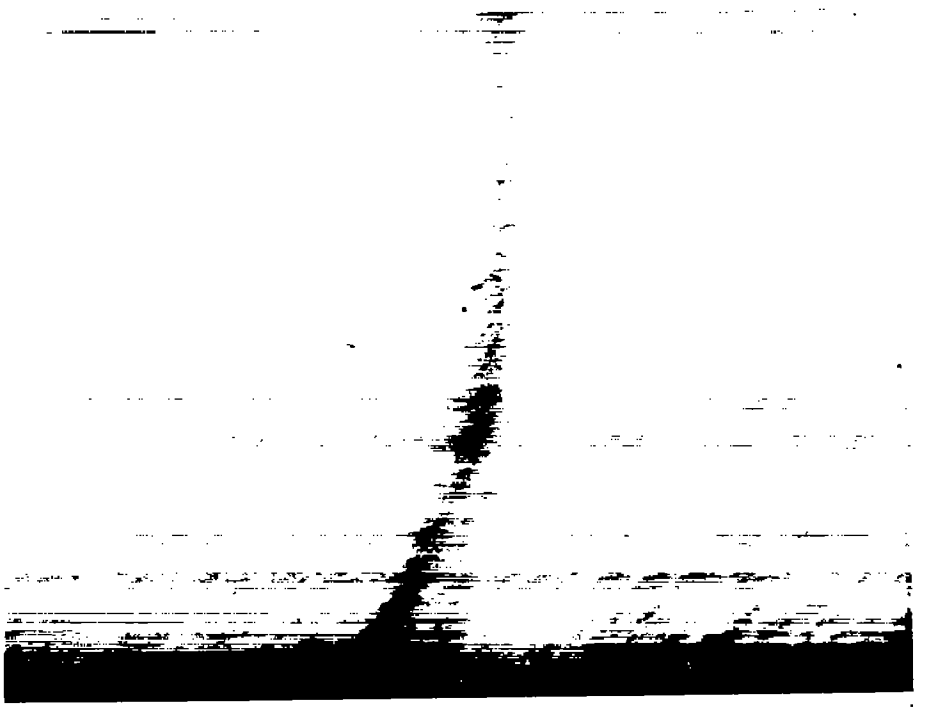

C-46566

(o) 6.25 Inches after reflection.

Figure 41. - Concluded. Reflected shock wave in air ($\gamma = 1.4$) at $M_1 = 2.15$, $p_1 = 0.9$ inch mercury absolute, at increasing time after reflection.

the distance back along the plate from the leading edge. In our case the velocity over the stationary wall after the passage of the initial shock is u_2. The distance the fluid at any point has traveled is given by this velocity u_2 multiplied by the time of travel. If we wish to define a Reynolds number in this manner, it becomes

$$Re \equiv \frac{\rho_w u_2 x \left(1 + \frac{U_s}{U_{rs}}\right) \frac{u_2}{U_s}}{\mu_w}$$

The x used here denotes the distance the reflected shock has traveled back from the reflecting wall to the point in question and, to allow the use of this convenient variable, it is necessary to include several extra factors to obtain a Reynolds number as just described. These factors allow for the differences in speed between the return shock and the initial shock, and between the initial shock and the following flow. Using this definition for Reynolds number, we may now make an estimate of the value of Re at which the boundary layer becomes turbulent. Re-examining figure 41 for the purpose of determining a reasonable value for x, the distance from the reflecting wall at which the laminar interaction has disappeared, it is clear that at best we can obtain only an estimate of this value by interpolating between pictures. If we say that the laminar interaction has disappeared between figures 41(m) and (n), we obtain thus a value for x of 0.462 feet. Calculating the Reynolds number as previously defined, we obtain (see appendix D)

$$Re_t = 1.47 \times 10^6$$

Thus, by varying the time after reflection of a reflected shock in air at an initial Mach number of 2.15 and interpreting the change in the interaction as caused by transition of the boundary layer from laminar to turbulent, we are able to calculate a Reynolds number at which the boundary layer behind the initial shock presumably becomes turbulent.

It is possible to make a cross check of this phenomenon by maintaining all variables constant (including the time after reflection) and varying only the pressure level at which the phenomenon occurs. A series such as this was made at $M_1 = 2.15$. The film was exposed each time in this series ≈ 320 μseconds after reflection. The pressure level in the low-pressure chamber was varied from 0.6 to 3.0 inches of mercury absolute in steps of 0.3 inch of mercury. This series of photos is presented in figure 42. Notice that here again the lower leg of the triangular pattern shortens and disappears. If we interpret this as before and make a similar interpolation and calculation, we obtain a value (see appendix D)

$$Re_t = 1.56 \times 10^6$$

4785

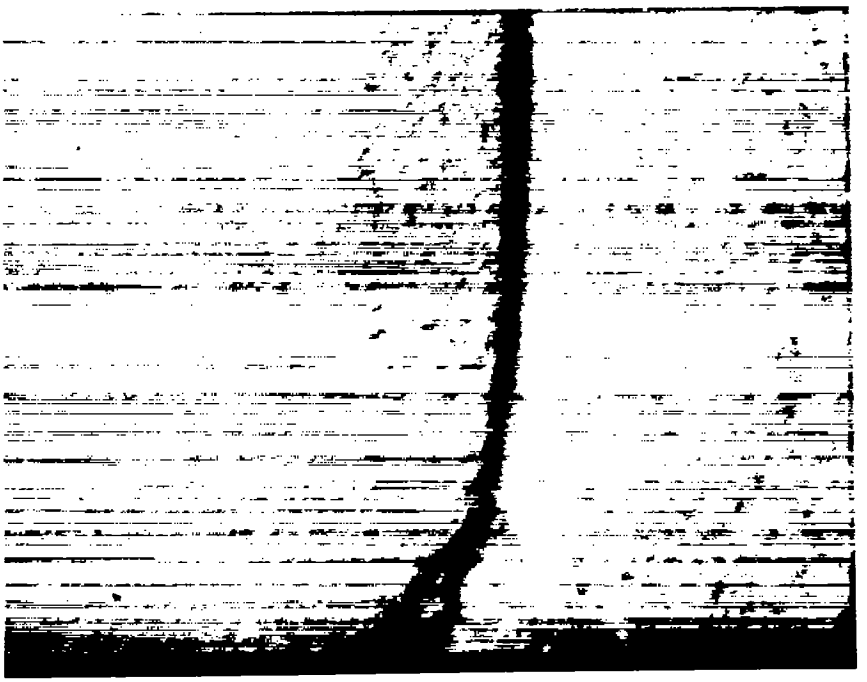

(a) p_1 = 0.6 inch mercury absolute.

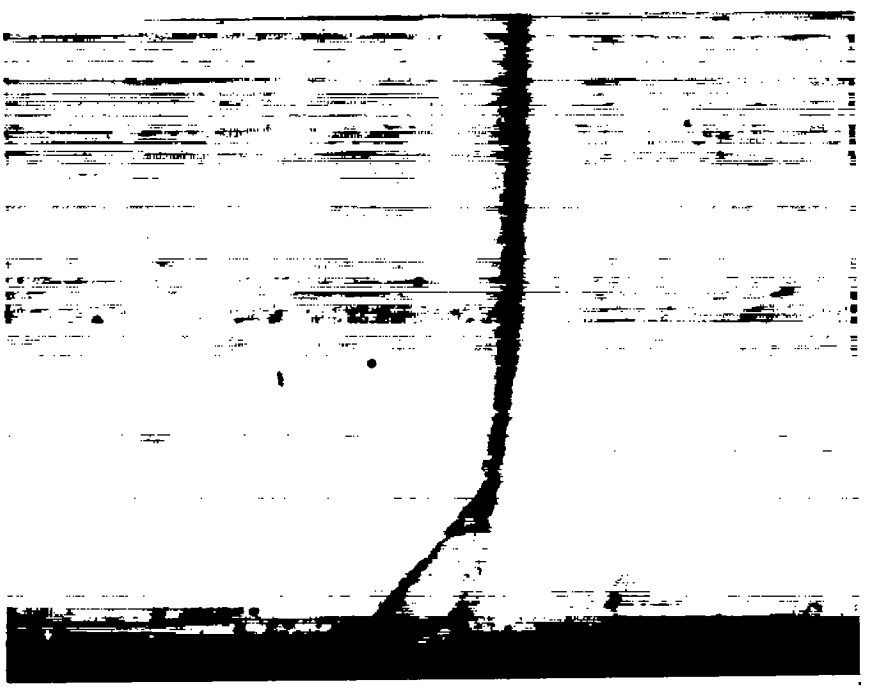

C-46567

(b) p_1 = 0.9 inch mercury absolute.

Figure 42. - Reflected shock wave in air (γ = 1.4) at M_1 = 2.15, approximately 3.9 inches after reflection, at increasing initial pressures (densities).

4785

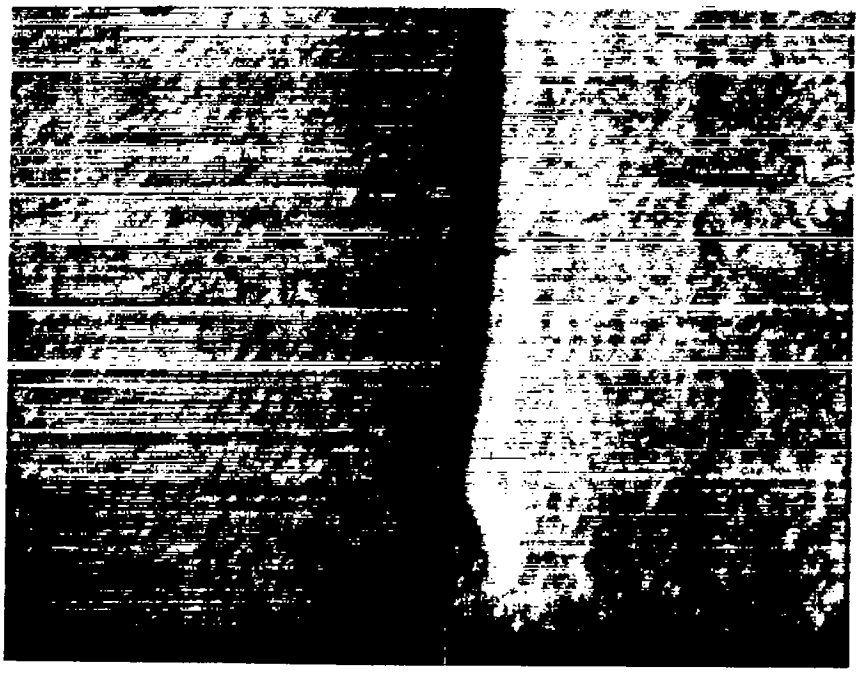

(c) p_1 = 1.2 inches mercury absolute.

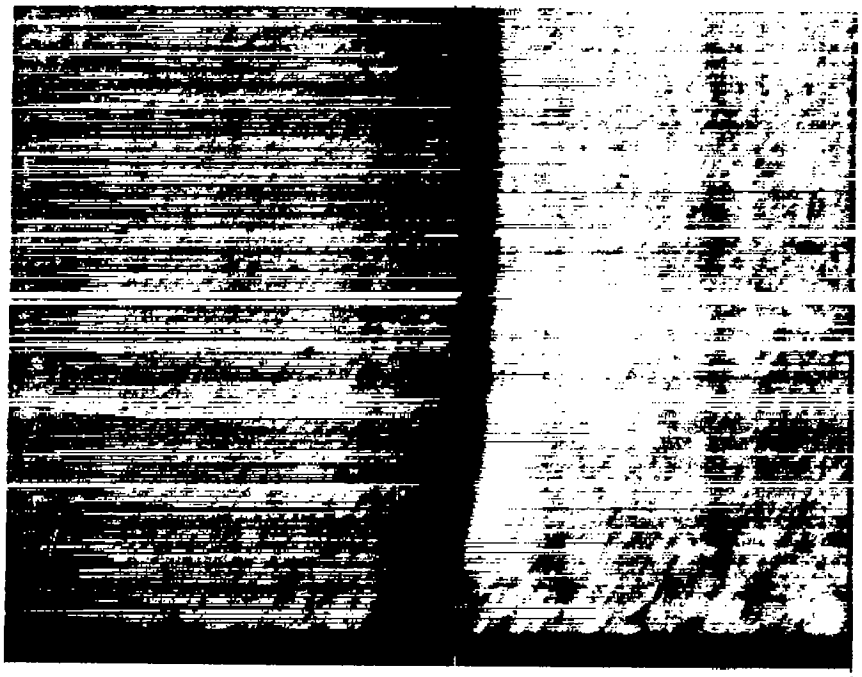

C-46568

(d) p_1 = 1.5 inches mercury absolute.

Figure 42. - Continued. Reflected shock wave in air (γ = 1.4) at M_1 = 2.15, approximately 3.9 inches after reflection, at increasing initial pressures (densities).

4785

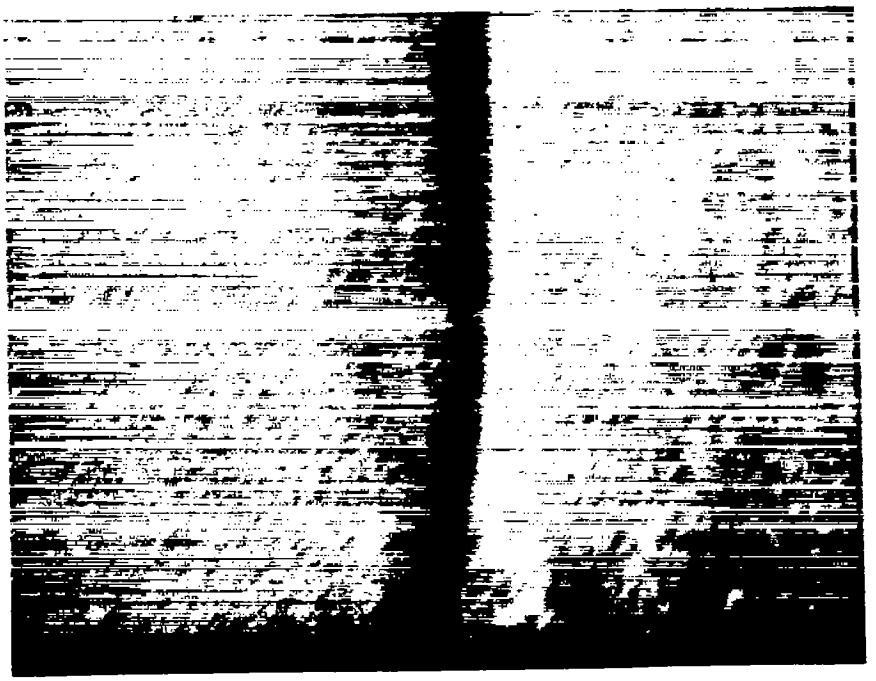

(e) p_1 = 1.8 inches mercury absolute.

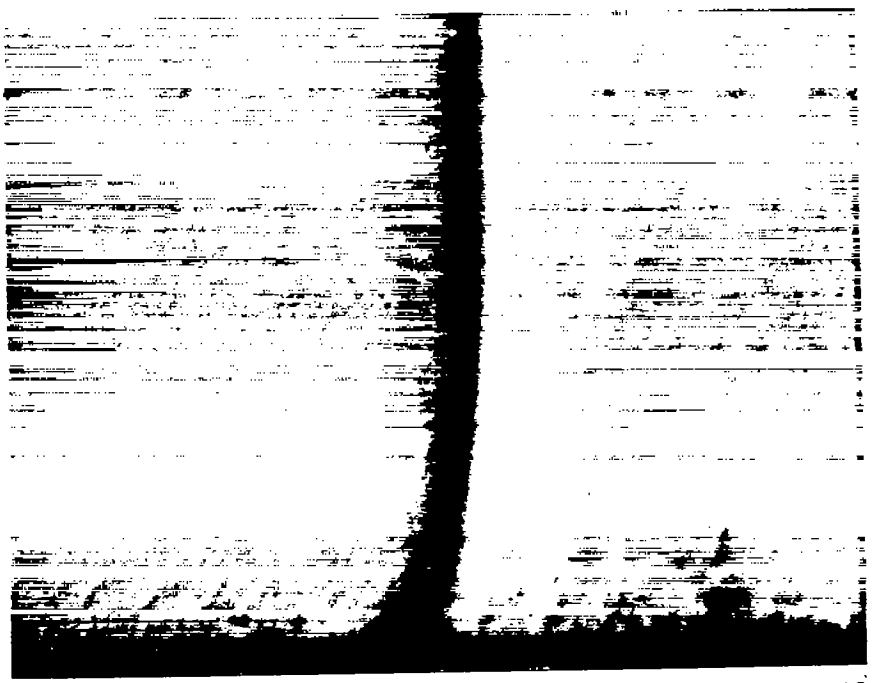

C-46569

(f) p_1 = 2.1 inches mercury absolute.

Figure 42. - Continued. Reflected shock wave in air (γ = 1.4) at M_1 = 2.15, approximately 3.9 inches after reflection, at increasing initial pressures (densities).

4785

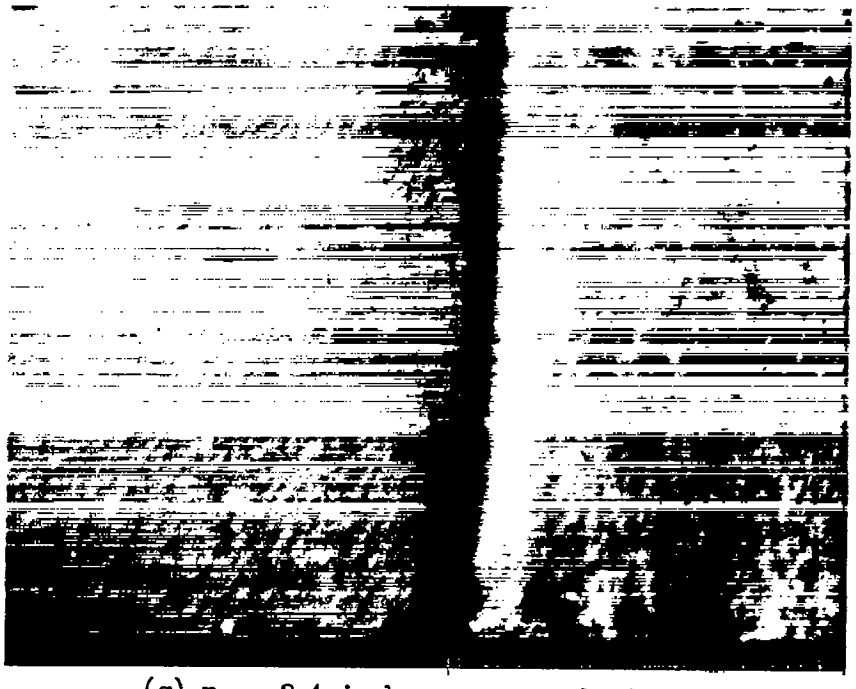

(g) p_1 = 2.4 inches mercury absolute.

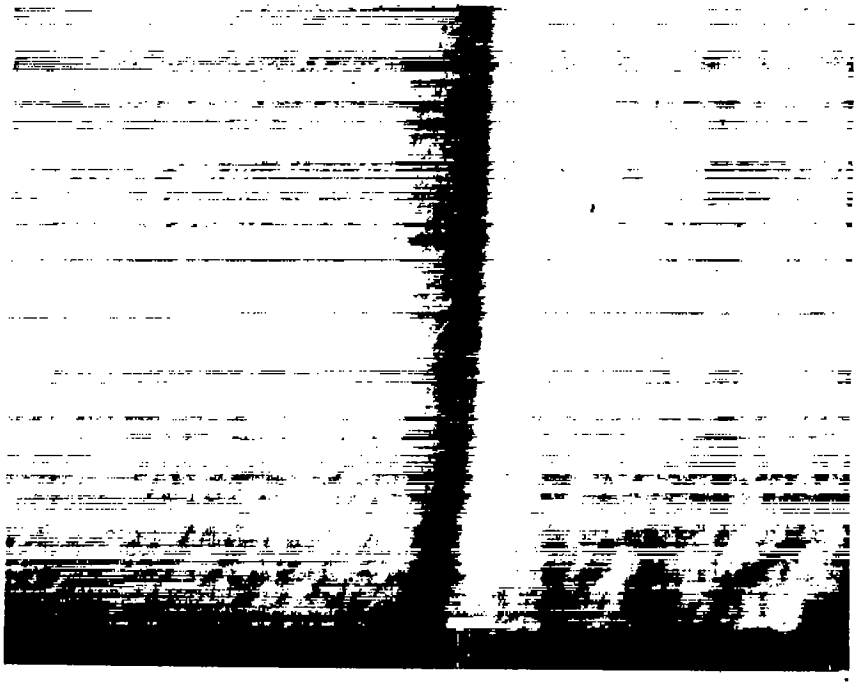

C-46570

(h) p_1 = 2.7 inches mercury absolute.

Figure 42. - Continued. Reflected shock wave in air (γ = 1.4) at M_1 = 2.15, approximately 3.9 inches after reflection, at increasing initial pressures (densities).

4785

CY-12

(i) p_1 = 3.0 inches mercury absolute.

Figure 42. - Concluded. Reflected shock wave in air (γ = 1.4) at M_1 = 2.15, approximately 3.9 inches after reflection, at increasing initial pressures (densities).

for the Reynolds number at which the laminar interaction disappears (at $M_1 = 2.15$ in air), and which we interpret to mean the transition of the boundary layer to turbulence. This value cross-checks with that obtained from the former series within 6 percent.

Certainly this is no more than a crude quantitative check of the transition of the boundary layer to turbulence. We assume that the phenomenon occurring is the detectable indication, in this experiment, of the transition of the boundary layer to turbulence and, of course, this may not be so. However, since there have been developed no really satisfactory techniques for this determination, this method may be used as a check to further experiments made along this line, until some improved techniques are devised.

A series of photos was made along with the latter Reynolds number variation experiment, at the same Mach number ($M_1 = 2.15$) and over the same range of pressure-level variation, but at approximately 1000 μseconds (≈3 times the previous delay time) after reflection. These photos are presented in figure 43. It is to be noted that the shock in these photos resembles very closely the shock interaction immediately after the disappearance of the laminar interaction. We conclude therefore that once the boundary layer becomes turbulent there are no further large changes in the interaction. Perhaps there is one further item of note. From figures 43(c) to (g) (pressures 1.8 to 3.0 in. Hg abs), the shock - boundary-layer interaction on the glass wall (which we see in the other view in the photos) has a number of noticeable undulations, and most interesting to note is the fact that these undulations reach out ahead of what might be called the average interaction, particularly at the top and bottom walls (or perhaps the corners). Since instantaneous pictures cannot tell us if this is a time varying or a steady situation, this phenomenon remains unexplained.

DISCUSSION OF THE GROWTH OF THE INTERACTION AS FURTHER VERIFICATION OF THE PROPOSED MODEL

We have seen now how the phenomenon which "handles the difficulty" predicted for the laminar boundary layer in region 2 appears, and how it may be described (fig. 36 of section IV). The shape of the interaction is easily calculated by using the proposed model and assumptions (appendix C), and the results check satisfactorily with the values obtained experimentally (figs. 28 and 29). From the pictures of figures

4785

CY-12 back

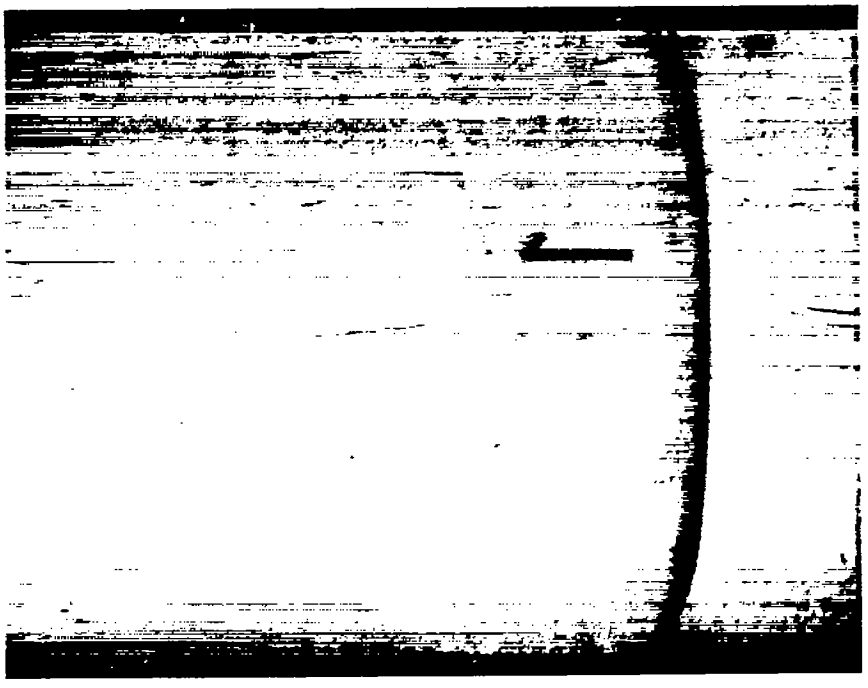

(a) p_1 = 1.2 inches mercury absolute.

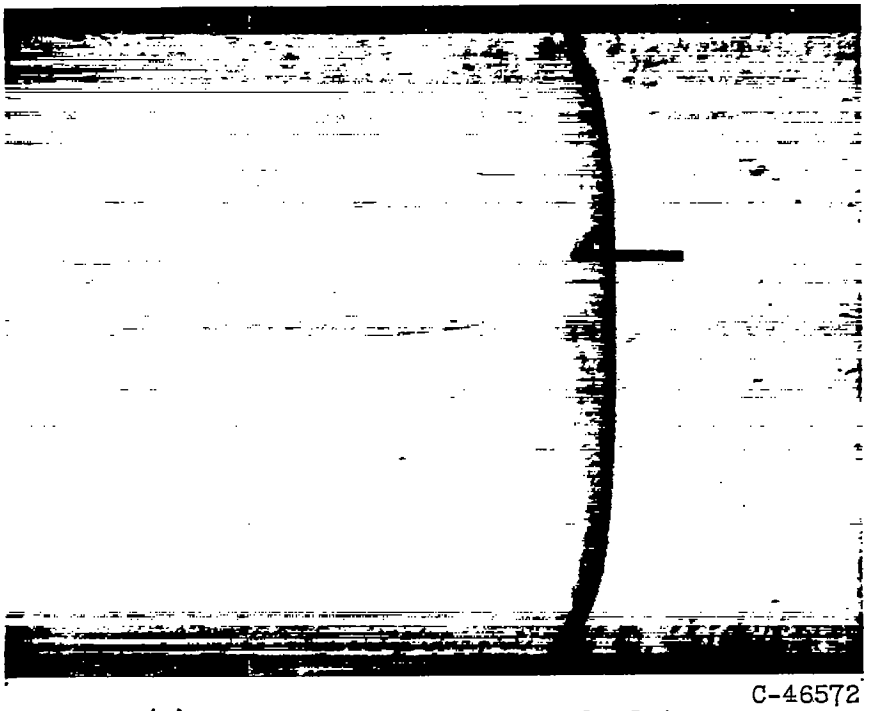

C-46572

(b) p_1 = 1.5 inches mercury absolute.

Figure 43. - Reflected shock wave in air (γ = 1.4) at M_1 = 2.15, approximately 11 inches after reflection, at various pressure levels.

4785

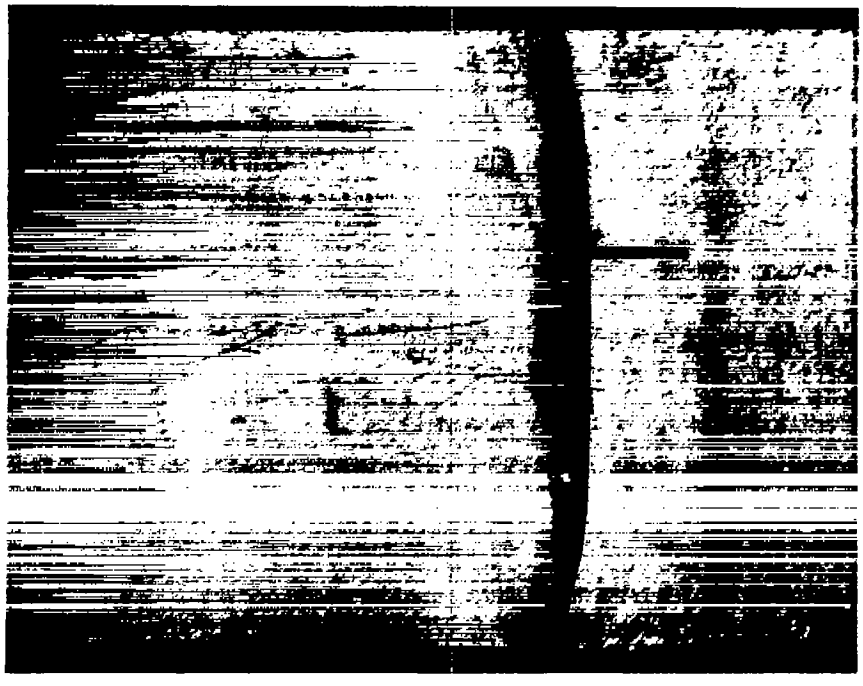

(c) p_1 = 1.8 inches mercury absolute.

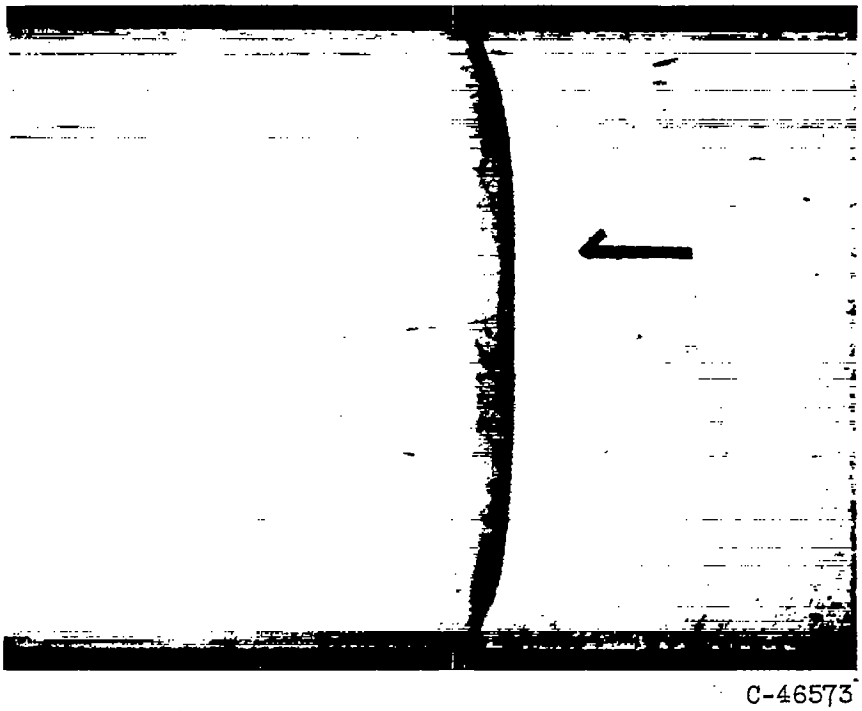

C-46573

(d) p_1 = 2.1 inches mercury absolute.

Figure 43. - Continued. Reflected shock wave in air (γ = 1.4) at M_1 = 2.15, approximately 11 inches after reflection, at various pressure levels.

4785

(e) p_1 = 2.4 inches mercury absolute.

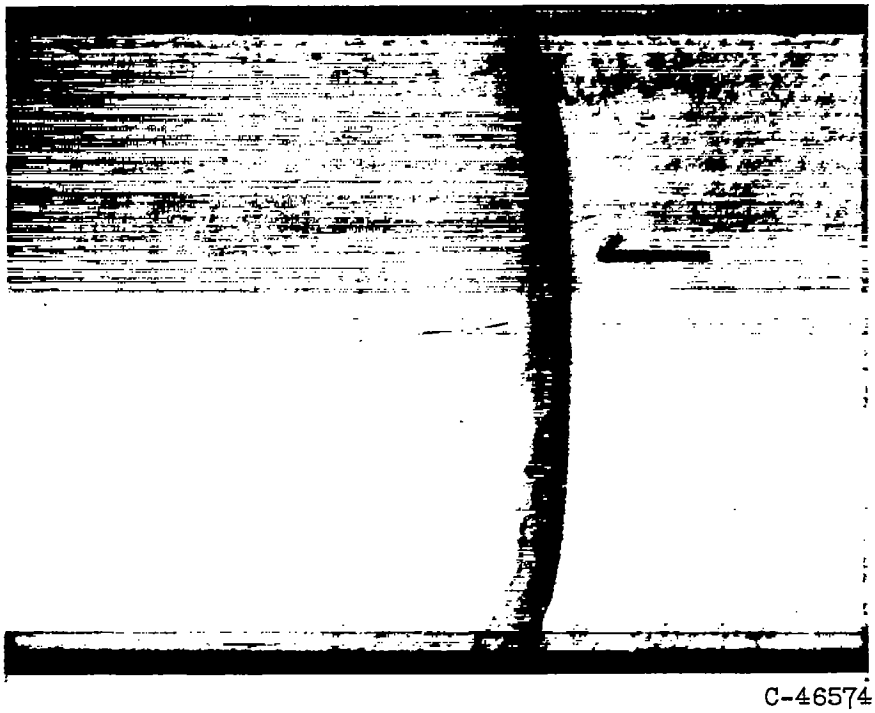

C-46574

(f) p_1 = 2.7 inches mercury absolute.

Figure 43. - Continued. Reflected shock wave in air (γ = 1.4) at M_1 = 2.15, approximately 11 inches after reflection, at various pressure levels.

4785

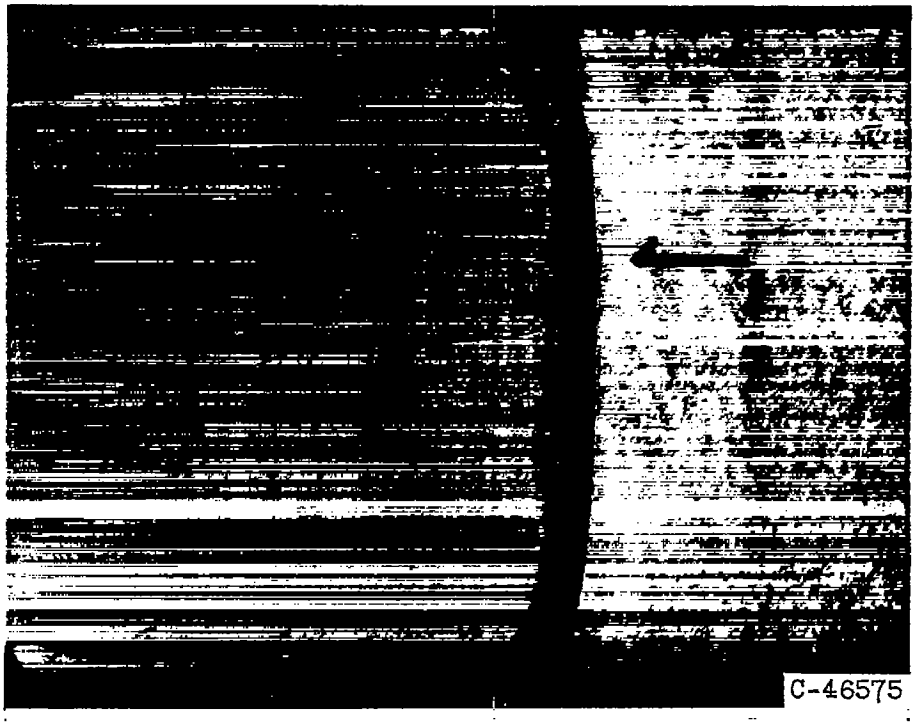

(g) p_1 = 3.0 inches mercury absolute.

Figure 43. - Concluded. Reflected shock wave in air (γ = 1.4) at M_1 = 2.15, approximately 11 inches after reflection, at various pressure levels.

4785

30 to 33, it is clear that the interaction pattern remains similar to itself (see y/ξ in table I) but grows with distance from the reflecting wall (i.e., with time). If we tabulate the information from figures 30 to 33, we have

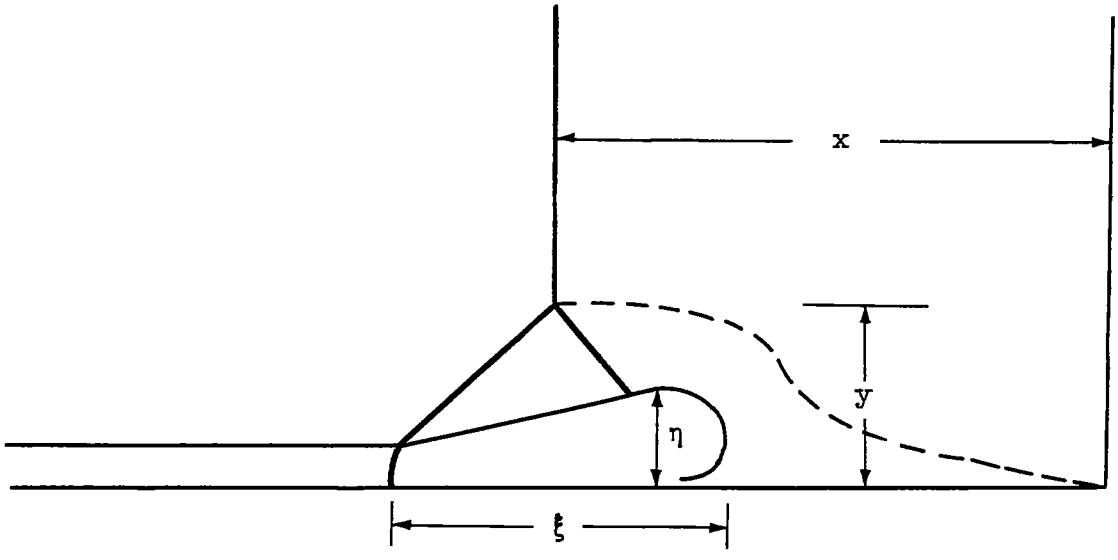

TABLE I

Figure	x, ft	y, ft	ξ, ft	η, in.	y/ξ	y/x
30	0.07	0.00716	0.0252	0.03	0.284	0.102
31	.14	.01365	.0496	.07	.275	.0975
32	.177	.0171	.0612	.095	.279	.0967
33	.22	.0218	.0796	.125	.274	.099

Since the interaction remains similar to itself as it grows (i.e., y/ξ is constant), it is sufficient, of course, to calculate the rate of growth of any linear dimension of the pattern in determining the time dependence of the growth of the entire interaction. For this purpose we choose to calculate the rate at which the dimension η of the figure varies with time.

If we imagine η to be the diameter of a two-dimensional volume (a cylinder of arbitrary length) being filled by a tube of boundary-layer fluid, we have the following picture:

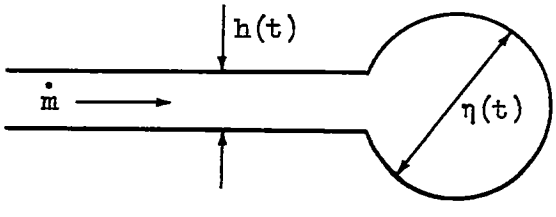

and we may write (if $\eta = 2r$), per unit width:

$$\dot{m} = \rho_{stag_{bl}} \frac{d(\text{vol.})}{dt} = \rho_{stag_{bl}} \frac{d(\pi r^2)}{dt} \tag{IV-2}$$

Now, if

$$\dot{m} = \rho_{bl}\bar{u}\, h \tag{IV-3}$$

and

$$h = k_1 t^{1/2} \tag{IV-4}$$

where $\dot{m}$ is mass flow per unit time per unit depth, h is height $h(t)$ of tube filling the cylinder, and $\bar{u}$ is the velocity in the boundary-layer tube relative to the cylinder being filled, then we may write (combining eqs. (IV-2), (IV-3), and (IV-4)):

$$\rho_{stag_{bl}} \frac{d(\pi r^2)}{dt} = \rho_{bl}\bar{u}k_1 t^{1/2} \tag{IV-5}$$

or (if we assume M_{bl} and $\bar{u}$ constant)

$$\frac{d(\pi r^2)}{dt} = k_2 t^{1/2}$$

Thus

$$r^2 = k_3 t^{3/2}$$

and then

$$r = \sqrt{k_3 t^{3/2}} \tag{IV-6}$$

Thus we have

$$\eta = k\, t^{3/4} \tag{IV-7}$$

Thus we would expect the laminar interaction of region 2 to grow as $t^{3/4}$ (or, since $x = \bar{u}t$, as $x^{3/4}$). Examining table I, we notice that $\eta \propto x^1$ as accurately as we can measure it, and this compares favorably with the variation predicted by the rather crude analysis just given.

As we shall see in the following section, the reflected shock does not return at constant speed. This conflicts with the assumption that $\bar{u}$, the fluid pickup speed, is constant. However, assuming a time dependence for $\bar{u}$ would not change the argument for the growth of the phenomenon, and would improve the quantitative estimate only slightly. An estimate (appendix E) of the size of the phenomenon calculated by using the previous analysis gives

4785

$$\eta = \sqrt{\frac{8}{3\pi} \frac{\rho_{bl}}{\rho_{stag_{bl}}} hx} \qquad \text{(IV-8)}$$

For $M_1 = 2.15$ at a distance $x = 0.22$ foot from the reflecting wall, equation (IV-8) gives $\eta = 0.098$ inch. This compares favorably with the value from table I of $\eta = 0.12$ inch at $x = 0.22$, if we consider that the value of h can only be estimated. We have in fact used $h = \delta^*$ (see appendix E), and this estimate could be off by a factor of 2 or 3 in describing the effective height of boundary-layer fluid entering and filling the growing cylinder of stagnation fluid.

CY-13

We have mentioned previously the possibility of a "re-entrant jet" (section IV). If a portion of the main fluid does pass under the bubble as a re-entrant jet, then we would expect our measurement of η to be somewhat higher than that which we calculated from the preceding analysis, the jet (invisible in any of our photos) raising the bubble somewhat away from the wall. Our measurements and calculation are consistent with this possibility. Perhaps the existence of a re-entrant jet explains the discrepancy between our calculated rate of growth proportional to $x^{3/4}$ and the measured linear rate. It is clear in any case that the model herein proposed suggests that the reflected shock is picking up and carrying with it a portion of the oncoming fluid (the fluid in the boundary-layer stagnation-pressure bubble). With the growth just described, the oblique shock which appears to initiate the entire interaction phenomenon and which precedes the main normal shock "processes" increasing amounts of main fluid. The leading edge of this oblique shock advances at a speed greater than that of the shock and thus maintains a growing lead over the main shock as the reflection proceeds into the oncoming flow. This type of interaction may certainly be called violent, since it leads to disturbances many times the size of boundary layer involved.

V - ATTENUATION OF THE REFLECTED SHOCK

MODEL FOR THE ATTENUATION PHENOMENON

If we examine the model for the interaction of the shock with the laminar boundary layer as presented in detail in figure 36, we note that it will appear as in figure 44 if we consider the entire interaction in the shock tube.

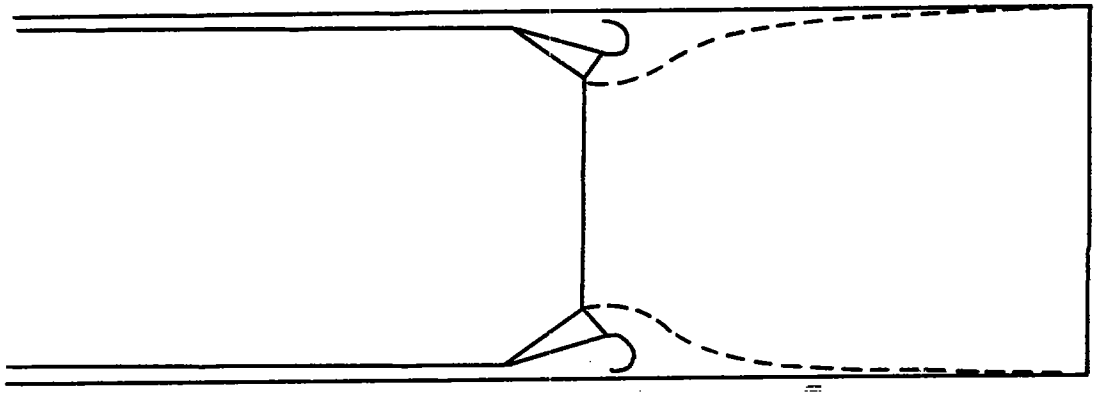

Figure 44. - Reflected shock traveling in shock tube.

It was pointed out in section IV, and it is clear from figure 44, that the fluid approaching the shock may be divided into three parts. First, there is the boundary-layer fluid which cannot enter the region behind the shock and collects in a "ball" of fluid under the foot of the shock. Then there is that part of the main fluid which passes through the bifurcated portion of the shock and into the region behind the shock between the dotted lines of figure 44 and the walls (top and bottom). Last, there is the remaining larger part of the main fluid which passes through the single normal shock and is presumably contained by the dotted-line boundaries of figure 44 in the region behind the reflected shock. This division of flow implies that the fluid being acted upon by the reflected shock wave is separated into three portions by the interaction, each portion being processed in a different manner on its path into the region behind the shock. The boundary-layer fluid which cannot manage the shock pressure rise collects in a ball at the foot of the shock. The main fluid which passes through the bifurcation forms a sort of "super bubble" over the inner ball of collected boundary-layer fluid, and remains separated from the major portion of main fluid which passes through the single normal shock. Since the triple point follows approximately a linear growth as the phenomenon grows, the dip (at top and bottom) in the trace of fluid particles that have passed through the triple point indicates that there is motion of the central portion of main fluid after

it is passed through the shock. Let us consider this main body of fluid passing through the normal shock. It is clear that the situation here differs from that in which the flow is brought to rest by an ideal reflected shock. There is no reason to assume in the present case that the fluid compressed by the shock is brought to rest in the region behind the reflected shock anywhere but at the reflecting wall. In fact, the dark vertical swath of figure 25 (which coincides with the opening dip in the dotted boundary lines for this flow) suggests that another milder (at least in gradient) compression does take place before the fluid that has passed through the normal shock is finally brought to rest at the reflecting wall. From an over-all point of view of the phenomenon, one might say that the main fluid sacrifices a part of itself to form a nozzle (or preferably, a diffuser) and in this manner overcomes the difficulty introduced by the energy-deficient fluid in the boundary layer. For the purpose of the subsequent analysis it assumed that the nozzle is formed by all the fluid passing between the triple points and the walls. We realize, of course, that the picture of the phenomenon as represented in figure 44 is by no means steady, because of the growth of the interaction as the reflected shock travels back up the tube. Thus the dotted lines of figure 44 outline the flow instantaneously and are not streamlines of the flow at all. However, the growth is not very rapid. In fact, from table I we can see that y, the height of the triple point from the wall grows as $0.095\ x$, where x is the distance of the phenomenon from the reflecting wall. Thus it is not unreasonable to examine the situation with the effects of the growth considered, but still assuming that at any instant the phenomenon does not differ any great amount from, and is reasonably well depicted by, the steady picture that it resembles. At a given instant, then, we have the following description (fig. 45) of the portion of the main fluid passing through the single normal shock.

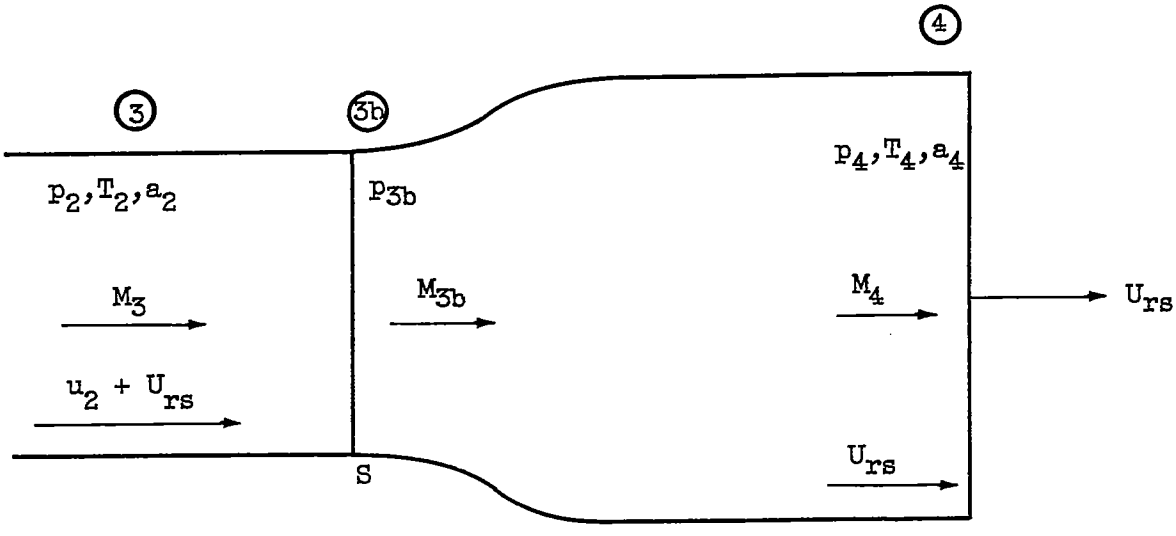

Figure 45.

We may now write (in the coordinate system moving with the shock, and assuming the picture of fig. 45 is a steady one)

$$M_3 a_2 = (u_2 + U_{rs}) \tag{V-1}$$

or

$$U_{rs} = M_3 a_2 - u_2 \tag{V-2}$$

Also, by definition and by the boundary condition that the fluid velocity at the wall is the same as that of the reflecting wall, we have at station 4: 4785

$$U_{rs} = M_4 a_4 \tag{V-3}$$

Since the total temperature is the same at stations 3 and 4 we may write

$$\frac{a_4}{a_2} = \sqrt{\frac{T_4}{T_2}} = \sqrt{\frac{1 + \frac{\gamma - 1}{2} M_3^2}{1 + \frac{\gamma - 1}{2} M_4^2}} \tag{V-4}$$

Combining equations (V-2), (V-3), and (V-4), we have the relation

$$\frac{M_4}{\sqrt{1 + \frac{\gamma - 1}{2} M_4^2}} = \frac{M_3 a_2 - u_2}{a_2 \sqrt{1 + \frac{\gamma - 1}{2} M_3^2}} \tag{V-5}$$

Since a_2 and u_2 vary very slightly due to attenuation of the initial shock wave, over the distance of interest to us they are constant and known. Thus equation (V-5) is a relation connecting M_3 with M_4. If we assume now that the flow in figure 45 is isentropic from station 3b to 4, we can then write

$$\frac{M_{3b}}{\left(1 + \frac{\gamma - 1}{2} M_{3b}^2\right)^{\frac{\gamma+1}{2(\gamma-1)}}} = \left(\frac{A_4}{A_{3b}}\right) \frac{M_4}{\left(1 + \frac{\gamma - 1}{2} M_4^2\right)^{\frac{\gamma+1}{2(\gamma-1)}}} \tag{V-6}$$

which follows from continuity and isentropy. If we now write the normal shock relations connecting M_3 and M_{3b}

$$M_3^2 = \frac{(\gamma - 1)M_{3b}^2 + 2}{2\gamma M_{3b}^2 - (\gamma - 1)} \tag{V-7}$$

we have a completely determined problem which may be solved by iteration once the dependence of A_4/A_{3b} on x (the distance from the reflecting wall) is known. For this purpose we might use the growth relation arrived at in section IV ($\eta \propto x^{3/4}$). However, the physical data are also available for the case $M_1 = 2.15$ and, as closely as we can make the measurements, they suggest a linear dependence on x. If we are to assume that this is so, we may write $y = ax$ for the height of the triple point from the wall. Then, since the interaction also takes place on the side walls (the glass), and $A_4 = S_1S_2$ is the area of our rectangular tube, we have

4785

$$A_{3b} = A_4 - 2ax(S_1 + S_2) + 4a^2x^2 \qquad \text{(V-8)}$$

from which to calculate A_4/A_{3b}. Thus the problem is completely solved (under our assumptions) in the region of the laminar-boundary-layer shock-wave interaction.

Recalling that the laminar interaction eventually disappears when the boundary layer becomes turbulent, we should point out that the whole attenuation model just presented will no longer be valid in the turbulent interaction region. In fact, since photographs of the interaction made at times when the boundary layer has become turbulent show the shock to be only slightly distorted from normal, we would expect the shock wave, after the laminar interaction has disappeared, to return to the theoretical reflected shock speed.

In the following section we will attempt a calculation based on the method just presented, and some comparisons will be made with available experimental data.

CALCULATION OF ATTENUATION OF THE REFLECTED SHOCK SPEED AT $M_1 = 2.15$ IN AIR

At a nominal value of $M_1 = 2.15$, we can calculate with the aid of figure 7 the Mach number of the initial shock just before it reflects from the wall 144 inches from the diaphragm station. Figure 7 (curve from ref. 8) gives:

$$\frac{\Delta p_{2,d}}{p_2} = \frac{0.124}{\left(\frac{U_s}{u_2}\right)^{7/5}\left(\frac{d}{x}\right)^{4/5}\left(\frac{a_2 d}{\nu_2}\right)^{1/5}}$$

which for our case is

$$\frac{\Delta p_{2,d}}{p_2} = 0.0208\ x^{4/5}$$

at $x = 12$ feet we have

$$\frac{\Delta p_{2,d}}{p_2} = 0.152$$

Thus

4785

$$p_{2,actual} = 0.85\ p_{2,ideal}$$

and, since we have nominal M_1 of 2.15,

$$\frac{p_{2,ideal}}{p_1} = 5.23$$

$$5.23 \times 0.85 = 4.45 = \frac{p_{2,actual}}{p_1}$$

Thus M_1 before reflection is 1.99 (for nominal $M_1 = 2.15$). Immediately we know (from fig. 10)

$$M_3 = 1.726$$

and from equation (V-7)

$$M_{3b} = 0.634$$

M_4 also has the value 0.634 just at reflection. Now if we calculate A_{3b} from equation (V-8), letting $a = 0.095$ (experimental value), we have at $x = 1/2$ inch:

$$\frac{A_{3b}}{A_4} = 0.93$$

Thus we

(1) Choose $M_3 = 1.70$

(2) From equation (V-5), $M_4 = 0.6148$

(3) From equation (V-6) and knowing $A_{3b}/A_4 = 0.93$, we have $M_{3b} = 0.7057$

(4) From equation (V-7), $M_3 = 1.487 \neq 1.70$

Since the value chosen for M_3 does not coincide with the calculated value we must reestimate M_3. Repeating this procedure, we try

(1) $M_3 = 1.65$

(2) From equation (V-5), $M_4 = 0.5727$

4785

(3) From equation (V-6), $M_{3b} = 0.645$

(4) From equation (V-7), $M_3 = 1.682 \neq 1.65$

Once more we try

(1) $M_3 = 1.657$

(2) We calculate $M_4 = 0.58$

(3) And $M_{3b} = 0.676$

(4) From which $M_3 = 1.66$

Check

Actually the procedure can be simplified very much by using the chart of figure 46. By choosing an M_3 and then going through the chart following the arrows, the iteration procedure was very rapid and the whole procedure was repeated at 1/2-inch intervals for x from 0 to 4 inches. The results are tabulated in table II.

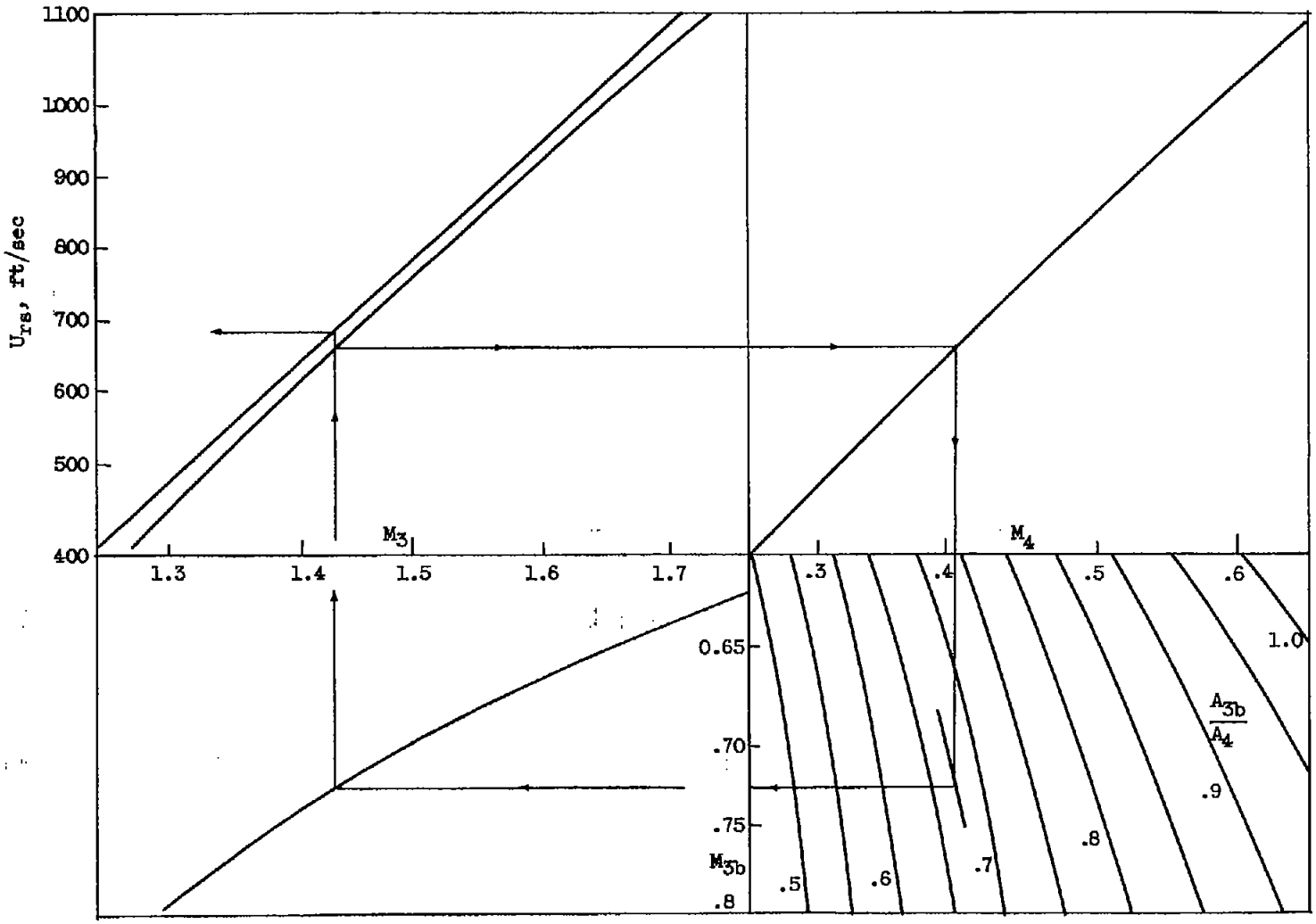

Figure 46. - Chart for iteration procedure necessary in calculating attenuating effect of the region 2 shock-wave - boundary-layer interaction on strength of reflected shock. $\gamma = 1.4$; $M_{1\ nominal} = 2.15$; shock tube, 142 inches long.

TABLE II

[$M_{1,nominal}$ = 2.15; M_1 at 144 inches = 1.99;
a_2 = 1461 ft/sec; u_2 = 1400 ft/sec]

x	A_{3b}/A_4	M_3	M_4	M_{3b}	U^*_{rs}	p_2/p_1	p_{3b}/p_2	p_{3b}/p_1	p_4/p_1	p_4/p_{3b}
0	1	1.726	0.634	0.634	1128	4.45	3.31	14.75	14.75	1.0
1/2	0.93	1.657	.58	.676	1022		3.03	13.5	14.62	1.08
1	.862	1.57	.514	.677	893		2.71	12.1	13.75	1.14
$1\frac{1}{2}$	.797	1.527	.481	.6915	830		2.55	11.37	13.40	1.18
2	.734	1.471	.438	.7115	750		2.36	10.51	12.96	1.23
$2\frac{1}{2}$	.672	1.422	.397	.728	678		2.192	9.79	12.50	1.28
3	.614	1.376	.361	.748	610		2.04	9.1	12.08	1.33
$3\frac{1}{2}$	.557	1.335	.326	.767	550		1.914	8.54	11.71	1.372
4	.5025	1.295	.294	.792	493		1.79	7.98	11.35	1.425

It is interesting to note that during the laminar interaction period the reflected shock speed falls monotonically and rather rapidly. It seems that such a drop in speed could hardly go unnoticed, and in fact it has not. However, on an xt diagram (the usual experimental method for determining shock speeds) acceleration appears as curvature of the shock trace. Over the short distance in which this slowdown occurs (the first few inches after reflection) this curvature has perhaps gone unnoticed. Let us examine this to see why. If we build an xt diagram (fig. 47) using the data in table II for the reflected shock speed (in which the shock slows down from 1128 ft/sec to half that speed in just a few inches), we note that the curvature is quite easily overlooked. In fact since the shock later accelerates (perhaps in part because of the disappearance of the previously mentioned attenuation configuration when the boundary layer becomes turbulent) the "S" shape encountered because of deceleration and acceleration could easily be averaged out as a straight line and the conclusion drawn that the reflected shock simply travels at lower speeds just after reflection. This has been observed experimentally. Experimental work done at Aberdeen Proving Grounds seems to bear this out.[1]

[1]Private communication from R. A. Strehlow, Dec. 1956.

4785

CY-14

4785

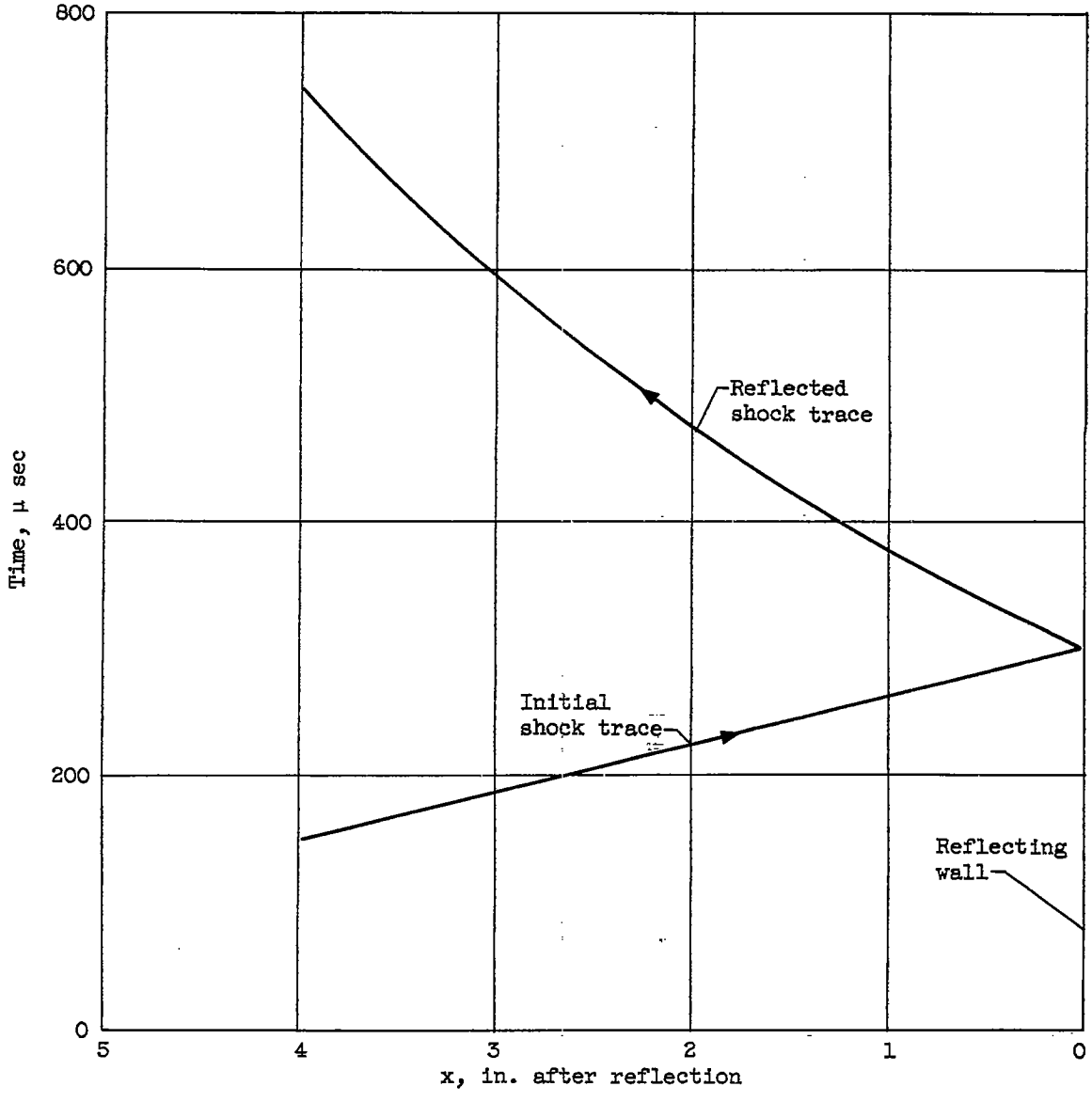

Figure 47. - Constructed xt diagram from calculation of reflected shock velocity, showing deceleration of reflected shock. $M_1 = 2.15$; $\gamma = 1.4$.

According to their findings, in all the gases for which they investigated experimental reflected shock velocity, they found that, for $M_1 > 1.3$ (the value predicted for the first pressure crossover in section III was 1.33 for $\gamma = 1.4$), the reflected shock velocity was less than the theoretical value near the reflecting wall. In all gases but argon (the only monatomic gas investigated), the reflected shocks later accelerated. In the case of nitrogen the reflected shock speed after acceleration corresponded almost exactly to the theoretical value. This experimental information seems to bear out, at least qualitatively, the attenuation model proposed. In figure 48 is presented an experimental diagram[1] for a shock traveling in nitrogen with $M_1 = 2.06$. The concave upward curvature of the reflected shock trace just after reflection is clearly visible. Following this deceleration is the acceleration previously mentioned which raises the reflected shock velocity very nearly to the value which is theoretically expected.

4785

CY-14 back

[1]The author is indebted to Dr. Roger A. Strehlow of the Ballistics Research Laboratory at Aberdeen Proving Grounds for making this picture available.

4785

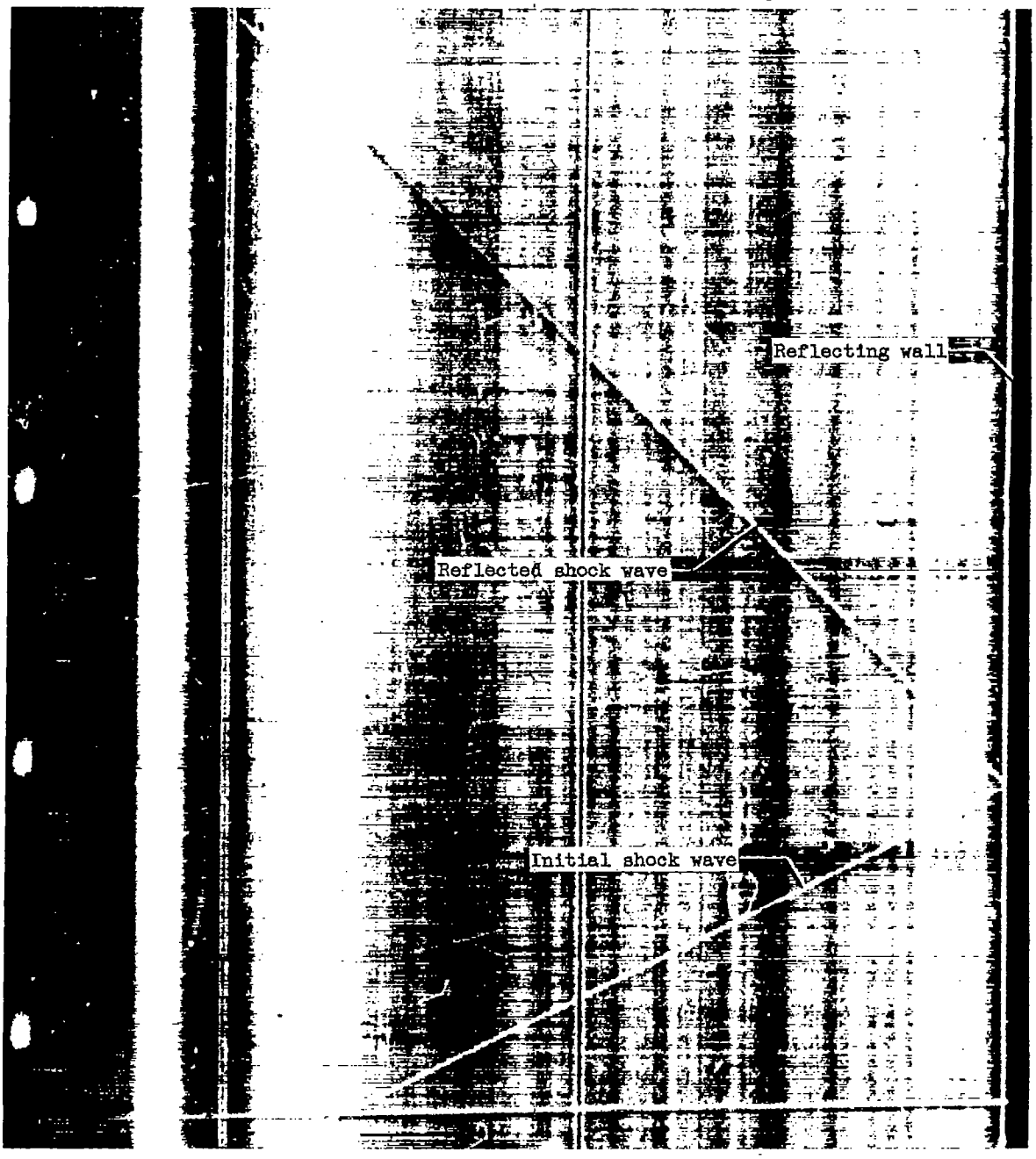

C-46538

Figure 48. - Experimental xt diagram showing deceleration of reflected shock wave immediately after reflection followed by subsequent acceleration of shock wave. $M_1 = 2.06$; $\gamma = 1.4$ (courtesy Ballistics Research Laboratory, Aberdeen Proving Grounds).

VI - A SUMMARY AND SOME SUGGESTED FURTHER STUDIES

The shock tube, although known since the end of the last century, has become in the past decade a tremendously useful and versatile research and laboratory tool. Some of its uses in the study of one-dimensional nonstationary gas dynamics have been mentioned without detail, and the particular usefulness of reflecting the initial shock wave from the closed end of the tube has been discussed more completely. Ideally (one-dimensionally) the initial shock signals a following flow in the shock tube which the reflected shock brings to rest. By this process there is produced conveniently in the shock tube a slug of stationary high-temperature gas which is very useful in a number of studies. It is clear that this is completely true only if the flow is one-dimensional. Because of the action of viscosity, however, a boundary layer with which the reflected shock must interact grows in the flow following the initial shock wave. A complete discussion of the methods by which this boundary layer is generally handled has been included. The results of this study indicate that the growing boundary layer has a very small effect on the shape of the initial shock, but does act to attenuate the shock somewhat (so that a nominal shock of $M_1 = 2.15$ is attenuated to $M_1 = 2.00$ in 144 inches of travel down a tube 2 by 4 inches in cross section).

4785

Using the picture of the boundary layer provided by the previous analysis, and changing coordinates to those moving with the reflected shock wave, it has been possible to examine the problem imposed by the deficiency of energy in the fluid of the boundary layer (due to viscosity) on the mechanism by which the initial shock afterflow (now no longer uniform) negotiates the pressure rise across the reflected shock wave. The analysis of these difficulties has been simplified by making the assumption that the boundary layer may be described as a jet of fluid entirely at M_{bl}, the Mach number of a thin layer of fluid near the tube wall. This assumption is reasonable, since an examination of the Mach number distribution across the boundary layer in a typical case indicates the variation to be monotonic from wall to main stream. Thus this assumption tends to give a conservative estimate for the appearance of difficulties in the shock-wave boundary-layer interaction. A display of the Mach number of the main stream (i.e., of the undisturbed reflected shock) and the Mach number of the boundary-layer jet (now described by M_{bl}) as functions of the Mach number of the initial shock immediately indicates two regions (and therefore two types) of interaction. In the first, the Mach number of the boundary layer is lower than that of the main stream; and, in the second, the Mach number of the boundary layer exceeds that in the main stream. A more careful study of the situation, by considering the pressure behind the undisturbed normal reflected shock (defined by the main uniform stream and normal shock-wave relations) as well as the pressure of the boundary-layer fluid described by M_{bl}, has shown that a third region appears in the initial Mach number regime. Of these three

regions, one, in which the stagnation pressure of the boundary layer is exceeded by the pressure behind the undisturbed normal reflected shock, is bounded by the other two regions in which this does not occur. An experiment was then devised to find out whether these two boundaries actually exist and if the predicted analytical values are correct. The results of this experiment show that these boundaries do actually exist and are predicted satisfactorily by the theory. To make this experimental verification, it was necessary, for detailed reasons which have been given, to use a particularly convenient mixture of monatomic and diatomic gases. However, when this was done, the results of the experiment successfully verified the predictions. Along with the former results, sufficient information was obtained from the experiment to make possible a proposed model for the interaction in the most complicated case. This model was further verified by measurements made during the experiment.

Since the problem just discussed involved a consideration of the laminar boundary layer only, the case for the turbulent boundary layer now had to be considered. At the present time there is no certain method for knowing when the boundary layer of the flow generated by the initial shock becomes turbulent, so an experiment was devised to obtain some information concerning this matter. The experiment was designed on the assumption that the transition from laminar to turbulent boundary layer would be indicated by a transition of the shock-wave boundary-layer interaction from an interaction corresponding to a laminar boundary layer to an interaction corresponding to the turbulent boundary layer. This turned out, apparently, to be the case. Below an experimentally determined value of Reynolds number of about 1.5×10^6 (the Reynolds number used is defined in the report), an interaction corresponding to the laminar boundary layer appeared. At the same Mach number (of the initial shock), but at Reynolds number greater than 1.5×10^6, the interaction was of a different character. This could be explained by supposing that the boundary layer was in the first case laminar and in the second case turbulent. An experimental cross check of Reynolds number variation gave the same value of transition Reynolds number within about 6 percent.

Because of the growth of the boundary layer with time, the laminar interaction with the reflected shock also grows in time, and an analysis has been made to determine this growth rate. The results checked reasonably well with the rate of growth measured experimentally. A calculation was made to determine the size of the interaction, and a good check was obtained with that experimentally determined.

Following this, a model has been proposed whereby the effect of the boundary-layer interaction on the strength of the reflected shock may be calculated. This model indicates that, because of the difficulty the energy-deficient boundary layer has in negotiating the pressure rise across the reflected shock, the entire pressure rise of the main fluid no longer takes place across the reflected shock. Instead, a portion of

the main fluid sacrifices itself to form a diffuser and brings the flow, now only partially compressed by a weaker shock, to its final state of rest at the closed end of the tube. A calculation for the attenuation of the reflected shock has been made in a particular case, and the constructed xt diagram for this case compares favorably with the experimental xt diagram for the same conditions.

4785

It should be pointed out that there remain some interesting questions for further investigation. First, it would be very desirable to know if the transition Reynolds number obtained in the present work at a given Mach number will hold universally at all Mach numbers, or if some variation with Mach number will occur. For this information the experiment of section IV could be repeated over a range of Mach numbers, and the resulting variation (if any) of Re_{trans} with Mach number could be obtained. It would also be of interest to change the closed-end boundary condition and investigate the changes in interaction that would occur with an average (steady-state) flow through the tube. This might be of interest and supply valuable information on the problem of rocket motor screaming. It is already known that shock waves travel down the rocket motor and are reflected at the nozzle end only during screaming operation. It might also be of extreme interest to extend the present work to the case of a steady (approximately) normal shock standing in the nose inlet of a supersonic air-breathing jet engine and to determine the connection between the spill induced by shock-wave boundary-layer interaction and the buzzing problem which exists presently with these engines (for instance, ref. 20).

APPENDIX A

MACH NUMBER DISTRIBUTION ACROSS THE BOUNDARY LAYER

If T, the temperature in the boundary layer, is a function only of η (η is defined in eq. (III-6)), the energy equation may be written (after ref. 7):

$$T'' + PrfT' = -Pr(\gamma - 1)M_e^2(f'')^2 \tag{A1}$$

where Pr is the Prandtl number (assumed constant); $f(\eta)$ is defined in equation (III-6) (also $f' = u/u_e$; see the following sketch of the stationary initial shock wave) and $M_e \equiv \frac{U_1 - u_2}{a_2} \equiv \frac{u_e}{a_2}$.

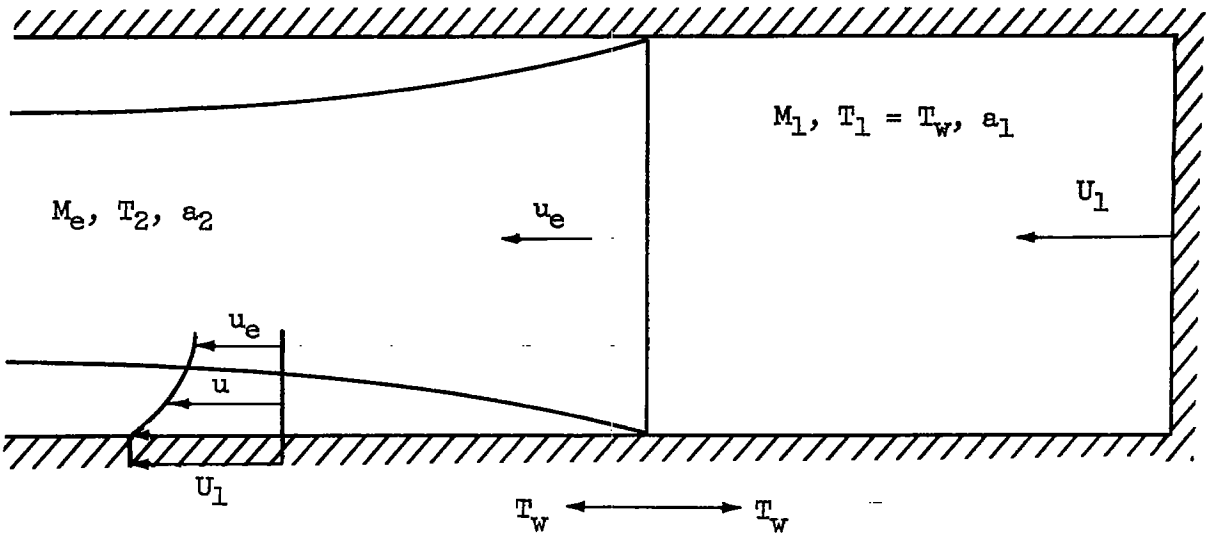

Since equation (A1) is linear, the solution for T/T_2 may be written as the superposition of solution for zero heat transfer (insulated wall) plus the effect of heat transfer. Thus if we write (from ref. 7)

$$\frac{T}{T_2} = 1 + \frac{\gamma - 1}{2}\left[\left(\frac{U_1}{u_e} - 1\right)M_e\right]^2 r(\eta) + \left\{\left(\frac{T_w}{T_2} - 1\right) - \frac{\gamma - 1}{2}\left[\left(\frac{U_1}{u_e} - 1\right)M_e\right]^2 r(0)\right\} S(\eta) \tag{A2}$$

For $Pr = 1$

$$r = 1 - \left(\frac{\frac{U_1}{u_e} - f'}{\frac{U_1}{u_e} - 1}\right)^2 \tag{A3}$$

and

$$s = \left(\frac{f' - 1}{\frac{U_1}{u_e} - 1}\right) \tag{A4}$$

where

$$f' = \frac{u}{u_e}$$

From (III-6) the relation between η and y is

$$\eta = \sqrt{\frac{U_1 - u_2}{2x\nu_w}} \int_0^y \frac{T_w}{T}\, dy$$

So

$$y\sqrt{\frac{U_1 - u_2}{2x\nu_w}} = \int_0^\eta \frac{T}{T_w}\, d\eta \tag{A5}$$

Combining equations (A2), (A3), (A4), and (A5), we have

$$y\sqrt{\frac{u_e}{2x\nu_w}} = \frac{T_2}{T_w}\left\{\eta + \frac{\frac{T_w}{T_2} - 1}{\frac{U_1}{u_e} - 1}(f - \eta) + \frac{\gamma - 1}{2} M_e^2\left[\frac{U_1}{u_e}(f - \eta) + f(1 - f') + f''(0) - f''\right]\right\} \tag{A6}$$

From Rankine-Hugoniot relations

$$\frac{T_2}{T_w} = \frac{(\gamma + 1)\frac{U_1}{u_e} - (\gamma - 1)}{\frac{U_1}{u_e}\left[(\gamma + 1) - (\gamma - 1)\frac{U_1}{u_e}\right]} \tag{A7}$$

$$M_e^2 = \frac{2}{(\gamma + 1)\frac{U_1}{u_e} - (\gamma - 1)} = \frac{(\gamma - 1)M_1^2 + 2}{2\gamma M_1^2 - (\gamma - 1)} = M_2^2 \tag{A8}$$

4785

Note also that

$$M_1^2 \equiv \left(\frac{U_1}{a_1}\right)^2 = M_e^2\left(\frac{U_1}{u_e}\right)^2\left(\frac{T_2}{T_w}\right) \tag{A9}$$

From reference 21 we may write (for $Pr = 1$)

$$\frac{T}{T_2} = A + B\left(\frac{u}{u_e}\right) + C\left(\frac{u}{u_e}\right)^2 \tag{A10}$$

where (by substituting eqs. (A3), (A4), (A7), (A8), and (A9) in (A2))

$$A = 1 + \left[\frac{\gamma - 1}{2}\left(\frac{(\gamma - 1)M_1^2 + 2}{2\gamma M_1^2 - (\gamma - 1)}\right)\right] = 1 + \frac{\gamma - 1}{2}M_e^2$$

$$B = 0$$

$$C = -\left[\frac{\gamma - 1}{2}\left(\frac{(\gamma - 1)M_1^2 + 2}{2\gamma M_1^2 - (\gamma - 1)}\right)\right] = -\frac{\gamma - 1}{2}M_e^2$$

We have now expressions for $T/T_2\left(= T/T_2(M_e;\ u/u_e)\right)$ (eq. (A10)) and, from figure 4 (or ref. 7, table I), u/u_e against η/η_δ. We have an expression for y in terms of η (for given initial Mach number) in equation (A6). Also, if we choose an initial Mach number, we have fixed M_e, T_2/T_w, and U_1/u_e (eqs. (A7), and (A8)).

Now we define η_δ as η at

$$\frac{\frac{U_1}{u_e} - \frac{u}{u_e}}{\frac{U_1}{u_e} - 1} = 0.999$$

we have

$$\frac{u}{u_e} = 1.002 \quad \text{at} \quad y = \delta \quad (\eta = \eta_\delta)$$

and

$$\eta_\delta = 2.59$$

We may now calculate and tabulate u/u_e and T/T_2 against y at any given x (here, distance behind the initial shock). For $M_1^2 = 5$ ($M_1 = 2.24$), we have tabulated these quantities in the following table:

$[M_1^2 = 5;\ U_1/u_e = 3.0;\ T_2/T_w = 1.892;\ M_e = 0.5418;\ x = 0.2$ foot; $\eta_\delta = 2.59;\ M_{bl} = 1.045;\ M_3 = 1.84]$

η/η_δ	η	u/u_e	T/T_2	$(T/T_2)^{1/2}$	$\frac{u/u_e}{(T/T_2)^{1/2}}$	y(in.)	M(y)
0	0	3.000	0.5296	0.7277	4.123	0	1.045
0.1	0.259	2.4001	.7201	.8486	2.828	0.00246	1.276
.2	.518	1.8949	.8477	.9207	2.058	.00553	1.467
.4	1.036	1.2893	.9611	.9804	1.315	.0127	1.712
.6	1.554	1.0709	.9914	.9957	1.076	.0203	1.807
.8	2.072	1.0134	.9984	.9992	1.014	.0281	1.837
.9	2.331	1.0053	.9994	.9997	1.006	.0320	1.839
1.0	2.59	1.002	.9998	.9999	1.002	.0359	1.840

4785

CY-15 back

$M(y)$ is the Mach number of the flow as seen in the coordinate system of the reflected shock and is calculated from $u/u_e/(T/T_2)^{1/2}$ (the quantity tabulated in column 6 of the table) by the following relation

$$M(y) = \left[\frac{u/u_e}{(T/T_2)^{1/2}}\right] M_e - \left[\frac{U_1 + u_{rs}}{(\gamma gRT)^{1/2}}\right] \tag{A11}$$

$M(y)$ is shown plotted against y in figure 9.

4785

4785

APPENDIX B

A WEAK SHOCK REFLECTED AT A WALL

If we consider a weak shock traveling into a stationary fluid and allow the shock to be reflected from a wall perpendicular to the direction of motion of the shock, we may describe this phenomenon in the xt plane as in the following sketch:

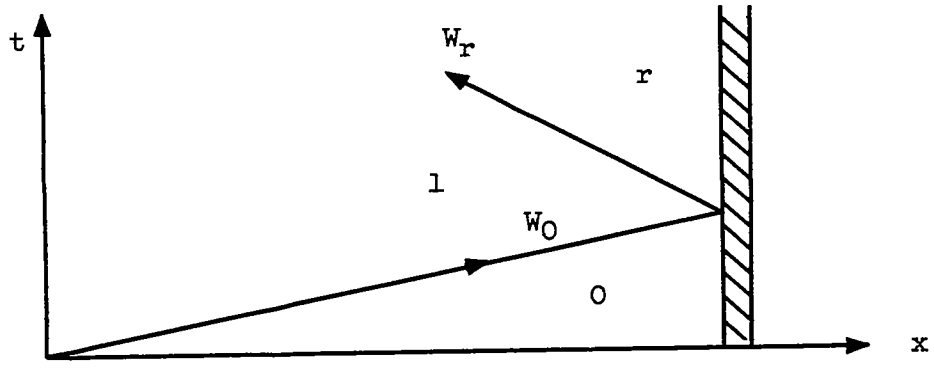

Considering the weak shock to be a simple P-wave we may write Q = constant across the wave. Thus

$$Q = na - u = \text{Constant} \qquad \text{(ref. 13)}$$

or

$$na_1 - u_1 = na_0 - u_0 \tag{B1}$$

where $n = \frac{2}{\gamma - 1}$, a = local speed of sound, u = particle velocity, and 0 and 1 are subscripts in regions 0 and 1, respectively, of the preceding sketch.

From the steady-flow energy equation and Prandtl's relation ($w_0 w_1 = a^{*2}$), it may be shown that the speed of a weak shock (to first order in particle velocity) is

$$w_0 = \frac{a_0 + a_1 + u_1}{2} \tag{B2}$$

Across the reflected shock, we consider P constant. Thus

$$P = na_r + u_r = na_1 + u_1 \tag{B3}$$

We may also write an expression for the speed of the reflected shock with respect to the fixed wall (in a manner analogous to that for equation (B2))

$$w_r = \frac{a_1 + a_r + u_1}{2} - u_1 \tag{B4}$$

or

$$w_r = \frac{a_1 + a_r - u_1}{2} \tag{B5}$$

Now from (B1) (and since $u_0 = u_r = 0$) we have:

$$a_1 = a_0 + \frac{\gamma - 1}{2} u_1 \tag{B6}$$

and from equations (B2) and (B6):

$$w_0 = a_0 + \left(\frac{\gamma + 1}{4}\right) u_1 \tag{B7}$$

From equation (B3)

$$a_r = a_1 + \frac{\gamma - 1}{2} u_1 \tag{B8}$$

Combining (B5), (B6), and (B8), we have

$$w_r = a_0 + \left(\frac{3\gamma - 5}{4}\right) u_1 \tag{B9}$$

Equations (B7) and (B9) are expressions for the velocity of the initial and reflected shock waves (to first order in particle velocity) with respect to the laboratory coordinate system. From section III we have (eq. III-13)

$$\left.\frac{dM_{bl}}{dM_1}\right]_{M_1=1} = \frac{3\gamma - 5}{\gamma + 1}$$

This corresponds to $\frac{dw_r}{dw_0}$ given previously, and from

$$\frac{dw_r}{dw_0} = \frac{dw_r/du_1}{dw_0/du_1} = \frac{\frac{3\gamma - 5}{4}}{\frac{\gamma + 1}{4}} = \frac{3\gamma - 5}{\gamma + 1}$$

which checks the limit $M_1 \to 1$ for $\frac{dM_{bl}}{dM_1}$.

APPENDIX C

CALCULATION OF ANGLES OF THE INTERACTION PATTERN

In calculating the angles of the interaction pattern we have assumed the proposed model of section IV, which is shown in the following sketch:

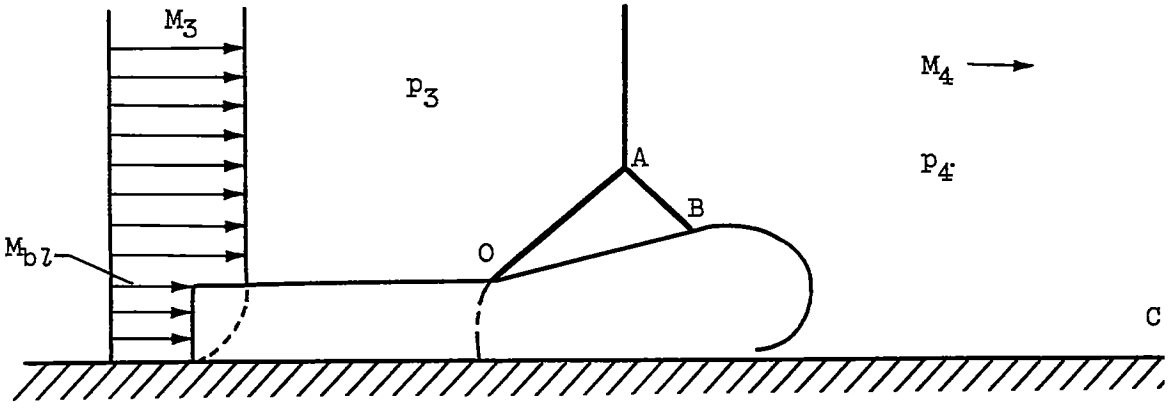

If we have a given M_1, then M_3 and M_{bl} are known from equations II-23 and III-7, respectively, or from figure 10. With M_{bl} known, the stagnation pressure of the boundary-layer fluid may be calculated from isentropic relations or, for the case of compression preceded by a normal shock (as in the preceding sketch), by the Rayleigh pitot formula (ref. 12, eq. 100)

$$\frac{p_{stag_{bl}}}{p_3} = \left[\frac{(\gamma + 1)M_{bl}^2}{2}\right]^{\frac{\gamma}{\gamma-1}}\left[\frac{\gamma + 1}{2\gamma M_{bl}^2 - (\gamma - 1)}\right]^{\frac{1}{\gamma-1}} \tag{C1}$$

Making the assumption that the pressure in region OAB is equal to the stagnation pressure of the boundary-layer fluid, we may use (from ref. 12) the relations for oblique shocks:

$$M_3^2 \sin^2(COA) = \frac{(\gamma + 1)\dfrac{p_{stag_{bl}}}{p_3} + (\gamma - 1)}{2\gamma} \tag{C2}$$

and

$$M_4^2 \sin^2(COA - COB) = \frac{(\gamma - 1)\dfrac{p_{stag_{bl}}}{p_3} + (\gamma + 1)}{2\gamma \dfrac{p_{stag_{bl}}}{p_3}} \tag{C3}$$

Since M_4 is known from normal shock relations, we can solve for the unknown angles COA and COB from these two relations. This has been done, and the results tabulated in the following table. The angles COA and COB are plotted against M_1 in figures 28 and 29, along with measured values.

4785

C-16

[γ = 1.4]

M_1	M_3	M_{bl}	$\frac{p_{stag_{bl}}}{p_3}$	Calculated		Measured	
				COA°	COB°	COA°	COB°
1.4	1.37	0.945	1.77	71.4	8.5		
1.6	1.51	0.95	1.77	58.4	11.0		
1.8	1.625	0.97	1.806	53.2	12.0	55.5 55.0 58.0	13.0 12.5 12.5
2.0	1.731	1.00	1.892	50.2	12.8		
2.15	1.81	1.03	1.96	48.5	13.4	55.0 51.0 53.0 51.0 49.0 50.0 50.0 49.0	14.0 13.6 15.1 13.5 14.5 14.7 16.0 12.5
2.4	1.91	1.085	2.10	47.0	14.45		
2.6	1.98	1.13	2.22	46.2	15.3		
2.8	2.05	1.18	2.37	46.0	16.35		
3.0	2.105	1.24	2.53	46.5	17.4	47.0 51.0 47.0 48.0	19.0 18.0 15.0 19.0
3.4	2.20	1.34	2.86	47.0	19.4		
3.8	2.27	1.45	3.25	49.0	21.6		
4.0						49 47	20 22
4.24	2.33	1.575	3.72	51.2	23.7	49	23
4.6	2.37	1.68	4.13	54.0	25.6		
5.0	2.41	1.81	4.67	57.2	27.6		

APPENDIX D

REYNOLDS NUMBER FOR THE REFLECTED SHOCK - BOUNDARY-LAYER INTERACTION

The Reynolds number as defined in section IV is

$$Re \equiv \frac{\rho_w u_2 x\left(1+\frac{U_s}{U_{rs}}\right)\frac{u_2}{U_s}}{\mu_w} \tag{D1}$$

4785

For the series of photographs in figure 41, the Mach number of the initial shock was kept constant. At constant ambient temperature, constant M_1 means that every term of the preceding expression is constant with the exception of x, the distance of the reflected shock from the reflecting wall. Rewriting the expression (D1), we have:

$$Re \equiv \frac{\rho_w u_2 x\left(1+\frac{M_1}{M_{bl}}\right)\frac{u_2/a_1}{M_1}}{\mu_w} \tag{D2}$$

For given M_1 and a_1, the values of u_2, u_2/a_1, and M_{bl} may be calculated from expressions (II-17) and (III-7) of the text. Values of ρ_w and μ_w are available in reference 12 as a function of temperature. It has been pointed out previously that the wall temperature is assumed to be unchanged with the passage of the shock and thus ρ_w and μ_w are obtained at the ambient (initial wall) temperature. Thus, for $M_1 = 2.15$, $a_1 = 1130$ feet per second, and $p_1 = 0.9$ inch mercury absolute (= 2.285 cm Hg abs), we have:

From (III-7),

$$M_{bl} = 1.03$$

From (II-17),

$$u_2/a_1 = 1.41$$

Thus,

$$u_2 = 1590 \text{ feet per second}$$

From reference 12

$$p_2/p_1 = 5.226 \qquad \text{at} \qquad M_1 = 2.15$$

Thus (since $T_w = T_1$)

$$\rho_2 = \rho_1\left(\frac{p_2}{p_1}\right) = \rho_{standard}\left(\frac{p_1}{p_{standard}}\right)\left(\frac{p_2}{p_1}\right)$$

$$\rho_2 = 0.002378 \times \frac{2.285}{76} \times 5.226 = 3.73\times10^{-4} \text{ slug/cu ft}$$

4785

and (from ref. 12) $\mu_w = 1.21\times10^{-5}$ lb/ft-sec

$= 3.76\times10^{-7}$ slug/ft-sec

Thus (by interpolating for x from the photographs of figure 41, $x = 0.462$ ft)

$$Re_{tr} = \frac{3.73\times10^{-4} \times 1590 \times 0.462 \times 3.085 \times 0.656}{3.76\times10^{-7}} = 1.47\times10^{6}$$

CY-16 back

Similarly (by interpolating the photographs in fig. 42, $p_1 = 1.35$ in. Hg abs), from the experiment during which the Reynolds number was varied (at $M_1 = 2.15$) by varying the density only (distance from reflected wall was kept constant at $x = 0.325$ ft),

$$Re_{tr} = \frac{5.6\times10^{-4} \times 1590 \times 0.325 \times 3.085 \times 0.656}{3.76\times10^{-7}} = 1.56\times10^{6}$$

APPENDIX E

CALCULATION OF THE SIZE OF THE SHOCK-WAVE - BOUNDARY-LAYER INTERACTION

From reference 5, equation 6.9 (in our nomenclature, and for $Pr = 1$ and $\gamma = 1.4$), assuming $T_w = T_1$, we have:

$$\frac{\delta^*}{\Delta} = \frac{u_2}{U_1 - u_2}\left[1 + \frac{2U_1 - u_2}{5U_1 + u_2} - (\sqrt{2} - 1)\frac{u_2}{5U_1 + u_2}\right] \tag{E1}$$

4785

δ^* is the boundary-layer displacement thickness defined by

$$\rho_2(U_1 - u_2)\delta^* = \int_0^\infty \left[\rho u - \rho_2(U_1 - u_2)\right]dy \tag{E2}$$

and is positive if defined as given here. $\rho(y)$ is the density across the boundary layer; $u(y)$ is the velocity in the boundary layer in a coordinate system moving with the initial shock. Δ is defined in equation 6.4 of reference 5 as

$$\Delta = \sqrt{\frac{4\mu_w x_i}{\pi\rho_w\left[U_1 - u_2(\sqrt{2} - 1)\right]}} \tag{E3}$$

where x_i is the distance behind initial shock.

Combining equations (E1) and (E3) and solving for δ^* at $M_1 = 2.0$ (the Mach number to which a nominal shock of $M_1 = 2.15$ has decayed in 144 in. of travel), and solving for μ_w and ρ_w from reference 12 at $T_w = 530^\circ$ F, we obtain (since fixing M_1 at a given temperature fixes U_1 and u_2)

$$\delta^* = 0.7\times10^{-3}\sqrt{x_i} \tag{E4}$$

where x_i is in feet.

Now in terms of x, the distance the reflected shock has traveled from the reflecting wall,

$$x_i = \left(1 + \frac{U_1}{U_{rs}}\right)x = \left(1 + \frac{M_1}{M_{bl}}\right)x \tag{E5}$$

Thus:

$$\delta^* = 0.7\times10^{-3}\sqrt{\left(1 + \frac{M_1}{M_{bl}}\right) x} \tag{E6}$$

Now from section IV we have (eq. (IV-7))

$$\eta = k\sqrt{t^{3/2}} \tag{E7}$$

4785

where

$$k = \sqrt{\frac{8}{3\pi}\frac{\rho_{bl}}{\rho_{stag_{bl}}}\bar{u}\,k_1}$$

and k_1 is defined by the expression for $h(t)$, the height of the stream of fluid entering the ball (section IV).

$$h(t) = k_1 t^{1/2}$$

Now since

$$x = \bar{u}\,t \tag{E8}$$

We may write (E7) as

$$\eta = \sqrt{\frac{8}{3\pi}\frac{\rho_{bl}}{\rho_{stag_{bl}}}\bar{u}\,k_1 t^{3/2}}$$

Thus substituting from (E8) we have:

$$\eta = \sqrt{\frac{8}{3\pi}\frac{\rho_{bl}}{\rho_{stag_{bl}}}hx} \tag{E9}$$

If we use δ^* for h we have finally:

$$\eta = \sqrt{\frac{8}{3\pi}\frac{\rho_{bl}}{\rho_{stag_{bl}}}\delta^* x} \tag{E10}$$

Substituting from (E6) for δ^* we can calculate η for given initial conditions at a given distance from the reflecting wall. For example, at

$$M_1 = 2.0$$

$$T_1 = 530^\circ \text{ F}$$

$$x = 0.22 \text{ foot}$$

we have (for $\gamma = 1.4$, from fig. 10)

$$M_{bl} = 1.0$$

thus

$$\frac{\rho_{bl}}{\rho_{stag_{bl}}} = 0.634$$

and from (E6)

$$\delta^* = 0.7\times10^{-3}\sqrt{3\times0.22} = 0.568\times10^{-3} \text{ foot}$$

and from (E10):

$$\eta = \sqrt{\frac{8}{3\pi}(0.634)(0.568\times10^{-3})(0.22)}$$

$$\eta = 8.21\times10^{-3} \text{ foot}$$

or

$$\eta = 9.84\times10^{-2} \text{ inch at } x = 0.22 \text{ feet}$$

REFERENCES

1. Glass, I. I., and Patterson, G. N.: A Theoretical and Experimental Study of Shock Tube Flows. Jour. Aero. Sci., vol. 22, no. 2, Feb. 1955, pp. 73-100.

2. Glass, I. I., Martin, W., and Patterson, G. N.: A Theoretical and Experimental Study of the Shock Tube. UTIA Rep. No. 2, Inst. Aerophys., Univ. of Toronto, Nov. 1953.

3. Glick, H. S., Squire, W., and Hertzberg, A.: A New Shock Tube Technique for the Study of High Temperature Gas Phase Reactions. Fifth International Symposium on Combustion, Reinhold Pub. Corp.

4. Hartunian, Richard A.: Some Viscous Effects in Shock-Tube Flow. M. Aero. E. Thesis, Cornell Univ., June 1954.

5. Rott, N., and Hartunian, R. A.: On the Heat Transfer to the Walls of a Shock Tube. Cornell Univ., Nov. 1955. (USAF Contract AF 33(038)-21406.)

6. Trimpi, Robert L., and Cohen, Nathaniel B.: A Theory for Predicting the Flow of Real Gases in Shock Tubes with Experimental Verification. NACA TN 3375, 1955.

7. Mirels, Harold: Laminar Boundary Layer Behind Shock Advancing into Stationary Fluid. NACA TN 3401, 1955.

8. Mirels, Harold: Attenuation in a Shock Tube Due to Unsteady Boundary-Layer Action. NACA TN 3278, 1956.

9. Donaldson, Coleman DuP., and Sullivan, Roger D.: The Effect of Wall Friction on the Strength of Shock Waves in Tubes and Hydraulic Jumps in Channels. NACA TN 1942, 1949.

10. Hollyer, Robert N., Jr.: A Study of Attenuation in the Shock Tube. Eng. Res. Inst., Univ. of Mich. July 1, 1953. (U.S. Navy Dept., Office Naval Res. Contract N6-ONR-232-TO IV, Proj. M720-4.)

11. Bershader, D., and Allport, J.: On the Laminar Boundary Layer Induced By a Travelling Shock Wave. Tech. Rep. II-22, Princeton Univ., May 1956. (NR061-020, N6 ori-105, Task II.)

12. Ames Research Staff: Equations, Tables and Charts for Compressible Flow. NACA Rep. 1135, 1953. (Supersedes NACA TN 1428.)

13. Courant, R., and Friedrichs, K. O.: Supersonic Flow and Shock Waves. Interscience Pub., Inc., 1948.

14. Hertzberg, A., Smith, W. E., Glick, H. S., and Squire, W.: Modification of the Shock Tube for Generation of Hypersonic Flow. CAL Rep. No. AD-789-A-2, AEDC TN-55-15, Mar. 1955.

15. Howarth, L.: Concerning the Effect of Compressibility on Laminar Boundary Layers and Their Separation. Proc. Roy. Soc. (London), ser. A, vol. 194, no. A1036, July 1948, pp. 16-42.

16. Resler, E. L., Lin, S. C., and Kantrowitz, A.: The Production of High Temperature Gases in Shock Tubes. Jour. Appl. Phys., vol. 23, no. 12, Dec. 1952, pp. 1390-1399.

17. Hess, R. V.: The Interaction of a Shock Wave with a Thermal Boundary Layer. (Unpublished)

4785

18. Schardin, H.: Toepler's Schlieren Method - Basic Principles for Its Use and Quantitative Evaluation. Trans. 156, David Taylor Model Basin, July 1947.

19. Ackeret, J., Feldmann, F., and Rott, N.: Untersuchungen an Verdichtungsstössen und Grenzschichten in schnell bewegten Gasen. Reps. of Inst. Aero. ETH (Zurich), no. 10, 1946 (See also NACA TM 1113.)

20. Dailey, C. L.: Supersonic Diffuser Instability. Jour. Aero. Sci., vol. 22, no. 11, Nov. 1955, pp. 733-749.

21. Crocco, L.: Sullo strato laminare nei gas lungo una lamina plana. Rend. Math. Univ., Roma, t. 2, 1941, p. 138.

4785

NACA - Langley Field, Va.